The role of pyruvate dehydrogenase kinases (PDKs) in rewiring of cell metabolism under energy stress

Hanan Ashrafi

This dissertation is submitted in partial fulfilment of the requirements for the degree of Master of Science in Biomedical Sciences

Department of Biomedicine
Faculty of Medicine, University of Bergen
Spring, 2019
Bergen, Norway

Acknowledgement

The work presented in this thesis was carried out in the Cellular Network Group (CELLNET) led by Professor James Lorens, Department of Biomedicine, University of Bergen, in the period from August 2018 to June 2019.

First of all, I would like to thank my main supervisor Ina Katrine Nitschke Pettersen, for her all laboratory guidance, valuable suggestion and support throughout this study period. Thank you for being so nice to me and always having the time for my questions and sharing your scientific knowledge. I have learned a lot from you.

My sincerest gratitude goes to my co-supervisor Karl Johan Tronstad for having faith in me and letting me be a part of his great research group and allowing me to learn new skills and techniques. Thank you for having the time for the meetings, excellent advice and comments on my work.

Besides my advisors, I would like to thank rest of my lab members; Lena Hansen, Sissel Elisabeth Dyrstad and Fredrik Hoel for their excellent laboratory guidance, valuable suggestions and the time for helping me to learn new techniques. I found Gro Vatne Røsland so encouraging and positive towards me and Silje also deserves a thank for being so nice and a helpful friend in the lab.

I am also grateful to Sissel Vik Berge and Endre stigen for their contribution in the excellent organization of the lab and providing us with every laboratory consumable when needed. Working in the well-organized and welcoming environment of CELLNET research group was never a stressful event for me.

Finally, I would like to thank my parents, in-laws, siblings and friends for their endless support and interest in my work. Last but not the least, a big thanks to my husband Ishtiaq, my only friend far from home, for all his dedication, support and love towards me. Thank you for having patience and understanding me throughout this busy year.

Thank you!

Hanan Ashrafi

Bergen, Norway, 2019

Table of Contents

Abbreviations

2DG	2-Deoxy-D-glucose
ADP	Adenosine diphosphate persulfate
Akt	Protein kinase B
AMPK	AMP activated protein kinase
ATP	Adenosine triphosphate
BSA	Bovine serum albumin
CCCP	Carbonyl cyanide m-chlorophenyl hydrazine
cDMEM	Complete Phoenix DMEM
CI	Complex I, NADH – ubiquinone oxidoreductase
CII	Complex II, Succinate dehydrogenase
CIII	Complex III, Ubiquinol cytochrome *c*
CIV	Complex IV, Cytochrome c oxidase
CPT I / II	Carnitine palmitoyl transferase I / II
CV	Complex V, F1F0 ATP-synthase
DCA	Dichloroacetate
DMSO	Dimethyl Sulfoxide
ECAR	Extracellular acidification rate
EMT	Epithelial mesenchymal transition
ETC	Electron transport chain
FA	Fatty acid
FAD+	Oxidized flavin adenine
FADH2	Reduced flavin adenine dinucleotide
FCCP	Trifluoromethoxy carbonylcyanide phenylhydrazone
FFA	Free fatty acid
GAPDH	Glyceraldehyde 3-phosphate dehydrogenase
GLUT	Glucose transporter
GTP	Guanosine triphosphate
hi FBS	Heat Inactivated Fetal Bovine Serum
Hif-1α	Hypoxia inducible factor 1 alpha
IMM	Inner mitochondrial membrane

kDa	Kilodalton
MMLV	Moloney murine leukemia virus
MPC	Mitochondrial pyruvate carrier
mRNA	messenger RNA
mtDNA	Mitochondrial DNA
mTOR	Mammalian target of rapamycin
NAD^+	Oxidized nicotinamide adenine
NADH	Reduced nicotinamide adenine
NADPH	Nicotinamide adenine dinucleotide phosphate
OCR	Oxygen consumption rate
OMM	Outer mitochondrial membrane
OXPHOS	Oxidative phosphorylation
PA	Palmitic acid
PBS	Phosphate buffered saline
PDH	Pyruvate dehydrogenase
PDK	Pyruvate dehydrogenase kinase
PDP	Pyruvate dehydrogenase phosphatase
PMF	Proton motive force
PMSF	Phenylmethylsulphonylfluoride
PPAR	Peroxisome proliferator-activated receptor transcription factors
PPP	Pentose phosphate pathway
PVDF	Polyvinylidene fluoride
ROS	Reactive oxygen species
SDS-PAGE	Sodium Dodecyl Sulfate Poly Acrylamide Gel Electrophoresis
TCA	Tricarboxylic acid cycle
UCP	Uncoupling protein

Summary

Irregularities in cellular energy metabolism have been linked to many human diseases, including metabolic disorders, mitochondrial diseases, cancer, and neurodegeneration. In order to survive and function properly, an adequate supply of energy is necessary. When cells are exposed to energy stress or pathologic stimuli, they have the ability counteract decreased energy status by activating adaptive mechanisms, which can theoretically be referred as metabolic rewiring. More scientific knowledge about the molecular mechanisms involved in metabolic rewiring may facilitate development of new targeted therapeutic strategies.

In this study, we investigated the effects of genetic manipulation and the mechanisms of metabolic adaptation in cultured cells, and how these correlates with changes in key metabolic and physiological functions under different conditions of energy stress. We particularly mimicked pyruvate dehydrogenase (PDH) dysregulation in MDA-MB-231 cell line by inducing overexpression of all four isoforms of pyruvate dehydrogenase kinase (PDK1-4).

Successful overexpression of each of the PDK isoforms was confirmed by quantitative real-time PCR and western blot analysis. We found that increased PDK1-4 expression is associated with increased proliferation in modified MDA-MB-231 cells, particularly in PDK1, PDK3, and PDK4 overexpressing cells. We carried out a series of cell proliferation assays in high (25 mM), moderate (5 mM) and low (1 mM) glucose to investigate the effect of glucose supply on growth of PDK-overexpressing cells. We observed that PDK1-4 overexpression triggers a reduced cellular tolerance in glucose deprived condition and conversely, they exhibited an increased dependence on high glucose. Besides, Inhibition of PDK by Dichloroacetate (DCA) was found to cause a drastic reduction in proliferation in these cells.

Subsequent metabolic adaptation was observed towards increased mitochondrial respiration and glycolysis in the PDK-overexpressing cells, mostly in the PDK1 expressing cell. However, pyruvate oxidation was reduced by PDK overexpression, as expected. One remarkable finding of this study is PDK-overexpression was found to trigger a metabolic switch towards increased fatty acid oxidation. In cells overexpressing PDK1 or PDK2, fatty acid oxidation was increased in low glucose condition, whereas in PDK3 or PDK4 overexpressing cells, fatty acid oxidation was increased in high glucose condition.

Our findings suggest that PDK overexpression is associated with subsequent metabolic rewiring in cultured cells, characterized by increased dependency of glucose for growth,

changed utilization of energy substrates, and increased rates of both glycolysis and mitochondrial respiration.

1 Introduction

In order to survive, having a source of energy is essential. Mammalian cells possess special mechanisms to produce energy from the breakdown of food we eat. The energy is utilized by the cells in the form of a versatile energy molecule, adenosine triphosphate (ATP). Energy homeostasis must be balanced by supporting the adequate production of ATP so that living cells can grow, reproduce, maintain structures and respond to environmental changes [1]. If the cell is unable to meet appropriate metabolic requirements, the homeostasis might be threatened, which may induce cell death and pathological conditions including cancer, neurodegeneration, metabolic syndrome, cardiovascular disease and more [2, 3]. To prevent such effects, cells need metabolic flexibility to adapt to conditional changes in energy supply and demand. This might be achieved by switching between substrates or activating rescue mechanisms to avoid potential stresses [4]. A cell's ability to be metabolically flexible is determined by the mitochondrial function, since mitochondria are the central organelles for metabolic processes [5]. This thesis focuses on characterizing adaptive mechanisms of cultured cell lines with regards to manipulation of mitochondrial function in varying conditions of energy stress.

1.1 The Mitochondrion: origin, structure, genetics, and function

Mitochondria derived their names from the Greek word 'mitos' meaning thread and 'chondros' meaning small granules, due to their thread-like structure when observed under a light microscope [1]. They occupy a substantial portion of the eukaryotic cell cytoplasm and are considered as metabolic headquarter of the cell. Mitochondria arose from the engulfment of an α-proteobacterium by a primitive eukaryotic cell over two million years ago. A relic of this event is that the mitochondrion maintained its double membrane character as its ancestors and is the only organelle that has its own DNA [6, 7]. All human cells contain mitochondria, except mature erythrocytes [8]. The size, shape and copy number of mitochondria in a cell depend on the type of cell and the cell's metabolic energy demand [9].

Mitochondria can be found as stiff, elongated cylinders or dynamic tubular network of interconnected mitochondria, with a diameter 0.5–1 μm. They have been found as remarkably mobile and plastic, and continuously changing their shape, as observed under light microscope [9, 10]. The structure consists of a mitochondrial matrix surrounded by the inner and outer mitochondrial membranes (IMM and OMM); between the two membranes, there is a narrow intermembrane space (IMS) (see Figure 1.1). The matrix contains most of the mitochondrial

proteins, including the enzymes involved in the tricarboxylic acid (TCA) cycle, fatty acid (FA) oxidation, iron-sulfur (Fe-S) biogenesis, and others [11] .The mitochondrial DNA (mtDNA) is also found in the matrix. In the IMM, the mitochondrial oxidative phosphorylation (OXPHOS) machinery consisting of the electron transport chain (ETC) complexes (complxes I-IV) and the ATP synthase complex (complex V) is located, and also protein complexes involved in transporting ions, metabolites and proteins through the IMM. [12]. The IMS contains some proteins for cristae remodeling and apoptosis factors. The OMM contains porin proteins that allow influx and efflux of metabolites and proteins involved in mitochondrial fission and fusion [13, 14].

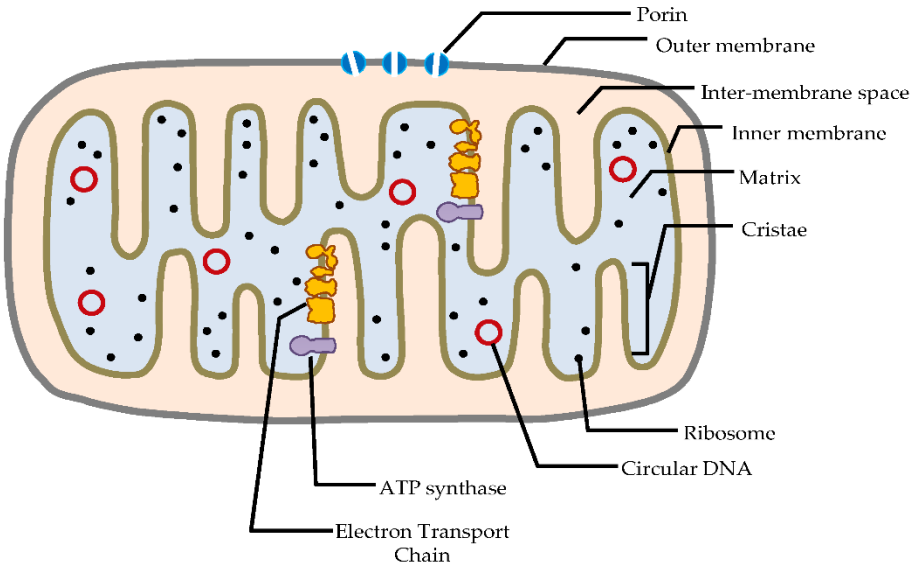

Figure 1.1 Simplified illustration of human mitochondrion with its structural parts. The mitochondrion has two membranes: inner and outer membrane (IMM and OMM); between these two, there is an intermembrane space. The IMM is folded into cristae that encloses the mitochondrial matrix. The electron transport chain (ETC) is in the IMM and the matrix holds the mitochondrial DNA (mtDNA) and ribosomes. Adapted from [15]

The mitochondrial genome contains multiple copies of small circular DNA that are maternally inherited and is distinct from the nuclear genome. The mtDNA contains coding information for 13 protein subunits of the ETC complex, 22 for transfer RNAs and two for ribosomal RNAs; encoding 37 genes in total. However, more than 98% of the protein complement needed for overall mitochondrial function are encoded by the nuclear genome [13, 16].

Mitochondria produce most of the cellular ATP and important contributors in different signaling pathways that are crucial for organism survival. They are also involved in cellular adaptation to environmental stimuli, production of reactive oxygen species (ROS), apoptosis

and in intracellular Ca^{2+} signaling [6]. The mitochondrial biomass and functional quality is maintained by a combination of process including metabolic adaptation, mitophagy, mitochondrial biogenesis and often accompanied by changes in morphology (e.g fission, fusion) [7].

1.2 Cell metabolism

The word 'metabolism' comes from the Greek 'metabolē' which means 'change'. It is the sum of chemical reactions occurring in the living organisms that allow organisms to maintain life [17]. The sum constitutes more than 8,700 reactions and 16,000 metabolites that have been annotated in the Kyoto Encyclopedia of Genes and Genomes (KEGG). The core metabolic reactions can be categorized as catabolic- the breakdown of substrates to produce energy and anabolic- using energy to build up components [18]. Thus, metabolism serves three purposes in an organism: 1. breaking down food into energy for vital processes, 2. conversion of food or fuel to building blocks of life such as protein, lipids and nucleic acids, and 3. the excretion of metabolic wastes (e.g. nitrogenous wastes). All the chemical reactions are organized into different metabolic pathways and carried out through a series of steps; each step facilitated by an enzyme. Enzymes function as catalysts to allow reactions to proceed rapidly and regulate the rate of metabolic reaction [3, 19].

1.2.1 Energy substrates and whole-body energy homeostasis

The main energy substrates of body metabolism are carbohydrates, lipids and proteins that come from the foods we eat. After digestion, the simplified food molecules are distributed to all tissue through the circulation via blood vessels. A set of tightly regulated transport mechanisms are involved in the uptake of molecules by the cells from the bloodstream [20]. Inside the cells, metabolic processes that convert sugar, FAs, and amino acids into energy occurs in multiple sites through specialized metabolic pathways. For instance, in the cytosol, we find glycolysis whereas in mitochondria; TCA cycle, FA oxidation and OXPHOS system contribute to the production of ATP [2]. Figure 1.2 show an overview of substrate conversion in different metabolic pathways.

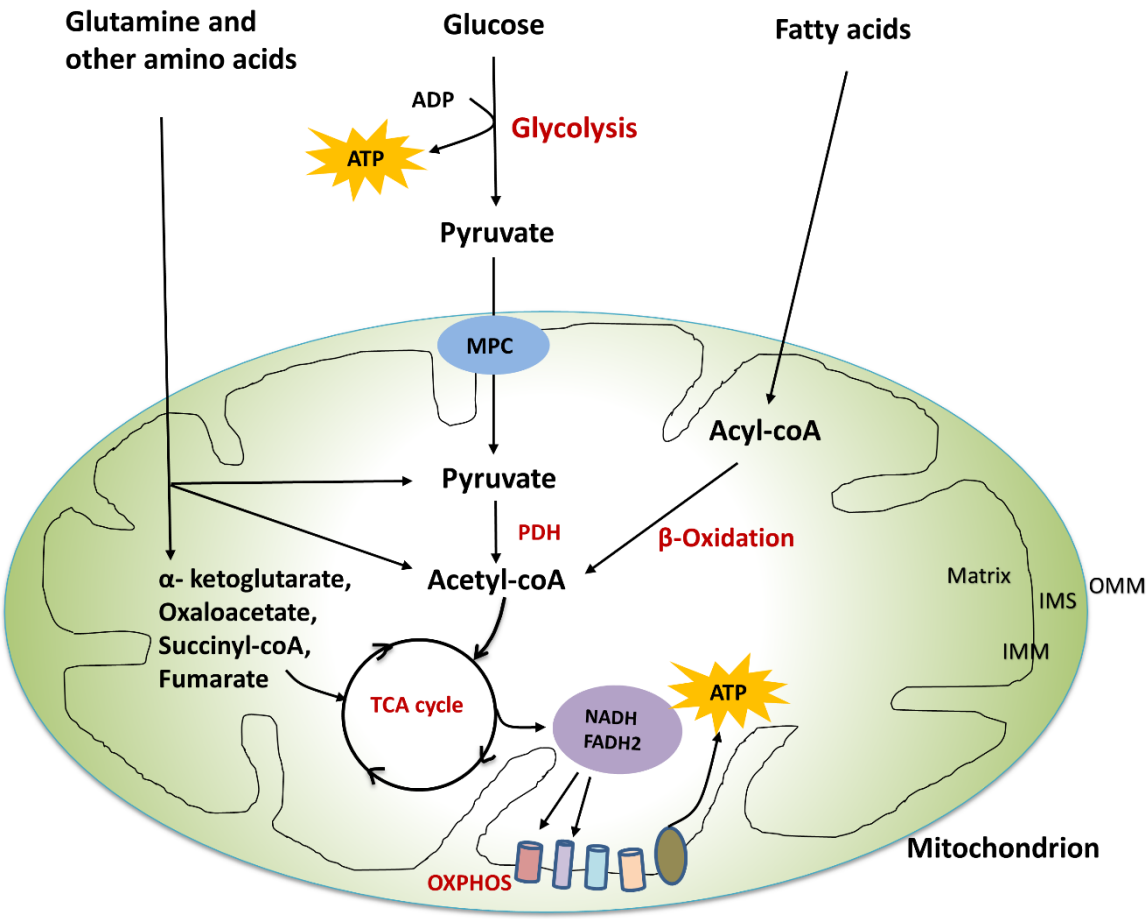

Figure 1.2 An overview of interplay between different metabolic pathways. Intermediates or end products from glucose metabolism, lipid metabolism and amino acid metabolism can serve as energy substrates for TCA cycle that eventually produce fuel molecules for ATP production. Modified from [21]

How the body will utilize different substrates depend on the type of the tissue, oxygen availability, metabolic state (fed or starved) and energy demand (resting or exercise). For example, red blood cells (RBC) only utilize glucose since they lack mitochondria. Similarly, the brain alone uses 130g of glucose per day since it cannot use FAs [22]. Alternatively, FAs are the preferred fuel for skeletal and heart muscle cells during resting states [23]. However, when the preferred substrates are unavailable, alternative substrates may be utilized instead; an example includes the use of FA derived ketone bodies by the brain when glucose is not available [24]. During fasting, FAs are taken up by the liver cells and are used to make ketone bodies and ATP to fuel gluconeogenesis which helps to maintain glucose levels above 3.5 mmol/L [3]. In diabetes, a similar shift occurs due to deficient glucose uptake which may lead to diabetic ketoacidosis if not controlled [25]. Some tissues switch between substrates

depending on the workload, such as in skeletal muscle, plasma free fatty acids (FFA) provide most of the energy during resting or low intensity exercise. When exercise intensity increases, plasma FFA turnover does not increase and the additional energy demand is met by using muscle glycogen, blood glucose or intramuscular triglyceride [26].

Glycogen serves as a form of energy storage in liver and to some extent, in muscle. When energy intake is higher than the metabolic demand, extra glucose molecules can be stored as glycogen. Alternatively, the adipose tissues are the storage site for excess FAs, in the form of fat [27].

1.2.2 Glycolysis pathway

ATP is generated both in the cytosol and mitochondria. In the cytosol, the glycolysis, also known as Embden–Meyerhof pathway converts glucose into pyruvate via a 10-step process. The net yield of this enzymatic process is 2 molecules of pyruvate, 2 molecules of ATP, and in addition two NADH (reduced nicotinamide adenine dinucleotide) per molecule of glucose [3]. The net reaction of glycolysis can be written as:

$$\text{Glucose} + 2\ NAD^+ + 2Pi + 2\ ADP \rightarrow 2\ \text{Pyruvate} + 2\ NADH\ ^+\ 2H^+ + 2\ ATP + 2\ H_2O$$

The glucose utilized in this process is mobilized from intracellular glycogen or transported from the bloodstream into cytosol through glucose transporters (GLUTs). The GLUT family transporters are subdivided into three classes and the physiological role of class I GLUT (GLUT1 to GLUT4) is associated with facilitating glucose transport into insulin-sensitive cells [28]. However, how the produced pyruvate will be utilized, depends on the level of oxygen present. In the presence of oxygen (aerobic condition), pyruvate is transported to the mitochondrial matrix to be oxidized in the TCA cycle. Under anaerobic condition (low or no oxygen), pyruvate is primarily converted to lactate by lactate dehydrogenase, and NADH is oxidized to NAD^+ [3, 29]. A detailed description of the glycolysis pathway is depicted in Figure 1.3.

The flux through glycolysis must be regulated to meet cellular demand depending on the condition both inside and outside of the cell. In general, enzymes that catalyze essentially irreversible reactions would be expected as potential sites of control. In glycolysis, hexokinase, phosphofructokinase, and pyruvate kinase, are considered to have regulatory roles since the three reactions they catalyze are virtually irreversible. Their activities are allosterically controlled by reversible binding of many effector molecules or by covalent modification [30, 31].

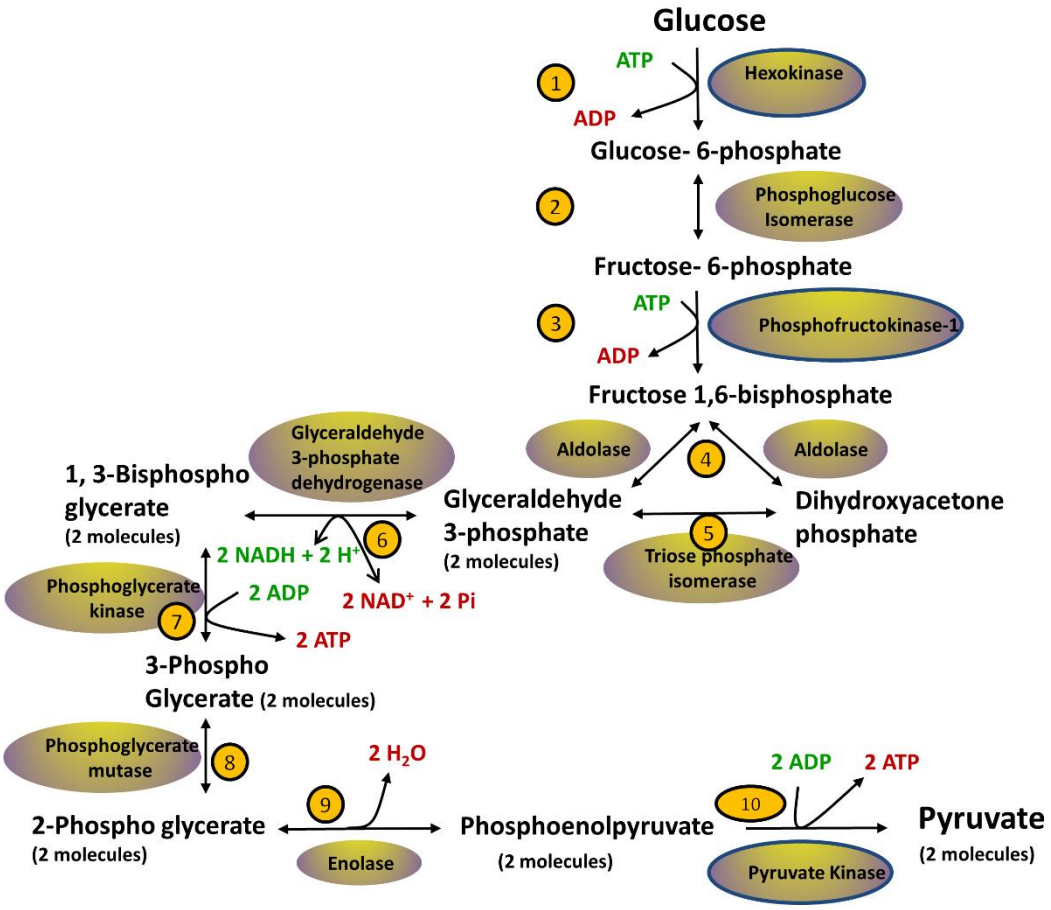

Figure 1.3 The series of chemical reactions in the glycolysis pathway. Each step is catalyzed by an enzyme and the three irreversible reactions in the pathway are circled blue. The net yield after the 10-step glycolysis pathway is 2 ATP, 2 NADH and 2 pyruvates. Figure based on [3]

1.2.3 Tricarboxylic acid cycle

The tricarboxylic acid (TCA) cycle, also known as citric acid cycle or Krebs cycle is a series of biochemical reactions that occurs in the mitochondrial matrix and is a central hub for aerobic energy metabolism. The cycle produces intermediates to be used in macromolecular synthesis and harvest high-energy electrons from carbon fuels to form NADH and $FADH_2$ (reduced flavin adenine dinucleotide). The NADH and $FADH_2$ that are produced throughout the cycle serve as electron donors for downstream cellular processes such as ETC to produce ATP [32, 33].

The common fuel for feeding the TCA cycle is acetyl-coenzyme A (acetyl-CoA) and pyruvate is a major source of acetyl-CoA in this cycle. After glycolysis, pyruvate is transported from the cytosol to mitochondrial matrix by mitochondrial pyruvate carrier (MPC, heterocomplex of MPC1 and MPC2), located in the inner mitochondrial membrane [34]. Inside the mitochondrial

matrix, pyruvate is primarily oxidized to acetyl-CoA by pyruvate dehydrogenase (PDH), also generating an NADH and a CO_2 in the process. PDH is highly regulated and thus control the flux of glycolytic acetyl-CoA into the TCA cycle (see section 1.4.1). Acetyl-CoA then fuses with oxaloacetate with the help of citrate synthase, to produce the first product of the classical 8-step cycle, citrate (a type of tricarboxylic acid, hence the name tricarboxylic acid cycle) [3, 35]. Figure 1.4 illustrates the full oxidation of acetyl-CoA through the 8-step process.

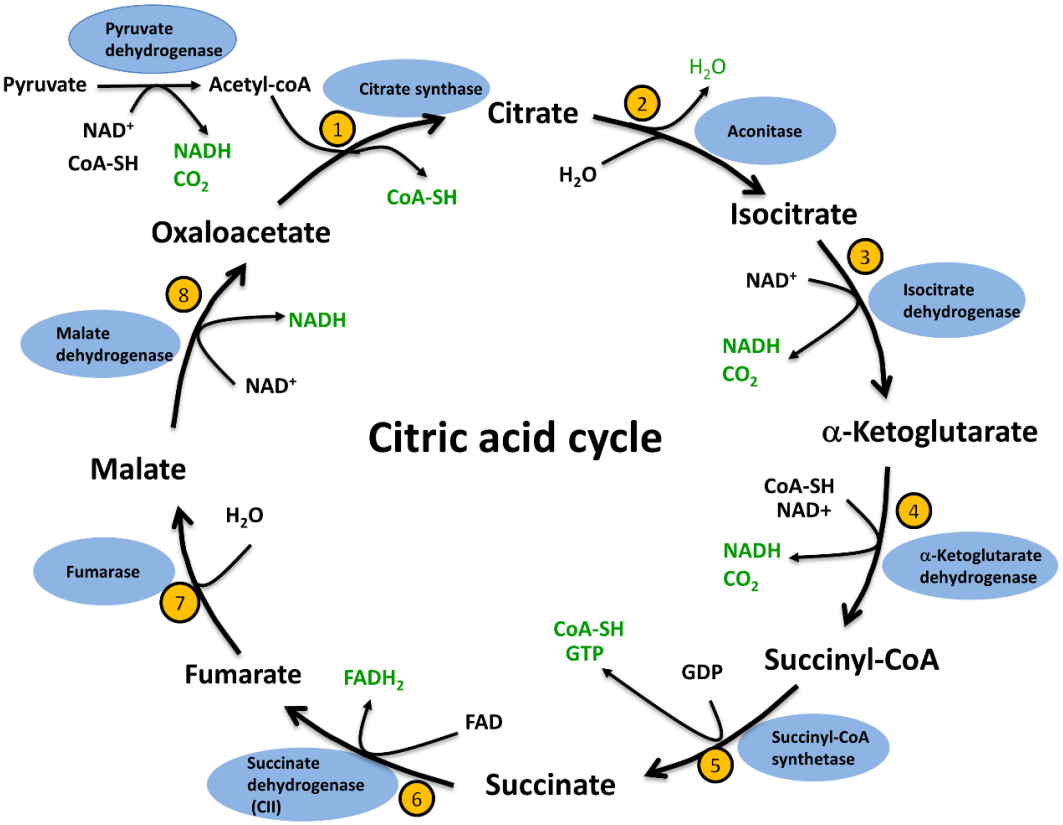

Figure 1.4 Biochemical reactions that drive TCA cycle. Acetyl-coA is the typical input of this cycle which condenses with oxaloacetate to form citrate with the help of citrate synthase and eventually oxidized in 8 consecutive reactions. In step 2, the mitochondrial aconitase make isocitrate which is then converted by isocitrate dehydrogenase to α-ketoglutarate with the production of 1 NADH (step 3). α-ketoglutarate dehydrogenase further catalyzes the conversion of α-ketoglutarate to succinyl Co-A and a second NADH in step 4. The step 5 produce succinate catalyzed by succinyl-CoA synthetase as well as 1 GTP is produced from 1 GDP. The conversion of succinate to fumarate by succinate dehydrogenase produce 1 $FADH_2$ in the process during step 6. Fumarase converts fumarate to malate and in the final step, malate dehydrogenase transform malate to oxaloacetate with the production of another NADH. Oxaloacetate further starts the cycle. The enzymes are shown in blue circles, the intermediate metabolites in black and the GTP, H_2O, and the electron donors, NADH and $FADH_2$ produced are marked as green. [35, 36]. Figure based on [37]

However, pyruvate is not the only source of acetyl-CoA, it can be generated from β-oxidation of FAs or from ketogenic amino acids. For example, glutamine is the most abundant non-essential amino acid in the human body, which enters the TCA cycle in the form of α-ketoglutarate [32]. The cycle produces 3 NADH, 1 $FADH_2$, and 1 guanosine triphosphate (GTP) from 1 molecule of acetyl-CoA [35]. Since, one glucose molecule ends up in two pyruvates along with 2 NADH and 2 ATP after glycolysis; the net yield of this whole journey after complete mitochondrial oxidation is 10 NADH, 2 $FADH_2$, 2 GTP, and 6 CO_2. The key control points involved in the regulation of the TCA cycle are the allosteric enzymes isocitrate dehydrogenase and α-ketoglutarate dehydrogenase. The activity of these two enzymes are affected by the concentration of ATP and NADH. Isocitrate dehydrogenase is inhibited by NADH by directly displacing the NAD^+. α-ketoglutarate dehydrogenase is inhibited by the products of the reaction it catalyzes, succinyl CoA and NADH. In addition, both of these enzymes are inhibited by ATP; when the cell has a high level of ATP, the rate of the cycle is reduced.

1.2.4 Mitochondrial electron transport chain and oxidative phosphorylation

Oxidation/reduction reactions in the TCA cycle produce reduced electron carriers in the form of NADH and $FADH_2$, which serve as electron donors to the ETC, located in the IMM. The oxidation of these carriers is coupled to ATP generation by the OXPHOS system [38]. OXPHOS involves transport of electrons through the ETC to the final electron acceptor, molecular oxygen (O_2) and phosphorylation of ADP to form the universal high energy molecule, ATP. The ETC is made up of four protein complexes, commonly known as complex I-IV coupled to a phosphorylating complex, the ATP synthase (complex V) (see Figure 1.5). NADH coenzyme Q reductase (complex I) receives electrons from NADH and transfers to coenzyme Q (Co-Q, reduced form of ubiquinone). Succinate dehydrogenase (complex II, a part of TCA cycle) also transfers electrons to Co-Q that is received from $FADH_2$. Electrons are shuttled from Co-Q via cytochrome C oxidoreductase (complex III) to cytochrome C (Cyt C). Cyt C is located at the cytosolic side of the respiratory chain and is responsible for further transport of electron to cytochrome C oxidase (complex IV). Cytochrome C oxidase is the last enzyme of the ETC and transfers a pair of electrons to molecular O_2 where it is reduced to form H_2O [39].

Complex I, III and IV function as proton pumps. For every pair of electrons transported, complex I and III each extrudes two pairs of protons; while complex IV pump out one pair of

protons from the mitochondrial matrix into intermembrane space. As protons accumulate, they establish an electrochemical proton gradient (membrane potential), representing a protonmotive force (PMF). The potential energy stored in the PMF is then harvested by the ATP synthase, which drives the energetically favorable flux of protons back into the matrix. The energy released in this process enables conversion of ADP to ATP [40, 41]. The net production of ATP is around 32 molecules from the catabolism of one glucose molecule [38], however the overall yield might be influenced by the mitochondrial membrane integrity or effects of uncoupling proteins.

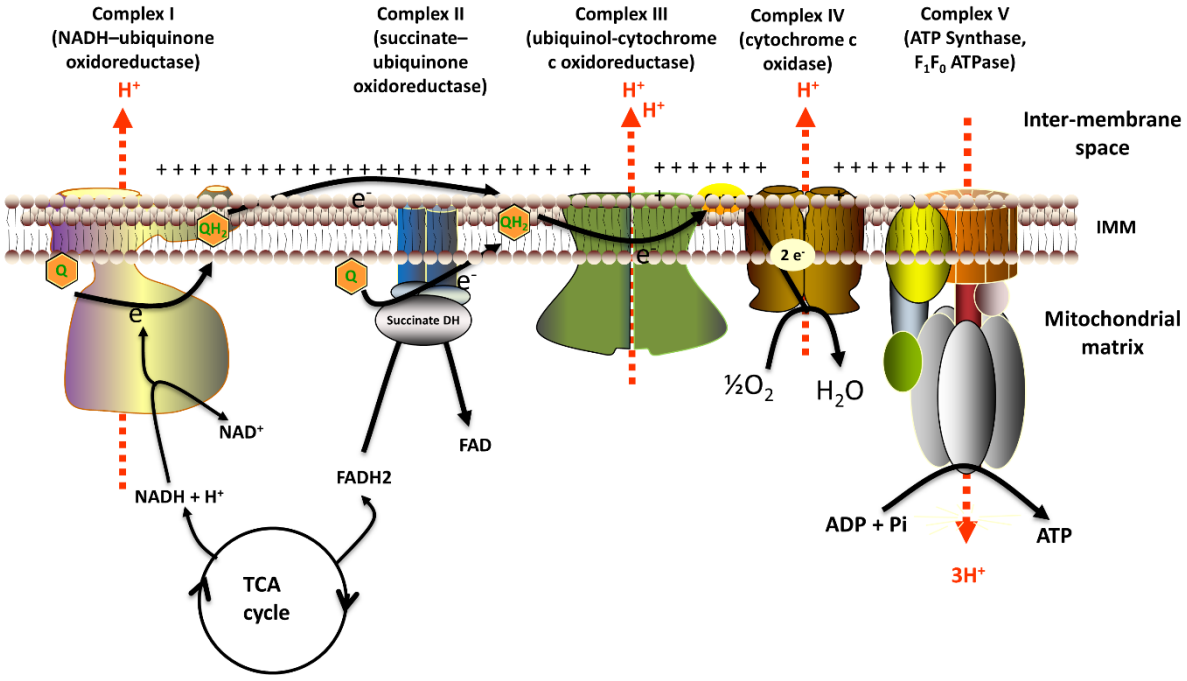

Figure 1.5 Bioenergetics of the ETC and OXPHOS system. Electrons from NADH and $FADH_2$ are shuttled to complex I and II, and are transported throughout the ETC. Transfer of electrons pump out protons from the matrix into the IMS through complex I, III and IV, thereby creating a proton gradient. This gradient drives the ATP synthase to flux protons back into the matrix to produce ATP. Figure based on [42]

1.2.5 Fatty acid transport and oxidation

Fatty acids are energy rich molecules and yield the most ATP as energy per gram basis. Therefore, FAs are the foremost storage form of fuel in animal cells and are involved in the formation of biomolecules (e.g triglycerides, phospholipids, ketone bodies) and in signaling pathways. They regulate countless metabolic pathways by acting as ligand for peroxisome proliferator nuclear receptors (PPARs) [43].

Due to the hydrophobic nature of FAs, they are co-transported as bound to albumin in the circulation [44]. Upon release by lipoprotein lipases, FA primarily enter the cell with the help of specific transporters on the cell surface, such as cluster of differentiation 36 (CD36) [45]. Once inside the cell, the FAs are activated by long chain acyl-CoA synthetases (ACS) which conjugates a coenzyme A (CoA) to the FA forming acyl-CoA.

Catabolism of FAs to produce energy generally takes place in mitochondrial matrix via β -oxidation. Hence, the enzyme carnitine palmitoyltransferase-1 (CPT1), present in the inner surface of the OMM, converts acyl-CoA to acyl-carnitine. CPT1 is the rate-limiting enzyme and is inhibited by malonyl-CoA, a precursor of FA biosynthesis, thus provides a major site of regulation of mitochondrial FA import [46, 47]. The fatty acyl-carnitine moiety is then transported across the IMM by the transport protein carnitine translocase (CAT). Inside the matrix, acyl-carnitine is converted back to acyl-CoA, by CPT2, and is then ready to be utilized in the β-oxidation pathway [48].

β-oxidation is a process in which an acyl-CoA ester undergoes a repetitive 4-steps reaction cycle involving dehydrogenation, hydration, another dehydrogenation and thiolytic cleavage [49]. The acyl-CoA is shortened by two carbons in each oxidation cycle, and ultimately results in release of NADH, $FADH_2$, and acetyl-CoA [50]. The acetyl-CoA produced then enters TCA cycle and are used by the ETC to produce energy. Thus, complete oxidation of a 16-carbon palmitic acid (PA) will yield eight molecules of NADH, $FADH_2$, and acetyl-CoA each; giving rise to up to 120 ATP molecules, through complementary actions by the TCA cycle and OXPHOS system.

1.3 Cellular stress and metabolic adaptation to stress

Cells, either growing *in vivo* or *in vitro* are exposed to various external and internal stimuli which may induce stress. Some of the conditions that may result in cellular energy stress are mutation, metabolic disease, temperature changes endurance exercise, ROS damage, caloric restriction, excessive nutrient uptake, hypoxia etc. Such stressors can damage intracellular

components including DNA, RNA, protein and lipids. At the same time, stressors can trigger different rescue responses in the cell depending on the level of insult and duration of the stress. They activate a variety of defense and pro survival mechanisms to re-establish the homeostasis by 1. Inducing repair mechanism, 2. Mechanisms that result in temporary metabolic adaptation, 3. Inducing autophagy, or 4. Triggering cell death. The rescue capacity of a cell depends on the flexibility of involved pathways and is a major determinant of its fate [51, 52].

1.3.1 Metabolic flexibility

Metabolic flexibility is the ability of an organism to respond or adapt to conditional changes in metabolic energy supply and demand. This concept has been promulgated primarily in the context of mitochondria to select fuel between glucose and FAs. Several tissues such as the liver, adipose tissue, skeletal muscle and heart systematically govern metabolic flexibility via sensing, uptake, transport, expenditure and storage of nutrients by maintaining communication at the endocrine level. Exercise is another physiological condition that can alter fuel consumption to meet increased energy demand depending on the duration and intensity of the exercise [4, 53]. A study on fuel selection of skeletal muscle in lean and obese individuals revealed a remarkable example of metabolic flexibility [54]. After overnight fasting, the skeletal muscles of lean individuals increased FA uptake and oxidation, however, insulin-stimulated conditions showed suppressed FA condition and increased glucose uptake, oxidation and storage displaying remarkable metabolic flexibility. Insulin-resistant obese patients did not show increased FA oxidation after fasting or reduced FA oxidation upon insulin infusion [55], reflecting metabolic inflexibility. Such inability to alter fuel oxidation in response to changes in nutrient availability has been implicated in insulin resistance, type 2 diabetes, mitochondrial dysfunction and obesity related complications [4].

1.3.2 Molecular mechanisms of metabolic adaptations and stress responses

Molecular mechanisms facilitating metabolic adaptations to energy stress include the activation of the energy sensor, AMP-activated kinase (AMPK). As a stress sensor, AMPK turns on a metabolic shift towards mitochondrial oxidation that generate ATP, while inhibiting anabolic pathways involving biosynthesis and proliferation that consume ATP [56]. Glucose-expending therapies such as exercise and caloric restriction also induce an energy challenge that lead to the activation AMPK. Other upstream activators of AMPK are Liver Kinase B1 (LKB1) and Ca^{2+}/calmodulin-activated protein kinase (CAMKK) that trigger AMPK activation in response

to increased intracellular Ca^{2+} levels [57]. AMPK also induce autophagy in response to stress through a 'dual-safe' mechanism that involves inactivation and direct phosphorylation of mTORC1 and ULK1 protein kinase respectively [58].

Response to oxidative stress (e.g reactive oxygen species or ROS damage) activates enzymatic antioxidant defense via ROS-metabolizing enzymes including glutathione peroxidase, catalase, and superoxide dismutase (SOD). Some exogenous antioxidants such as Vitamin A, C, and E found in foods also act as free-radical scavengers. Other responses such as heat shock response or unfolded protein response (UPR) mediate an increased chaperon protein activity that improves the protein folding capacity of the cell, thus counteract the stress and promote survival [51, 59].

However, if the level of stress is very severe or prolonged and the condition goes unresolved, such an unhealthy energy balance may have systemic effects on energy storage and utilization, and this can lead to the potential harmful secondary effects. Some examples of cellular energy failure include decreased membrane potential of mitochondria, intracellular accumulation of Ca^{2+} or Na^{+}, increased lactate concentration, excess ROS production and aerobic glycolysis [51, 60] . Aerobic glycolysis, which primarily has been characterized in cancer cells (Warburg effect), is a condition in which glucose is converted to lactate with increased rate of glycolysis even in the presence of oxygen [61]. The activation of oncogenic serine/threonine kinase, Akt supports aerobic glycolysis by promoting glucose dependency of the cells. Akt has also a role in preventing autophagy by interacting with the mammalian target of rapamycin (mTOR) [62]. Akt activation is an important mediator of insulin induced signaling and can also enhance glycolytic flux by increasing GLUT1 expression [63]. The increased Akt activity has been reported in many human cancers. Therefore, the Akt/mTOR/AMPK network is one of the major signaling pathways that is associated with cellular energy stress and metabolic flexibility [62, 64].

Besides, excess ROS production contribute to early aging and causes DNA mutation that promote tumorigenesis. Moreover, accumulation of peroxidized polyunsaturated FAs, ROS, mutation damaged protein or altered glycosylation etc. lead to the aggregation of unfolded/misfolded protein in brain cells, which is a hallmark of many neurodegenerative diseases [52].

1.4 Biological and pharmacological modulators of cellular energy metabolism

Modulation of cell metabolism may occur through interactions of enzymes and other proteins, co-factors and molecular energy sensors, and can to some extent be targeted by pharmacological agents (e.g DCA, rotenone) [65]. Regulators of energy metabolism control vital parts or components of metabolic pathways and function as nodes in rewiring of metabolism. In fact, the concept of modulation is to improve or optimize energy metabolism either by shifting metabolism towards a preferred substrate or by improving mitochondrial coupling or stimulating glucose oxidation. The following section lists some of the key modulators of energy metabolism and the mechanisms of their actions.

1.4.1 Pyruvate dehydrogenase (PDH) and Pyruvate dehydrogenase kinases (PDKs)

The PDH complex is a multi-enzyme complex in mitochondria that catalyzes the irreversible oxidative decarboxylation of pyruvate. It is a mitochondrial enzyme that connects glycolysis to the TCA cycle, as it controls the conversion of pyruvate, Coenzyme A (CoA) and NAD^+ into acetyl-CoA, NADH and CO_2. The acetyl-CoA produced, along with the acetyl-CoA coming from FA oxidation, amino acids and ketone bodies are utilized in the TCA cycle to produce fuel for mitochondrial respiration [54, 66].

PDH complex has three different catalytic components: E1, pyruvate dehydrogenase that catalyzes the decarboxylation of pyruvate; E2, transfers the acetyl groups to CoA to form acetyl-CoA; E3, catalyzes the oxidation of lipoyl moieties on E2 with concomitant reduction of NAD^+ [67].

PDH is more active when the cells are healthy and in well-fed state. However, suppression of PDH activity is crucial during nutrient depletion when glucose is not available. During fasting or insulin resistant state, the PDH activity is tightly controlled by the upregulation of pyruvate dehydrogenase kinases (PDKs) that phosphorylate specific serine residues in the alpha-subunit of the E1 enzyme, resulting in inhibition of PDH complex (see Figure 1.6) [68]. Therefore, PDKs are important modulators of metabolism, acting as a gatekeeper enzyme of glucose oxidation [69]. Four mammalian isoforms of PDK (1 to 4) have been identified so far and they have tissue specific expression and different phosphorylation target sites. PDK1 is ubiquitously expressed and is the principle enzyme that regulate hepatic PDH [70]. PDK2 and PDK4 are widely distributed in tissues like kidney, heart, and liver in humans and rodents. PDK4 is also highly expressed in tissues that have high glucose and fatty acid oxidation rate such as skeletal muscle [54, 71]. PDK3 is the kinase regulating PDH activity in kidney, brain and testes [70,

72]. PDH inhibition can be counteracted by reciprocal dephosphorylation of E1α subunit by two pyruvate dehydrogenase phosphatases (PDP1 and PDP2). PDKs are downregulated in the presence of insulin, Ca^{2+} and inhibitors and their activity can be transcriptionally regulated via signaling cues such as PPAR-α, AMPK and hypoxia inducible factor 1 (HIF1) [73].

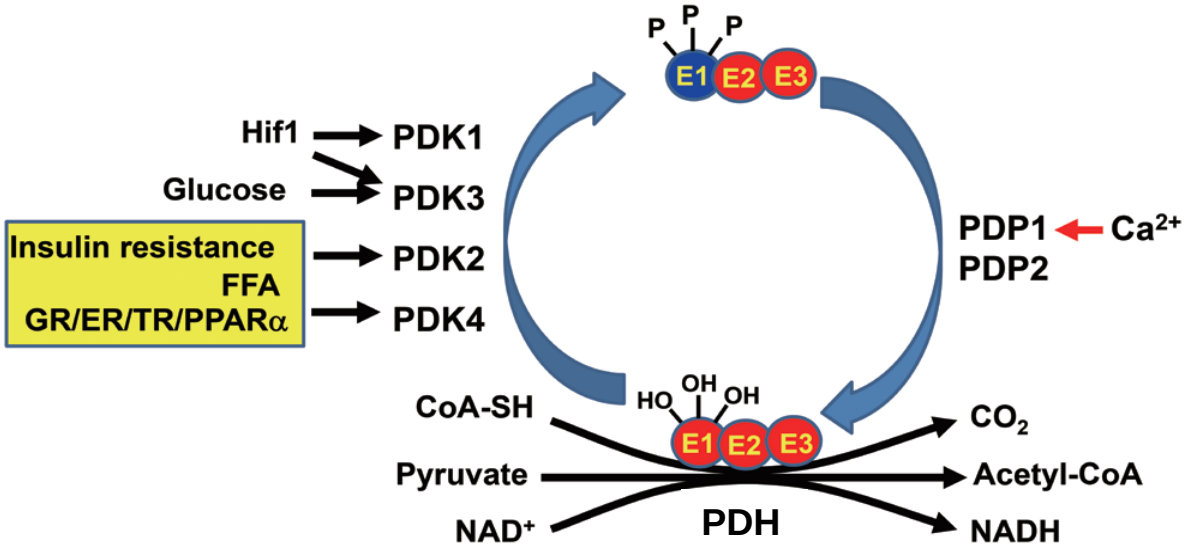

Figure 1.6 Regulation of pyruvate dehydrogenase complex (PDH) and physiological factors involved in regulating pyruvate dehydrogenase kinase (PDK1-4) activity.
The PDH complex consists of three components: pyruvate dehydrogenase (E1), dihydrolipoyl acetyltransferase (E2), and dihydrolipoyl dehydrogenase (E3). Pyruvate dehydrogenase (E1) catalyzes decarboxylation of pyruvate into acetyl-coA. Phosphorylation of E1 by PDK1-4 inactivates E1, and subsequently the whole complex. This inactivation is reversed via dephosphorylation of E1 by pyruvate dehydrogenase phosphatase (PDP). Adapted from [68].

1.4.2 Pharmacological inhibitors of PDK

An elevated expression of PDK has been reported in many cancers that cause a shift in the glucose metabolism towards glycolysis over OXPHOS, a phenomenon called 'Warburg effect', described by Otto Warburg in 1924 [69]. This term is synonymously exchanged with aerobic glycolysis (described in section). Although this process is less energy efficient, glycolysis is a rapid process that provide cancer cells potential advantages over OXPHOS to cope with environmental constraints, including hypoxia [74]. Therefore, targeting PDK can provide potential therapeutic benefits for developing new cancer therapies [69, 75]. The known PDK inhibitors act by binding to one of the four binding sites: 1. A pyruvate binding site, 2. An allosteric site, 3. A nucleotide binding site, and 4. A lipoamide binding site. The naturally occurring PDK inhibitors are pyruvate, NAD^+, and CoA which activate PDH by inhibiting PDK [71]. Dichloroacetate (DCA) is a small (150 Da) molecule and is a well-established

inhibitor of PDK. DCA can penetrate membranes and is rapidly absorbed, it can also readily cross the blood brain barrier. PDK isoforms have a conserved pocket, mainly pyruvate-binding site to which DCA binds. PDK2 is the most sensitive to DCA, PDK1 and PDK4 are equally sensitive whereas PDK3 is the least sensitive [76]. To inhibit PDK, DCA concentration ranges between 10-250 μM in physiological level, when taken orally. But in contrary to the physiological point of view, *in vitro* studies involving immortal cell lines require very high concentration of DCA (may be up to 100 mM) [66]. Other known PDK inhibitors include PS-10, Betulinic acid (BA), Phenylbutyrate and some derivatives of DCA such as Mito-DCA and Mitaplatin [71].

1.4.3 Uncoupling proteins

Uncoupling proteins (UCPs) are important modulator of metabolism as they uncouple respiration from ATP synthesis by mediating a regulated discharge of proton gradient into the matrix. Thus, the typical result will be dissipation of the mitochondrial membrane potential and reduced ATP yield [77]. UCPs are the transporters of IMM and have functions in thermogenesis, reduction of ROS production or maintaining redox balance. There are five UCP homologs in mammal; among them, UCP1-UCP3 are related, while UCP4 and UCP5/BMCP1 have more distant relationship. Each of them has a molecular mass of 31-34 kDa and the functional carrier protein is a homodimer [78]. UCP1 is predominantly expressed in brown adipose tissue (BAT) where it can mediate cold-induced thermogenesis. UCP2 is expressed in different tissues and is involved in diet-induced thermogenesis as well as regulation of glucose homeostasis. UCP3 is mainly present in skeletal muscle, but also found in BAT and heart tissue. UCP3 is thought to have a role in mitochondrial fatty acid oxidation and regulating ROS-induced oxidative damage [79, 80].

1.4.4 Respiratory inhibitors and uncouplers

Inhibitors of ETC are substances that bind to specific components of the ETC and block their ability to reversibly change from an oxidized state to reduced state. Inhibition of mitochondrial ETC lead to autophagy-induced cell death through the generation of ROS [81]. Hence, in terms of oncogenic signaling, inhibition of mitochondrial respiration could provide therapeutic benefit for certain targeted therapies. Further, experimental and clinical procedures involving mitochondrial inhibitors and manipulators might give insights where the potential disturbance is located [82]. For experimental purposes, amytal, rotenone, antimycin A, sodium azide,

myxothiazol and cyanides are the most common inhibitors of ETC, and carbonyl cyanide m-chlorophenyl hydrazone (CCCP), p-trifluoromethoxyphenyl hydrazone (FCCP), phenol SF 6847, and hydrophobic salicylanilide S-13 are used as uncouplers (See Figure 1.7) [83, 84]. Oligomycin is the inhibitor of ATP synthase that prevents protons from passing back into the mitochondria required for ATP production by blocking its proton channel (f_0 subunit) [85]. CCCP or FCCP uncouple mitochondrial respiration from ATP synthesis by permitting transport of protons across the membrane leading to the depolarization of membrane potential that results in increased oxygen consumption but no ATP production. Rotenone and antimycin A are the inhibitors of complex I and III respectively, that block passage of electrons through these complexes. So, the addition of both these inhibitors results in no further electron transfer through the ETC [83, 86]. Azides and cyanides act on respiratory chain by inhibiting the heme groups of cytochrome oxidase (Complex IV) [84].

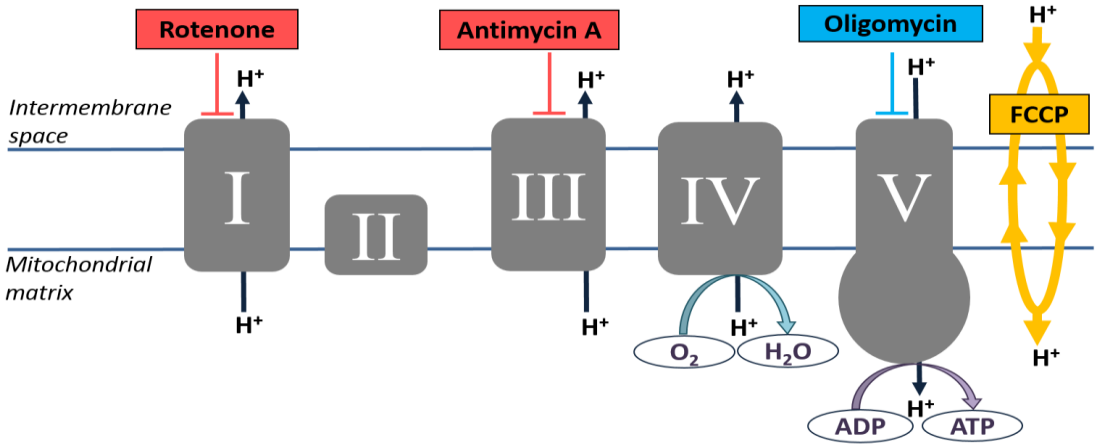

Figure 1.7 Modulators of the ETC. Rotenone inhibits ETC-Complex I, antimycin A inhibits ETC Complex III, oligomycin targets the ATP synthase (Complex V) and FCCP targets the IMM to enable proton flux across the membrane by disrupting the membrane potential. Adapted from [87]

1.5 Metabolism and disease

Occurrence of metabolic disorders is often associated with loss of mitochondrial function. Mitochondrial dysfunction has been implicated in a number of human diseases including cancer, cardiovascular diseases, epilepsy, neurodegenerative diseases, aging etc. Dysfunctional

mitochondria also found to have important role in the pathogenesis of chronic metabolic diseases characterized by insulin resistance in obesity and type-2 diabetes. These disorders arise from either dysfunction in the mitochondrial complexes or mutation in the mtDNA or nuclear DNA [88-90]. Defects in transferring of electrons out of the membrane cause electron accumulation in the ETC complex that allows binding of electrons to free oxygen to produce ROS, which contributes in pathologies like cancer, degenerative diseases and aging. Besides, excess energy intake may reduce lipid oxidation and increase ectopic lipid storage in the cells that lead to insulin resistance [90].

1.5.1 PDH dysregulation in diseases

PDH dysregulation is involved in severe disease conditions including cancer, neurological dysfunction, lactic acidosis, diabetes or other insulin-resistant states, growth retardation and even early death**.** PDH complex deficiency is itself a type of metabolic disease where the body lack the ability to break down foods to be used for producing energy and symptoms include lethargy, poor feeding and fast breathing [71, 91]. Fluge Ø et al suggested PDH impairment in Myalgic encephalopathy/chronic fatigue syndrome (ME/CFS) patients after analysis of blood serum from 200 ME/CFS patients and 102 healthy individuals [73]. Furthermore, PDH deficiency has been demonstrated in metabolic disorders that are caused by mutations, for instance in cancer. Stable overexpression of HIF1α and oncogenic Myc play an important role in the upregulation of glucose transporter GLUT1, all PDKs and glycolysis enzymes favoring the Warburg effect [71]. Interestingly, at least one of the PDK isoforms are found to be highly expressed with excess production of lactate in the cells with pathological conditions due to PDH impairment. For instance, involvement of increased PDK2 mRNA in glioblastoma [54]. Another study of hyperthyroidism involving rat heart emphasized increased *ex vivo* activity of PDK while PDH-mediated glucose oxidation was inhibited [92]. In primary biliary cirrhosis, a condition of autoimmune disease, PDH complex is the target for antimitochondrial autoantibodies, leading to inflammation and tissue destruction [73].

1.5.2 Metabolic rewiring in cancer

Metabolic rewiring, also known as metabolic reprogramming or remodeling is common in many pathological and physiological processes including stem cell formation, epithelial-to-mesenchymal transition (EMT), cancer progression and immune responses [93]. Rewiring of metabolism is a common event in cancer cells to promote survival, growth, proliferation and

long-term maintenance [94]. Vander Heiden et al. suggested that oncogenic mutations evade the need of stimuli for nutrient uptake and result in increased uptake of nutrients, particularly glucose [95]. This can be exemplified by the enhanced GLUT expression in several cancers due to the activation of certain oncogenes such as *ras*, *c-myc*, *src*, and transcription factors like HIF-1α [96]. Therefore, cancer cells preferentially increase the rate of aerobic glycolysis over OXPHOS, and this kind of metabolic rewiring has currently been recognized as a hallmark of cancer [74]. It also promotes glycolysis-branched pentose phosphate pathway (PPP) to produce nicotinamide adenine dinucleotide phosphate (NADPH), required for the impairment of ROS; thereby sustaining tumor cell survival and signaling [74, 97].

Deregulation of few metabolic enzymes has been reported in some cancers. Repeated upregulation of Hexokianse II has been implicated in increased glycolytic rate and inhibition of apoptosis [98, 99]. Loss of function mutations in two tumor suppressors, succinate dehydrogenase (SDH) and fumarate hydratase (FH), the TCA cycle enzymes lead to tumorigenesis through the activation of HIF signaling [100].

At the early stage of cancer progression, cells degrade the ECM by increasing motility and invasion abilities. These processes are energetically costly and are supported by the remodeling of cell–cell and cell-ECM interactions, activation of EMT, and rearrangements of focal adhesions [74, 101]. Similarly, immune cells also modify their metabolic requirements to activate their host-defense mechanisms against stress. For example, lymphoid cells undergo a metabolic switch from OXPHOS-dependent catabolic state to a glycolysis-dependent anabolic metabolism during the transition from a naïve/quiescent state to fully active effector immune cells [97].

1.6 Aim of the study

Our major aim was to characterize changes in key metabolic and physiological functions in cultured cells upon experimental manipulation of PDH activity. Our strategy was to mimic relevant metabolic defects and changes in glucose supply in cultured cell models to investigate which type of signals or features the cell displays under given metabolic defects.

The study particularly focused on manipulating PDH function by inducing upregulation of PDKs in cultured cells. Besides, stress-inducing metabolic environment (glucose restriction), direct intervention of metabolic pathways (addition of enzymatic inhibitors, metabolic stressors, mitochondrial uncoupling) was also applied to investigate effects on cell proliferation and metabolism. The specific aims are listed below:

A. To characterize proliferation and metabolism in cell lines overexpressing PDK1, PDK2, PDK3, and PDK4.
B. To characterize mechanisms of metabolic adaptation in PDK overexpressing cells under different conditions of energy stress[1]
C. To determine if overexpression of PDKs affect cellular glucose dependency.

[1] Part of the data generated from this study has been included in a manuscript under review for publication in Mitochondrion (Pettersen et al, revised version).

2 Materials and methods

2.1 Cell line

The cell line that was used in this study was a human immortalized triple negative breast cancer cell line, the MDA-MB-231. The cell line had previously been transduced to overexpress the four isoforms of PDK by Lena Hansen in Professor Karl Johan Tronstad's laboratory. Thus, there were four different cell lines overexpressing PDK1, PDK2, PDK3, and PDK4, as confirmed by qPCR. I participated in the transduction procedure to establish my own cells but was not successful to transduce all four PDK isoforms, therefore, I continued my project with the cell lines made by Lena Hansen. The parental line (Wild type) was used as a control. They are referred to as 231 WT, 231 PDK1, 231 PDK2, 231 PDK3, and 231 PDK4 throughout the study.

2.1.1 General maintenance and culture conditions

The cells were cultured in high glucose Dulbecco's modified eagle's medium; DMEM (Cat no. D5671, Sigma) supplemented with 10% hi FBS (Heat inactivated Fetal Bovine Serum, Cat no. A15-101, PAA), 1% Pen-Strep (10,000 units penicillin + 10 mg streptomycin per ml, Cat no. P0781, Sigma) and 0.5mM L-glutamine (Cat no. G7513, Sigma), thereby making complete DMEM (cDMEM). Media with different concentration of glucose, high (25 mM), moderate (5 mM), and low (1 mM) were prepared from 2.5 M glucose stock (Sigma-Aldrich) in glucose free 1X Gibco™ DMEM (Cat no. 11966-025, ThermoFisher scientific) supplemented with 10% hi FBS and 1% Pen-Strep, as required by different experiments.

The cells were routinely handled in a clean lamina flow hood to maintain sterility and checked under a Nikon ECLIPSE TS100 microscope to monitor confluency. They were cultured in 75 cm^2 T75 flasks to 80-90% confluence before splitting to new flask, or to 10 cm dishes for RNA and protein extraction. All the cultures were maintained at a Hera cell 150 (Heraeus) incubator with a humidified atmosphere of 5% CO_2 in air at 37 °C.

2.1.1 Thawing of cells

Complete culture medium was preheated in a 37°C water bath before the cryo-preserved cells (see details in section 2.1.5) were taken out from the nitrogen-tank. The vials were wiped with 70% alcohol and transferred to the laminar air hood. For thawing, 500 µl preheated cDMEM was added to each vial and mixed gently by pipetting. T75 culture flasks were prepared with

10 ml of preheated cDMEM and labelled before the cells were transferred from the corresponding cryo vial. The medium was replaced with fresh medium the next day. The cells were kept growing in the Hera cell 150 (Heraeus) incubator until they reach 80% confluency.

2.1.2 Propagation of cells

The cells were routinely passaged every 2-3 days when a culture reached 80-90% confluence. cDMEM, 1X PBS (Phosphate buffered saline, prepared from tablets Cat no. P4417, Sigma dissolved in MilliQ-H_2O) and Trypsin-EDTA solution (0.25%, Cat no. T4049, Sigma) were preheated to 37°C for 30 minutes in a water bath. A vacuum pump was used to remove the old medium from the culture flasks and the cells were gently washed with PBS. 3 ml trypsin-EDTA was added to each flask and incubated for 2-3 minutes to allow trypsin to break down the proteins that enable the cells to adhere to the culture flasks. The cells were observed under a light microscope to see if they were floating or not, otherwise the side of the flasks were gently tapped for complete detachment of the cells. 5 ml of warm cDMEM was added to neutralize trypsin activity and the cell suspensions were transferred to 15 ml tubes. The tubes were centrifuged at 1200 rpm for 5 minutes and the supernatants were carefully removed. The cell pellets were resuspended in fresh media and split 1:4 into new T75 flasks containing 10 ml of fresh cDMEM. The flasks were put back into the incubator.

2.1.3 Cell counting and determination of viability

Counting of the cells was important to prepare a definite number of cells depending on the experiment. A hemacytometer from Reichert Bright-Line (#1490) was used to count the cells when the cell concentration was low. But mostly, a Countess automated cell counter from Invitrogen was used to count the cells. This instrument makes use of a trypan blue exclusion test which is based on the principle that viable cells exclude this dye due to intact cell membrane whereas dead cells do not [102]. The counting procedure involves mixing 10 µl of cell suspension with 10 µl of trypan blue before transferring 10 µl of this mixture to a Countess cell counting chamber slide. The slide is then inserted into the allotted slot on the front of the machine. Upon pressing the start button, the counting starts and data including total, live, and dead cell count, and percent viability appears on the screen. The counting usually takes less than a minute.

2.1.4 Freezing of cells

Long term storage requires freezing the cells and preserving them in liquid nitrogen. After reaching 70-90% confluency, they were washed with PBS, trypsinized (as previously described in 2.1.3) and centrifuged at 1200 rpm for 5 min. The pellets were resuspended in freezing medium (10%v/v DMSO (Cat no. D5879, Sigma), 20%v/v hi FBS and 70%v/v cDMEM and kept on ice. 1.5 ml of each cell-freezing medium suspension was carefully aliquoted into small CryoTubeTM vials (#363401, Nunc). The vials were labeled with cell line names, passage number and date and then put into an isopropanol freezing box. The box was stored in -80°C overnight to have a smoother transition of temperature change by lowering the temperature 1°C/min. The day after, the cells were transferred from the -80°C freezer to a tank containing liquid nitrogen for long-term storage.

2.2 PDK overexpression in MDA-MB-231 cells by retroviral transduction

Four Moloney murine leukemia virus (MMLV) derived retrovirus gene expression vectors containing each of the four PDK cDNAs and one antibiotic resistance genes were transfected in HEK293 derived Phoenix-AMPHO (ATCC® CRL-3213™) packaging cells by Lipefectamin-200 transfection. The antibiotic resistance genes were puromycin, hygromycin, gentamycin, and blasticidin for PDK1, PDK2, PDK3, and PDK4 respectively. This transfection procedure was performed in Haukeland University Hospital, Bergen. Therefore, the experimental details are not explained for the transfection process.

The transduction of MDA-MB-231 cells by Phoenix packaging cells was done in Prof. Tronstad's laboratory. For retroviral infection, 1.5 $x10^6$ Phoenix cells were seeded in T75 flask containing cDMEM followed by 48 hours of incubation until they reach ~80% confluency. MDA-MB-231 cells were seeded in the same cDMEM in 6-well plates with a seeding density $1x10^5$. The next day, the virus-containing medium was collected from the Phoenix cells and filtered through a 30ml syringe with a 0.2µm Whatman filter. Protamine sulfate (5 µg/ml, #P-4020) was added, which aids the virus to penetrate the membranes. The media of the target cells were aspirated and replaced with virus-containing medium (1 ml/well) and left until the next day as reverse transcription and integration of the construct takes place between 24-36 h. The following day, the virus medium was replaced by cDMEM and the cells were transferred to 10 cm dishes, allowing the cells to proliferate. All equipment that came in contact with virus was treated with DUPONTTM Rely+on Virkon® for safe disposal.

2.2.1 Selection of the transformed cells

72 h post infection, the cells were ready for selection. The old media were replaced with new cDMEM and respective selection antibiotic was added in minimal concentration since too high concentration of the selective agent can inhibit growth of cells. Upon everyday monitoring, the concentrations were gradually increased to final concentrations of 1.5 µg/ml puromycin, 175 µg/ml hygromycin, 1 mg/ml gentamycin and 10 µg/ml blasticidin. The dead non-transformed cells were floating in the media that was replaced every 2/3 days with new media and selection antibiotics. Selection process continued to 15/16 days and finally very few transformed cells were left in the dishes. They were transferred to new dishes with fresh media and kept growing until confluent. Re-selection of the cells was done at different time points throughout the study period to make sure the overexpression still exists in the cell pool.

2.2.2 Preparation of cells for RNA and protein extraction

Equal number of 231 WT and PDK1-4 transduced cells were seeded in 10 cm petri dishes and were grown for 2/3 days to reach 80-90% confluency. After removing the media, the cells were washed with warm PBS. The PBS was aspirated, and the cells were gently scraped in 1 ml cold PBS and transferred to 1.5 ml Eppendorf tubes. The dishes were again washed with 0.5 ml cold PBS and the contents transferred to the same tubes. The tubes were centrifuged at 1200 rpm for 8 min. The supernatant was removed, and the cell pellets were preserved at -80°C freezer for RNA and protein extraction in future.

2.3 Analysis of PDK overexpression by RT-PCR

2.3.1 RNA isolation

Qiagen RNEasy Mini Kit was used to extract total RNA by following the manufacturer's protocol. Cell pellets were taken out from the -80°C freezer and loosen thoroughly by flicking on the tubes. 700 µl of buffer RLT was directly added to lyse the cells and mixed well by pipetting. Equal amounts (700 µl) of 70% ethanol was added to homogenized lysates and mixed well by pipetting. 700 µl of each sample was transferred to a RNeasy spin column placed in a 2 ml collection tube and was spun for 30 s at 8000 rpm. The flow-through was removed and the remaining 700 µl sample was added to the same column and the same procedure repeated. The RNA was bound to the spin column which was then washed with 350 µl buffer RW1 and spun for 30 s at 8000 rpm, the flow-through discarded. In a separate tube, 10 µl of DNase I

Enzyme was added with 70 µl of buffer RDD, mixed gently by inverting the tube and this DNase I incubation mix (80 µl) was directly added to the spin column membrane and left on the benchtop for 15 min. Again, the bound RNA was washed with 350 µl of buffer RW1 followed by spinning for 30 s at 8000 rpm. The next wash was done with 500 µl RPE buffer and centrifuged at 8,000 rpm for 2 min. After removing the flow-through, the samples were centrifuged for another 1 minute at maximum speed to remove any residual flow-through. Finally, the RNeasy spin column was placed in a new 1.5 ml collection tube, 30 µl of RNase free water was added and centrifuged for 15 s at 8000 rpm in two consecutive steps to elute the RNA. The concentration of the RNA yield was measured by NanoDrop ND-1000 Spectrophotometer based on the absorbance at 260 nm.

2.3.2 cDNA synthesis

The cDNA synthesis to be used for real-time quantification was performed by using High Capacity cDNA Reverse Transcription Kit in a 20 µl reaction. Firstly, 1000 ng RNA sample was prepared in 10µl (100 ng/µl) volume by diluting with milliQ water according to each sample concentration. Secondly, a master mix was prepared in 10 µl volume by combining 2 µl 10X RT buffer, 2 µl 10X RT random primers, 0.8 µl 25X dNTP Mix 100mM, 1 µl reverse transcriptase (all from applied biosystem, Cat No. 4368813) and 4.2 µl miliQ water. The 10 µl RNA sample and the 10 µl master mix were mixed well together to make 20 µl reaction volume (give rise to final concentration 50 ng RNA/µl) and the mixture was then transferred to a thermal cycler (MJ mini, Bio-Rad) and the loading program was set for 10 min at 25°C , 120 min at 37°C , 5min at 87°C and 4°C for holding. The cDNAs were ready to be used in qPCR and could be stored in -20°C.

2.3.3 Quantitative PCR (qPCR)

Probe based quantitative PCR (qPCR) was used in this study to detect mRNA expression of PDK isoforms in the PDK1-4 overexpressed cells. It is the most sensitive technique for detecting and quantifying even low-abundance mRNA in the target sample. This method measures florescence intensity emitted by the probe at each cycle of the reaction and the intensity gradually increases as the reaction advances. The software associated with the qPCR machine determines a threshold level to reduce background intensity. The point at which the reaction curve reaches the threshold level produces a Ct (cycle threshold) value which represent the number of cycles required for the fluorescent signal to cross the threshold [103].

A 10-fold (for PDK probes) and 100-fold (for reference probe) dilution series were made from the synthesized cDNA samples to run the qPCR reaction. To avoid error in mRNA quantification, eukaryotic 18s rRNA (4352930E, FAM™ Dye/MGB Probe, Thermo Fisher Scientific) was used as endogenous control in each of the samples. A 36 µl of reaction stock (+ 1.2% safety) was made containing 18 µl LightCycler 480 Probes reaction mix (04887301001, Roche, Basel, Germany), 1.8 µl TaqMan PDK1-4 probes (Hs 00176853_m1, Hs 00176865_m1, Hs 00178440_m1, Hs 01037712_m1, Applied biosystem), 1.8 µl reference probe (18s rRNA), 9 µl of RNase-free water and 5.4 µl of cDNA for each sample per well of 96-well plate. We wanted to look at the expression of other PDK mRNAs in each of the PDK overexpressing cells against each PDK probe. For this, a bulk quantity (183.6 µl, 6x sum of the aforementioned amounts) was first made in four 1.5 ml microtubes without the cDNAs. To achieve better control, equal volume of a reaction mix containing only 18s probe was prepared (PDK probe exclusion adjusted to water) in a separate tube. 30.6 µl of each reaction mix was manually pipetted in first six wells of a 96-well plate. Then 5.4 µl of 100-fold diluted cDNA samples were added in the wells containing 18s rRNA probe mix and 10-fold diluted cDNAs were added in the wells with 18s+PDK probe mix. Three technical replicates each of 10 µl were then manually transferred from the 96 well plate to a LightCycler® 480 Multiwell Plate 384 (Roche, Basel, Germany).

The 384 well plate was loaded to the LightCycler 480 system (Roche, Basel, Germany) to perform the qPCR following the program setting as listed in Table 2.1.

Table 2.1 Program setting of Light Cycle 480 system for qPCR

PCR Stages	**Temperature (ºC)**	**Time (mm:ss)**
Pre-incubation	95ºC	10:00 mins
Amplification (45 cycles)		
Denaturation	95ºC	00:10 secs
Primer annealing	60ºC	00:30 secs
Extension	72ºC	00:01 secs
Cooling	40ºC	00:30 secs

After completion of the cycles, Ct values generated curves representing the number of the cycles needed to detect the florescence from each sample by LightCycler® 480 system. The higher the Ct value, represents lower gene expression and vice versa [104]. The data was

collected from the LightCycler® 480 system, which could then be used to perform comparative analysis between expressed genes and housekeeping genes, as expressed as delta Ct value. The relative expression fold change of the expressed genes could be determined from the ct values. The analysis of Ct value uses the following equation [105]:

Ct = PCR cycle

ΔCt = Ct (gene test) – Ct (endogenous control)

$\Delta\Delta C_t$ = treated (Ct (gene test) – Ct (endogenous control)) – untreated (Ct (gene test) – Ct (endogenous control))

Relative quantification (RQ) = $2^{-\Delta\Delta Ct}$

Relative quantification is the fold change of the treated samples compared to the untreated. The RQ values for PDK gene expression were generated in Microsoft excel 2016 which were graphically presented and analyzed using Graphpad Prism 7.

2.4 Cell lysis and isolation of proteins

Cell pellets for protein isolation were prepared beforehand (see section 2.2.4). They were taken out from the -80 freezer and thawed on ice. The cells were lysed directly in the Eppendorf tubes by 300 µl of 1X RIPA lysis buffer supplemented with 1% Sodium Orthovanadate (SO) and 1% Phenylmethylsulfonyl fluoride (PMSF) obtained from Santa Cruz biotechnology, Cat. No. sc-24948, along with 1% phosphatase cocktail inhibitor (Sigma-Aldrich) and 1% protease cocktail inhibitor (PIC, Complete ULTRA Tablets, Mini, EDTA-free from Roche Diagnostics, Cat. No. 05892791001). The tubes were left on ice for 20 minutes after adding lysis buffer, then centrifuged at 4°C at 14000 rpm for 7 min. The DNA and cellular debris were pelleted, and the clear supernatant contained the total cell lysate. The supernatant was transferred to new microcentrifuge tubes which could be used immediately or stored at -80°C for later use.

2.4.1 Determination of protein concentration

Bicinchronic Acid (BCA) assay was performed to quantify total protein concentration in the lysate by using Pierce™ BCA Protein Assay Kit from ThermoFisher Scientific (#23225). The standard curve was generated from the serial dilution of the Bovine serum albumin (BSA) standard solution that comes with the kit, making eight ranging concentrations from 0 to 2000 µg/ml. 25µl of these nine samples were carefully aliquoted into a 96 well plate (Nunc™ MicroWell™ 96-Well Microplates) in duplicates. Similarly, 25µl of the lysed protein samples were aliquoted in the same plate in duplicates. The working solution of BCA was prepared by

mixing BCA reagent A and BCA reagent B in 50:1 ratio, and 200 µl of this working reagent was loaded into each well. They were mixed and incubated for 30 minutes at 37°C under light protection. The plate was then transferred to a plate reader (Thermo Scientific™ Multiskan™ FC Microplate Photometer) and the absorbance of the samples were measured at 562 nm. The absorbance values were inserted into an Excel sheet to obtain the standard curve that were used to determine the protein concentrations and to calculate the amount of proteins to be loaded into the SDS-PAGE.

2.4.2 Sodium Dodecyl Sulfate Poly Acrylamide Gel Electrophoresis (SDS-PAGE) and Western blot buffers

SDS-PAGE and Western blot of proteins require a few buffers to be repeatedly used throughout the process. Table 2.2 lists all the buffers that were used before proceeding to experimental details.

Table 2.2 List of buffers with composition and suppliers' information used for analysis of PDK proteins

Buffers	Stock solution	Preparation of working solution (1x/1L)	Suppliers
Loading buffer	XT Sample Buffer	Ready to use	Bio-Rad #1610791
Running buffer	10x Tris/Glycine/SDS	100 ml 10x stock + 900 Milli -Q H_2O gives 25 mM Tris, 192 mM Glycine & SDS 0.1%, pH 8.3	Bio-Rad #1610772
Transfer buffer	5x Tris/Glycine	200 ml 10x stock+ 200 ml 100% ethanol+ 600 ml Milli-Q H_2O gives 25 mM Tris, 192 mM Glycine, pH 8.3	Bio-Rad #1610734
Blocking buffer	Odyssey® Blocking Buffer in TBS containing 0.1% sodium azide	Ready to use	LI-COR Biosciences P/N: 927-50000
Washing buffer	Pierce™ 20X TBS	50 ml 20x stock+ 950 ml Milli-Q H_2O+ 1 ml Twin-20 gives 25 mM Tris, 0.15M NaCl, pH 7.2 to 7.5	ThermoFisher Scientific # 28358

2.4.3 SDS-PAGE

After the concentrations of the protein samples were determined, the volume of the samples was calculated based on the amount of the proteins (10 µg/well) we intended to have in each well. In order to obtain the 15 µl loading volume, the samples were mixed with equal volume of XT sample buffer and diluted with Milli-Q water so that the protein concentration is equal for every sample. The samples were then heated for 5 min at 95°C to denature the proteins. Two 4-20% gradient Mini-PROTEAN® TGX™ Protein Gels, 15-well #4561096 supplied by Bio-Rad were used for separating the proteins and were placed in the electrophoresis apparatus (Bio-Rad Mini Protean 3 cell system) filled with 1x running buffer. Precision Plus Protein™ Dual Color Standards (10–250 kD, #1610374, Bio-Rad) was used as molecular marker. 15 µl of the marker as well as the samples were loaded in pre-determined wells. The loading was done in a way such that each gel can produce two blots (after cutting in the middle), each containing all five protein samples (PDK1-4 + WT control) along with the marker. The electrophoresis first started at 90V for 15 min and then the voltage increased to 110V, the gels were run for next 1h until the blue tracking dyes end their journey out of the gels.

2.4.4 Transfer of proteins by blotting

The Polyvinylidene fluoride (PVDF) membrane (Trans-Blot® Turbo™ Mini-size LF PVDF) was used for blotting and was first activated in methanol for 30 sec, followed by washing with distilled water and then in 1x Transfer buffer. The transfer stacks were also prepared by soaking in transfer buffer and the gels were taken out of the gel cassettes. The transfer sandwich was made on the transfer cassette in the order: transfer stack in the bottom, the activated PVDF membrane, the gel, and another transfer stack on the top. Two transfer cassettes containing two sandwiches were then placed inside the Trans-Blot® Turbo™ Transfer System (Bio-Rad) for rapid transferring of the proteins within 7 min. After transfer was complete, the two membranes were rinsed with water and cut in the middle making four separate blots in order to be treated with four different antibodies.

2.4.5 Total protein staining and blocking

Total protein staining of the blots was done with REVERT™ Total Protein Stain kit (LI-COR Biosciences, # P/N: 926-11010) with methanol added. Following the manufacturer's protocol, the membranes were incubated with 5 ml REVERT Total Protein Stain solution for 5 min in gentle shaking. The staining solution was decanted thoroughly, and the membranes were

washed with REVERT wash solution twice for 30 secs. The membranes were then imaged at 680 nm IRshort channel (the staining solution has an excitation and emission spectrum near 700 nm) in Amersham Typhoon Gel and Blot Imaging Systems (GE healthcare). After imaging, the membranes were incubated in REVERT reversal solution for ~5 min, in gentle shaking until the stain was no longer visible. The membranes were rinsed briefly with water and proceeded immediately to blocking. For blocking, the membranes were placed in small western blot incubation boxes containing 5 ml of Odyssey Blocking Buffer (TBS) and continued to block with gentle shaking in room temperature for more than one hour. Blocking is done to prevent nonspecific binding of the detection antibodies in the membrane.

2.4.6 Preparation of the antibodies and immunoblotting

The primary and secondary antibodies that were used for immunoblotting were prepared according to the recipes listed in the Table 2.3 (see following page).

The four membranes were incubated with anti-PDK1, anti-PDK2, anti-PDK3, and anti-PDK4 primary antibodies overnight at 4°C on a roller mixer (Stuart). The next day, the primary antibody solutions were poured off (re-usable) and washed three times for 5 min with 1X TBS-T buffer. The anti-PDK1, anti-PDK2, and anti-PDK3 treated membranes were again incubated with diluted donkey anti-rabbit IgG secondary antibody, whereas anti-PDK4 treated membrane was incubated with goat anti-mouse IgG secondary antibody for around 2 h under light protection and gentle shaking. The membranes were again rinsed with 1X TBS-T for 5 min under vigorous shaking. The washing was repeated three additional times, the last step was only with 1X TBS to remove residual Twin-20. The membranes were then scanned at 800 nm IRlong channel in Amersham Typhoon Gel and Blot Imaging Systems (GE healthcare) to produce images of the desired protein bands. Amersham™ Imager 600 software was used to view and analyze the blot images.

Mouse anti-α-Tubulin and mouse anti-GAPDH were used as loading controls. The incubation procedure was same as PDK primary antibodies as described above, followed by incubation with anti-mouse secondary antibody and visualizing in the same platform.

Table 2.3 List of antibodies used in western blotting

Antibodies	Dilution & preparation in Odyssey Blocking Buffer (TBS)	Supplier
Anti-PDK1 antibody, 49 KDa, Rabbit monoclonal	1:1000, 5 ml blocking buffer+ 5 µl antibody+ 10 µl Twin-20 (0.2%)	Abcam #ab207450
Anti-PDK2 antibody, 46 KDa Rabbit polyclonal IgG	1:1000, 5 ml blocking buffer+ 5 µl antibody+ 10 µl Twin-20 (0.2%)	Invitrogen # PA5-35376
Anti-PDK3 antibody, 47 KDa Rabbit polyclonal IgG	1:1000, 5 ml blocking buffer+ 5 µl antibody+ 10 µl Twin-20 (0.2%)	Invitrogen # PA5-76332
Anti-PDK4 antibody, 46 KDa Mouse monoclonal	1:500, 5 ml blocking buffer+ 10µl antibody+ 10 µl Twin-20 (0.2%)	Abcam #ab110336
IRDye® 800CW Goat anti-Mouse IgG Secondary Antibody	1:20000, 5 ml blocking buffer+ 0.25 µl antibody+ 10 µl Twin-20 (0.2%)	LI-COR Bioscience P/N 926-32210
IRDye® 800CW Donkey anti-Rabbit IgG Secondary Antibody	1:20000, 5 ml blocking buffer+ 0.25 µl antibody+ 10 µl Twin-20 (0.2%)	LI-COR Bioscience P/N: 926-32213
Anti-α-Tubulin antibody, 50 KDa, Mouse monoclonal	1:1000, 5 ml blocking buffer+ 5 µl antibody+ 10 µl Twin-20 (0.2%)	Abcam #ab7291
Anti-GAPDH antibody, 35.8 KDa, Mouse monoclonal	1:1000, 5 ml blocking buffer+ 5 µl antibody+ 10 µl Twin-20 (0.2%)	Proteintech #60004-1

2.4.7 Quantification of blots

For quantification, ImageJ analysis software was used to calculate the relative amount of proteins in the samples compared to the loading control, α-Tubulin or GAPDH. The backgrounds were rejected, and the area intensity values of each protein band (both α-Tubulin/GAPDH and PDKs) were exported into an excel sheet. First, a normalization factor was calculated for the α-Tubulin /GAPDH by dividing the values of each protein sample with the WT control value. Second, these NF values were multiplied to the corresponding PDK protein values from the same blot.

2.5 Cell proliferation assays

2.5.1 xCELLigence system

A label-free RTCA (real-time cell analysis) platform called xCELLigence system from ACEA Biosciences was used in this study as one of the methods for assessing cell proliferation. The system utilizes an electronic readout called impedance analysis for real time monitoring of adherent cell proliferation and viability on tissue culture microplates. The RTCA instrument is composed of a RTCA impedance analyzer, electronic microwell plates and a RTCA station placed inside an incubator which is connected to a computer with RTCA software. For cellular proliferation assay, 16-well E-plate was used and the bottom of each well is 80% covered with gold-electrodes. As the cells proliferate, the more they attach and cover the electrodes, thus giving higher impedance. The impedance measurement is displayed as cell index (CI) (generated by RTCA software) value and provides quantitative information about the biological status of the cells, including cell number, viability, and morphology [106].

Proliferation study of PDK overexpressing cells started with one 1x T75 flask for each anfollowed normal propagation procedure as described in section 2.1.3. For each of the cell lines, 40,000 cells/ml were prepared in high glucose cDMEM (the cell number was previously been optimized in the laboratory). 100 µl of cDMEM was added in each well of an E-Plate VIEW 16 (ROCHE, Acea Biosciences Inc. San Diego, CA92121) and the program schedule was set for 100 h prior to measuring the background index of the plate inside the RTCA station. Thereafter, 100 µl of each cell suspension, that gives 4000 cells per well were added in the wells as triplicates and incubated for 30 min in room temperature. After incubation, the plate was inserted in the machine, connection was checked in the message and the experiment started. Therefore, the cells were maintained at optimal culture conditions (5% CO_2, 37^0 C) throughout the experiment up to 100 h.

The growth curves of the proliferating cells could be seen real-time in the monitor during the experiment. The measurements were paused every 24 h, the plate was taken out and 10 µl of media was collected from each of the wells to measure glucose consumption and lactate production rate. The impedance values were exported as excel file when the experiment was done.

2.5.2 Live-cell proliferation assay on IncuCyte platform

The IncuCyte™ ZOOM (Essen Bioscience) is a platform for continuous monitoring of cells that allows acquiring, analyzing and quantifying live cell images by using time-lapse imaging method. Viable cells are measured inside an incubator (37°C with 5% CO_2) in a physiologically relevant condition without being perturbed by the detection method. The system can house 6 micro-titer plates at a time and scan the plates on a customizable duty-cycle. There are three objectives with magnifications of 4x, 10x and 20x. To determine glucose-dependent proliferation of PDK-overexpressing cells 10x objective was used, as a general protocol.

The 231 WT and 231 PDK1-4 cells were seeded in a 96-well plate (Nunc, Cat. #167008), with seeding density 3000 cells/well in 100 µl of 1 mM, 5 mM, and 25 mM glucose medium. The plate was left to equilibrate at room temperature for 45 min. By this time, 1M of DCA working solution was made from 98% Sodium dichloroacetate (DCA, Lot# STBH0169, Sigma-Aldrich) in MQ H_2O. 5 µl DCA was added to the selected replicates of 25 mM glucose groups, leading to final DCA concentration 50 mM. The plate was left overnight at 37 °C, 5% CO_2 incubation. The next morning, the scanning schedule was created in the incuCyte ZOOM® Software such that images were captured under 10x magnification every 2 h for a total of 72 h. The cell plate was placed into the IncuCyte system and first allowed to warm to 37°C for 30 min prior to scanning. The algorithm in the ZOOM software generated growth curves from data points of every 2 h interval imaging acquired throughout the experiment. The data was exported in excel sheet and analyzed via Graphpad prism 7.

2.5.3 Resazurin Assay

To determine the viability of the PDK-overexpressing cells, the plates that came out from IncuCyte experiment were again undergone resazurin conversion assay. Resazurin (7-Hydroxy-3H-phenoxazin-3-one 10-oxide), the active ingredient of alamarBlue assay is a blue-colored non-fluorescent dye, that has been widely used as an indicator of cell viability in many cell proliferation and cytotoxicity assays [107]. It is non-toxic and can enter living cells, so when resazurin is present, viable cells reduce resazurin into a pink-colored fluorescent compound, resorufin. In a population of cells, this conversion of resazurin to resorufin is proportional to the number of viable, metabolically active cells which can be a way of assessing proliferation [108].

While running the IncuCyte experiment, the cells were continuously being incubated for 3 days, and soon after the IncuCyte was done, the resazurin assay started. The working

concentration of resazurin was made as 1:20 dilution (1X) in PBS from 2.5 mg/ml stock (Sigma, cat. no. R7017) and 20 µl 1X resazurin was added directly to each well and mixed by gentle shaking. The plate was light protected by wrapping in aluminum foil and placed in an incubator at 37°C in 5% CO_2. Following incubation for 3h, the fluorescence for metabolic reduction of resazurin to resorufin was measured by Tecan's Spark® multimode microplate reader platform at 550/600 nm (excitation/emission).

2.6 Monitoring mitochondrial respiration and glycolysis by Seahorse extracellular flux (XF) analyzer

The Seahorse extracellular flux (XF) Analyzer serves a powerful technique for measuring mitochondrial respiration and glycolysis simultaneously in the same cell. The technology uses fluorescent probes coated in a sensor cartridge sensitive to oxygen and protons to measure oxygen consumption rate (OCR) and extracellular acidification rate (ECAR) respectively, in the medium directly above adherent cells. ECAR is primarily the measurement of acidification of the surrounding media caused by lactate production from the conversion of pyruvate [29, 109].

Bioenergetic parameters of metabolic function can be revealed from measurement of OCR and ECAR values (Figure 2.1). To assess respiratory parameters, the first measurement is basal respiration which represents oxygen consumption needed to meet cellular energy demand under baseline conditions. The second measurement is ATP -linked respiration upon injection with ATP synthase inhibitor, oligomycin that causes a decrease in the OCR. The difference between basal and ATP-driven respiration is referred as leak respiration which represents any oxygen consumption that was not coupled ATP synthesis. The next parameter is to obtain maximum respiratory capacity after addition of a mitochondrial uncoupler (e.g CCCP, FCCP). This creates a cellular energy demand that stimulates the respiratory chain to act at its maximum capacity and as ETC increases, oxygen consumption goes up. Finally, non-mitochondrial respiration is measured after complete inhibition of ETC upon sequential addition of respiratory inhibitors (e.g rotenone and antimycin A) (Figure 2.1A) [73].

Similarly, to assess glycolytic key parameters, the first measurement is glucose-induced response in glycolysis under basal conditions. The second measurement is oligomycin-mediated inhibition of mitochondrial ATP production that allow the cells to depend more on glycolysis, thereby revealing maximum glycolytic capacity. The final step is inhibition of glycolysis through the addition of a glucose analogue, 2-deoxy-glucose (2-DG) with a

subsequent reduction in ECAR and the remaining ECAR is referred as non-glycolytic acidification (Figure 2.1B) [110].

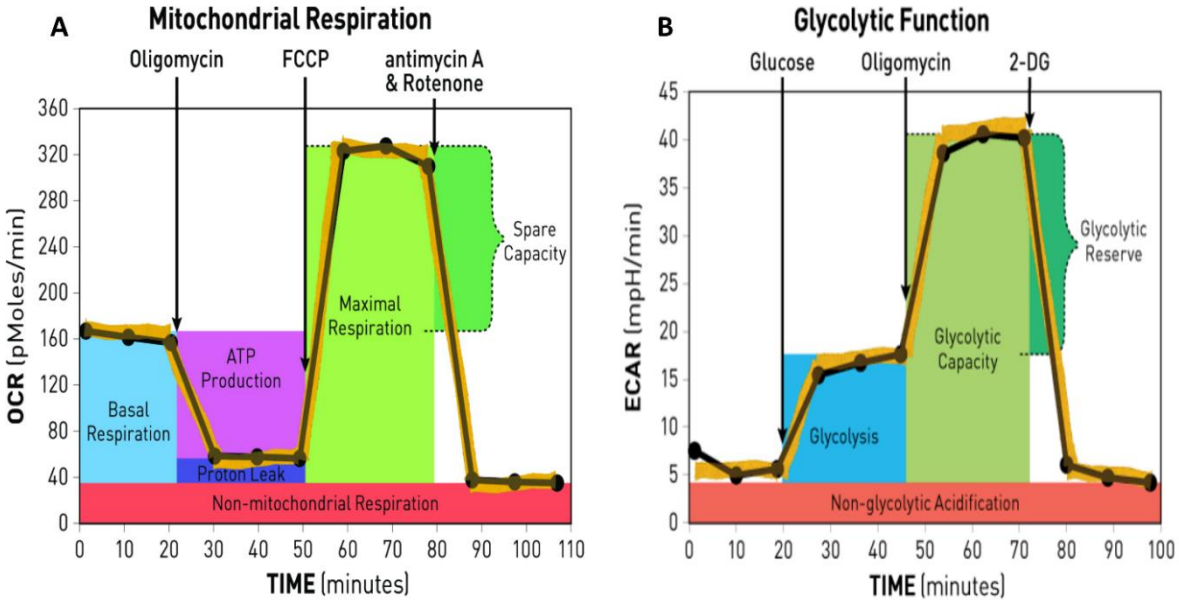

Figure 2.1 The fundamental parameters of mitochondrial and glycolytic functions.
(A) Key parameters of mitochondrial bioenergetics measured based on OCR values. The compounds, oligomycin, FCCP, and a mix of rotenone and antimycin A, are sequentially injected to measure basal respiration, ATP-linked respiration, maximal respiration, and non-mitochondrial respiration, respectively. Proton leak and spare respiratory capacity can be calculated from these parameters in terms of basal respiration **(B)** key parameters of glycolytic function measured based on ECAR. Sequential injections of glucose, oligomycin and 2-DG measure glycolysis, glycolytic capacity, and non-glycolytic acidification respectively from which glycolytic reserve can be calculated. Adapted from [87, 110].

2.6.1 Seeding of cells and preparing the sensor cartridge

The seahorse experiments for 231 PDK1-4 cells were performed according to standard protocols. The cell numbers and compound concentrations has previously been optimized in Prof Tronstad's laboratory. But the optimal CCCP concentration for newly transduced 231 PDK1-4 was not determined. As a result, 231 WT and 231 PDK4 cells were seeded 30000 cells/80µl/well in a 96-well assay plate (XFe96 Cell Culture Microplates, #101085-004) in two different glucose concentration (1 mM and 25 mM) to perform a CCCP titration assay. For the assessment of general metabolic function, all five cells were seeded in two assay plates with the same seeding density (30000 cells/well) under pre-treatment with three concentrations of

glucose (1 mM, 5 mM, and 25 mM). They were allowed to attach overnight at 37 °C with 5 % CO_2 in air.

To achieve consistent result, the sensor cartridges must be hydrated overnight. 200 µl of Seahorse XF Calibrant Solution was added to each well of a XFe96 utility plate (FluxPaks cat # 102416±100). The sensor cartridge was submerged in the calibrant solution and left overnight in a CO_2 free incubator (PrepStation, Agilent) at 37 °C to hydrate.

2.6.2 Mitochondrial and glycolysis stress tests

For metabolic study of PDK-overexpressing cells, the Seahorse XFe96 Analyzer (Agilent, Santa Clara, CA, US) was used to perform two standard assays, Agilent Seahorse XF Cell Mito Stress test and Glycolysis Stress test. These stress tests use sequential injection of certain compounds that have been mentioned in section 2.8.1. After overnight incubation in different glucose treatments, the growth media were replaced with unbuffered DMEM assay media (phenol red-free, D5030) supplemented with 10 mM D-glucose, 2 mM sodium pyruvate and 2 mM L-glutamine for the Mito stress test with the pH adjusted to 7.4. For glycolysis stress assay, media was replaced with glucose-free assay media supplemented only with 2mM glutamine at pH 7.4 The cell microplates with assay media were then incubated for at least 1 h in the PrepStation.

The inhibitors and modulators of the stress tests were adjusted to proper concentration in 3ml of respective unbuffered assay media. The final concentrations of the modulators in the well were 3 µM oligomycin, 1 µM CCCP, 1 µM rotenone and 1 µM antimycin A for Mito stress test and 10 mM glucose, 3 µM oligomycin and 100 mM 2-deoxyglucose were the final concentrations for glycolysis stress test (all obtained from Sigma-Aldrich). For CCCP titration assay, the CCCP concentrations ranged between 0.25 to 2 µM along with the 3 µM oligomycin ,1 µM rotenone and 1 µM antimycin A. 25 µl of each of these additives were pipetted into the injection ports A, B, C, D of the sensor cartridge in the order they are listed above so that seahorse instrument could sequentially inject the chemical modulators onto the cells to obtain metabolic flux profiles. The sensor cartridge with the utility plate was first inserted into the machine for calibration and then the utility plate was replaced with the cell culture plate. The protocol for the measurements is 3 cycles of 3 min measurement and 3 min mixing, between each injection of modulators.

At the end of the assay, media in the wells were removed and the plates were kept in -80°C freezer overnight to lyse the cells. Total protein content was measured by Pierce® BCA Protein

assay (described in section 2.4.1.) and the OCR and ECAR values obtained were normalized to protein (per µg) content.

2.7 Substrate oxidation assay by $^{14}CO_2$-trapping

$^{14}CO_2$ capture is a standard technique for evaluation of cellular oxidation of substrates. A modification of the traditional method (cells or cell lysate in a sealed vial) involves using cell cultures and filter plates designed to be used in a multiplate scintillation spectrophotometer [111]. The method uses a standard 96-well tissue culture plate and a filter plate having the filter plate (activated with NaOH) inverted on top of the cell plate, sealed with a silicon-gasket in the middle to obtain a gas-tight compartment (See Figure 2.2) [112].

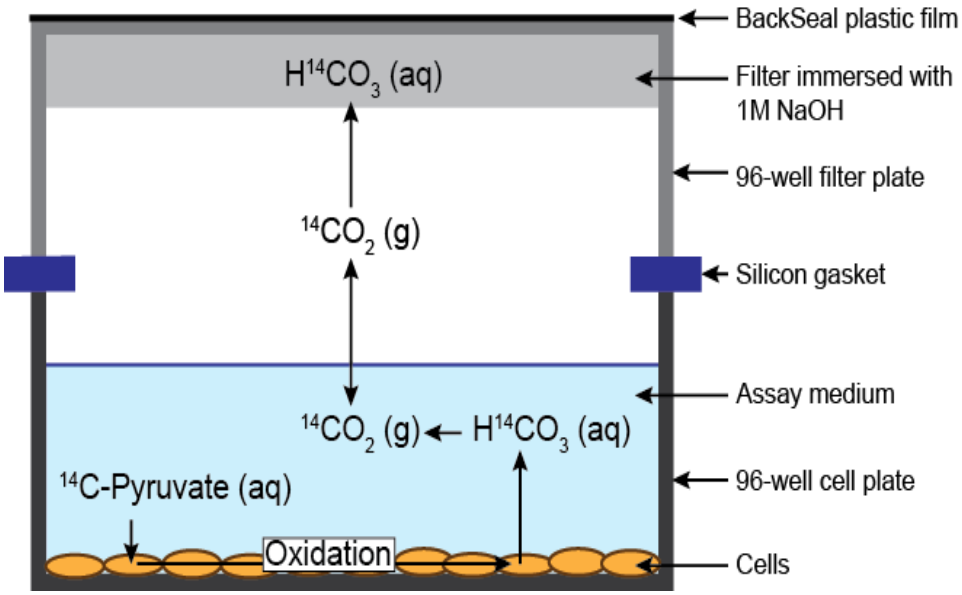

Figure 2.2 The principles of the $^{14}CO_2$ trapping system. The released CO_2 from the oxidation of ^{14}C-labeled substrate will be trapped by the alkaline suspension in the filter plate [112].

2.7.1 Preparation of samples and media

Substrate oxidation rate of PDK overexpressed cells were assessed by trapping released $^{14}CO_2$ as described by Wensaas et al. after being treated with two different radiolabeled carbon substrates (^{14}C) [112]. Cells were seeded as 45 000 cells/well in two 96-well CellBind® microplates in pre-treatment with different concentrations of glucose (1mM and 25 mM or 1mM, 5 mM, and 25 mM, depending on the experiment) and incubated overnight (37°C in 5% CO_2) for proper attachment. The radiolabeled substrates used were [1-^{14}C]pyruvic acid (0.25

µCi/ml) and [1-^{14}C]palmitic acid (1 µCi/ml), supplied by PerkinElmer (Waltham, MA, US). The assay media with these substrates were prepared in 5 ml of Dulbecco's Phosphate Buffered Saline (DPBS) (with $MgCl_2$ and $CaCl_2$, D8662, Sigma-Aldrich) supplemented with 10 mM HEPES, 0.5 mM glucose and 10 µM BSA (i.e. 7.06 µM for palmitic acid). Additionally, 1 mM L-carnitine was added in the assay medium for palmitic acid (PA) oxidation. To obtain final concentrations of 200 µM of sodium pyruvate and 100 µM of BSA-conjugated PA, calculated amount of respective non-radiolabeled substrate was added. The reduced amount of BSA in the assay medium for PA was because the cold fatty acid (non-radiolabeled) is conjugated to BSA (40µM BSA in 100µM cold PA). For uncoupled substrate oxidation, two optimized concentrations for CCCP, 10 µM for pyruvate and 30 µM for PA oxidation were prepared in DPBS. The optimal concentration of CCCP was made higher for PA than pyruvate, due to increased amount of BSA in PA medium, CCCP will bind to BSA.

2.7.2 The $^{14}CO_2$ trapping procedure

At first, the cells were monitored under a light microscope and the media was removed and saved in a new 96-well plate to be used for measuring glucose and lactate concentration. The two plates were labeled for two substrates, and 50 µl of the corresponding radioactive assay medium was added to the cells. 5 µl of 10 µM and 30 µM CCCP stock was added to the selected wells of pyruvate and PA plate, leading to final concentration 1 µM and 3 µM respectively. UK-5099 (5 µM, inhibits the transport of pyruvate into the mitochondria, by inhibiting the mitochondrial pyruvate carrier (MPC)) and Etomoxir (40 µM, inhibitor of fatty acid oxidation, by irreversible inhibition of carnitine palmitoyltransferase-1, CPT-1) were also added to some wells to monitor non-mitochondrial CO_2 production. In another experiment, after adding radioactive assay media, the cells were treated with a range of DCA concentrations (20 µM, 30 µM, 40 µM, 50 µM) in order to investigate DCA-mediated influence in substrate oxidation. A 96-well filter plate (UniFilter: GF/B) was prepared beforehand by immersing with 25 µl of 1M NaOH. After adding all treatments, the cell plate was clamped together with the filter plate in a sandwich like structure in the order: cell plate/silicon gasket/inversed filter plate (as described by [112], see Figure 2.2). The trapping apparatus was placed in an incubator (37°C) and was allowed to trap CO_2 for 4 h. The $^{14}CO_2$ captured in the filters could be monitored by addition of scintillation liquid (30 µl, MicroScint PS PerkinElmer) to the filters, followed by sealing with a TopSealA (PerkinElmer). Radioactivity was counted in a microplate scintillation counter (MicroBeta2 Microplate Counter, PerkinElmer). The cell plates containing the

radioactive media and treatments was used for protein measurement and cell-associated radioactivity.

2.7.3 Measurement of protein and cell associated radioactivity

The media was removed, washed twice with PBS, and 0.1M NaOH was added to lyse the cells. 50 µl of lysed cells were taken in a Nunc™ MicroWell™ 96-Well Microplate for measuring protein concentration using Pierce® BCA Protein Assay Kit as described in section 2.4.1. Another 50 µl of lysed cells were transferred to an Isoplate-96 Microplate (PerkinElmer) and 100µl of scintillation liquid (UltimaGold XR) was added to each well and sealed with a TopSealA. The plate was left to incubate for 2 h and the radioactivity was measured in the same MicroBeta scintillation counter. All the procedures and instrument handling were done in a specialized room for isotope handling and with appropriate personnel protection.

2.8 Media lactate and glucose measurements

Lactate that is produced as a metabolic by-product of glucose metabolism has also effects in cell growth and metabolic activity (Ozturk SS). Biosen C-Line GP+ (EKF Diagnostics, Cardiff, UK) was used to measure glucose and lactate concentrations in the media that were collected during xCELLigence and $^{14}CO_2$ trapping experiments. Biosen uses a special chip sensor technology for quick and efficient measurement of glucose and lactate within the measuring range 0.5–50 mmol/L and 0.5–40 mmol/L respectively. The sensor contains immobilized enzyme glucose oxidase / lactate oxidase which catalyzes the oxidation of β-D glucose / L-lactate contained in the sample and the hydrogen peroxide (H_2O_2) produced is detected at the electrode.

Before starting measurement, a solution of known concentration (EKF Multi-standard) was placed in the device to be automatically calibrated. Then 10 mM of pure glucose and lactate solutions were measured as control to check instrument accuracy. 4 µl of media was precisely taken in micro-tubes and mixed with 200 µl of hemolysis solution (1:50 dilution) by gentle pipetting. The samples were inserted into the analyzer where they were automatically taken up and moved to the sensor. The results were generated after 20-45 sec.

2.9 Data analysis

Data from all experiments were calculated and analyzed by Microsoft excel and Graphpad Prism 7 software and presented as either mean ± standard deviation (SD) or mean ± standard

mean error (SEM). Statistical analysis of data was performed by ordinary one or two-way ANOVA followed by Tukey's multiple comparisons test in Graphpad. $P<0.05$ was considered as significant to indicate a statistical difference. The bands from western blot data was quantified by using Image J. software.

3 Results

3.1 mRNA expression analysis confirms PDK overexpression in MDA-MB-231 cells

The stable transduction of PDK1-4 in MDA-MB-231 cells was done by Phoenix retroviral packaging system. To confirm successful overexpression in the stably transduced MDA-MB-231 cells prior to experimental proceeding, the increased expression of PDK1-4 mRNAs was confirmed by qPCR analysis. Expression of each of the PDK1-4 mRNAs was significantly upregulated in the respective target sub-lines compared to WT cells (Figure 3.1). Figure 3.1A show expression levels immediately after the selection process, and Figure 3.1B after a second selection process 3 months later to ensure that the cells still had the inserted construct.

The data from these two time points showed similar PDK1-4 mRNA expression profile. Both figures show elevated expression of each four PDK mRNAs in their host cells, though with some variation in magnitude. For instance, fold induction was highest in the PDK4 overexpressing cells compared to the WT cells. Still, all PDKs were considered highly expressed based on their high fold change in the respective cells. The relative increase in PDK1-4 expression ranged between 60- to 2000-fold in the first quantification (Figure 3.1A), whereas it was some lower in the second as it ranged from 30- to 350-fold (Figure 3.1B).

Decreased overexpression between the first and second measurement was particularly seen for the PDK1 and PDK4 mRNAs. Besides, the expression level of other non-overexpressed PDKs in each of the transduced cell lines as well as in WT was also measured, however, their expression was quite low and was not affected by the overexpression (data shown in supplementary Table 8.1). The expression for WT is not presented in the graph since the mean for WT expression was 1 by default, as fold-change for PDK mRNAs was calculated relative to the WT mRNA expression.

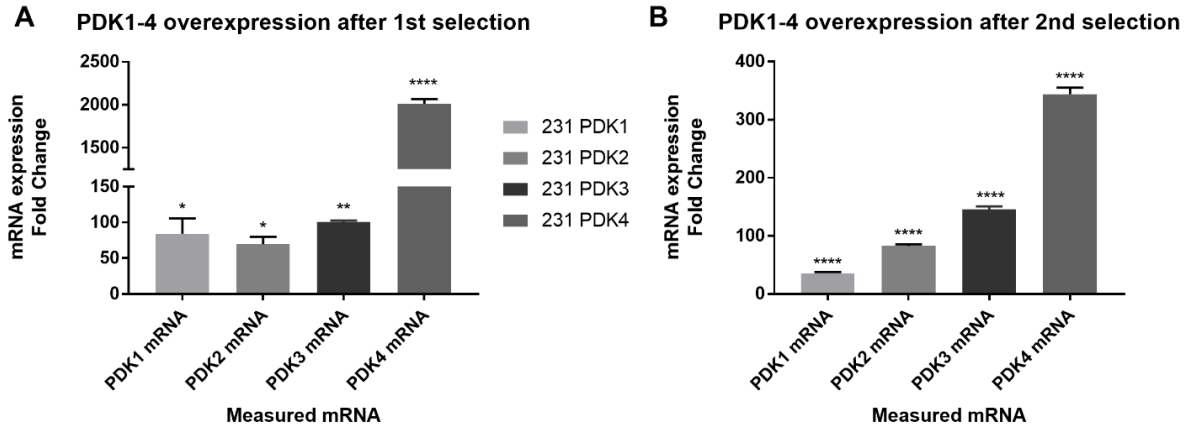

Figure 3.1 The upregulation of PDK1-4 mRNAs confirmed by quantitative real-time PCR in the cell lines overexpressing the respective target mRNA (A) The increased expression level of PDK1-4 mRNAs detected after the first selection process. **(B)** The increased mRNA expression was further confirmed after 3 months upon reselection of the cells. For quantification, the amount of PDK1-4 mRNA expression was normalized to 18S rRNA mRNA expression. The X-axis data shows the corresponding mRNA measured in each PDK-overexpressing cell and Y-axis data shows mRNA expression fold change relative to the WT control (ddCT method). Values are presented as mean ± SD and statistical comparisons was performed by one-way ANOVA. The asterisks indicate significant differences from the control group considering *P < 0.05; **P < 0.01; ***P < 0.001 and ****P < 0.0001.

3.2 PDK overexpression leads to increased protein expression

To further confirm PDK1-4 overexpression at protein level, western blot analysis was performed and the results are displayed in Figure 3.2. The level of overexpression was evaluated relative to the amounts of endogenous PDK isoforms measured in the WT cells. Detection with anti-PDK1 antibody showed an effective increase in PDK1 expression in the stably transduced 231 PDK1 cells (Figure 3.2A). There was low expression of PDK1 in the other transduced cell types, as well as in the parental WT cells. Similarly, high expression was observed for PDK2 protein in 231 PDK2 cell with no or low expression in other cells (Figure 3.2B). Similar expression patterns were observed in the other blots for PDK3 and PDK4 proteins (Figure 3.2C and Figure 3.2D). The PDK isoforms have molecular weight ranging between 46-49 KDa and all the bands were detected at ~46 KDa. Anti-GAPDH (and anti-α-tubulin, data not shown) was used as a loading control and confirmed equal sample loading in all wells. The intensity of the respective bands on the western blot image was quantified, and calculated relative to GAPDH expression (Figure 3.2E-H).

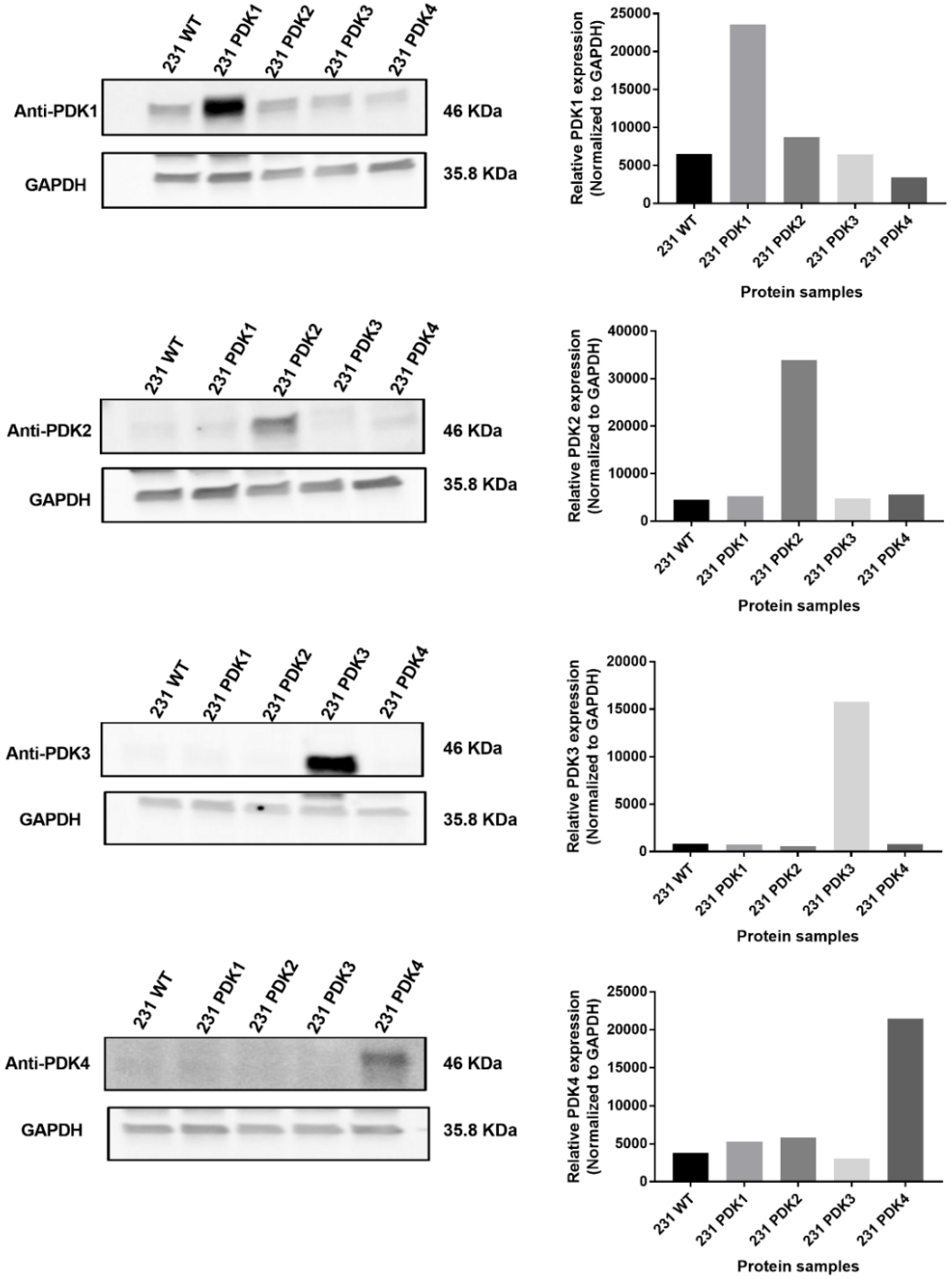

Figure 3.2 Western blot analysis to verify successful stable overexpression of PDK1-4 isoforms in terms of protein expression. A-D Representative blots showing increased protein expression of PDK1, PDK2, PDK3, and PDK4 against their specific antibodies in the respective PDK1-4 overexpressed cell lines, all were detected approximately at 46 KDa. Other PDKs show downregulation or poor expression including in the WT. **E-H** Quantification of relative PDK expression in each sample. X-axis represents the total protein samples in 231 PDK1-4 cells and Y-axis represents PDK1-4 protein expression levels that were normalized to GAPDH expression, each relative to the WT Control. Anti-GAPDH detects a band of approximately 35.8 KDa. The data presented here is representative of three independent experiments.

3.3 Effect of PDK overexpression on the proliferation of 231 PDK1-4 cells

3.3.1 Growth characteristics by impedance analysis indicates increased proliferation in PDK overexpressed cells

To determine if overexpression of the PDK isoforms causes changes in cell proliferation, we performed impedance analysis-based proliferation study by using the xCELLigence system. The cells were continuously monitored for 96 h and the generated growth curves are presented in Figure 3.3. The cell index (CI) values were normalized 5 h after the experiment started (i.e. 2h after cell seeding) in order to obtain the relative growth of the cell cultures, after proper cell attachment and spreading. The normalized CI values display distinct growth profile for each cell type. 231 PDK1, PDK3, and PDK4 cells showed significantly higher proliferation than the WT cells whereas PDK2 had the slowest proliferation. Despite differences in the proliferation rate, the CI values were gradually increasing for all of them over time. PDK1 and PDK4 overexpressing cells were growing at a similar rate for the first 24 h, but a slightly lower proliferation rate was observed for the 231 PDK4 cells for the rest of the experiment (see Figure 3.3A).

Based on the overall monitoring, we statistically compared the CI levels of all five cell types at specific time points 24 h, 48 h, 72 h, and 96 h (see Figure 3.3B). The relative differences between the cell lines at individual time points were almost the same, showing increased proliferation in the cells overexpressing PDK1, 3 and 4 compared to the parental WT cells. The differences in CI among the cell types, including the parental cells, were significant as calculated by two-way ANOVA. Of these cell types, the PDK1 cells displayed the highest proliferation rate among the all PDK candidates.

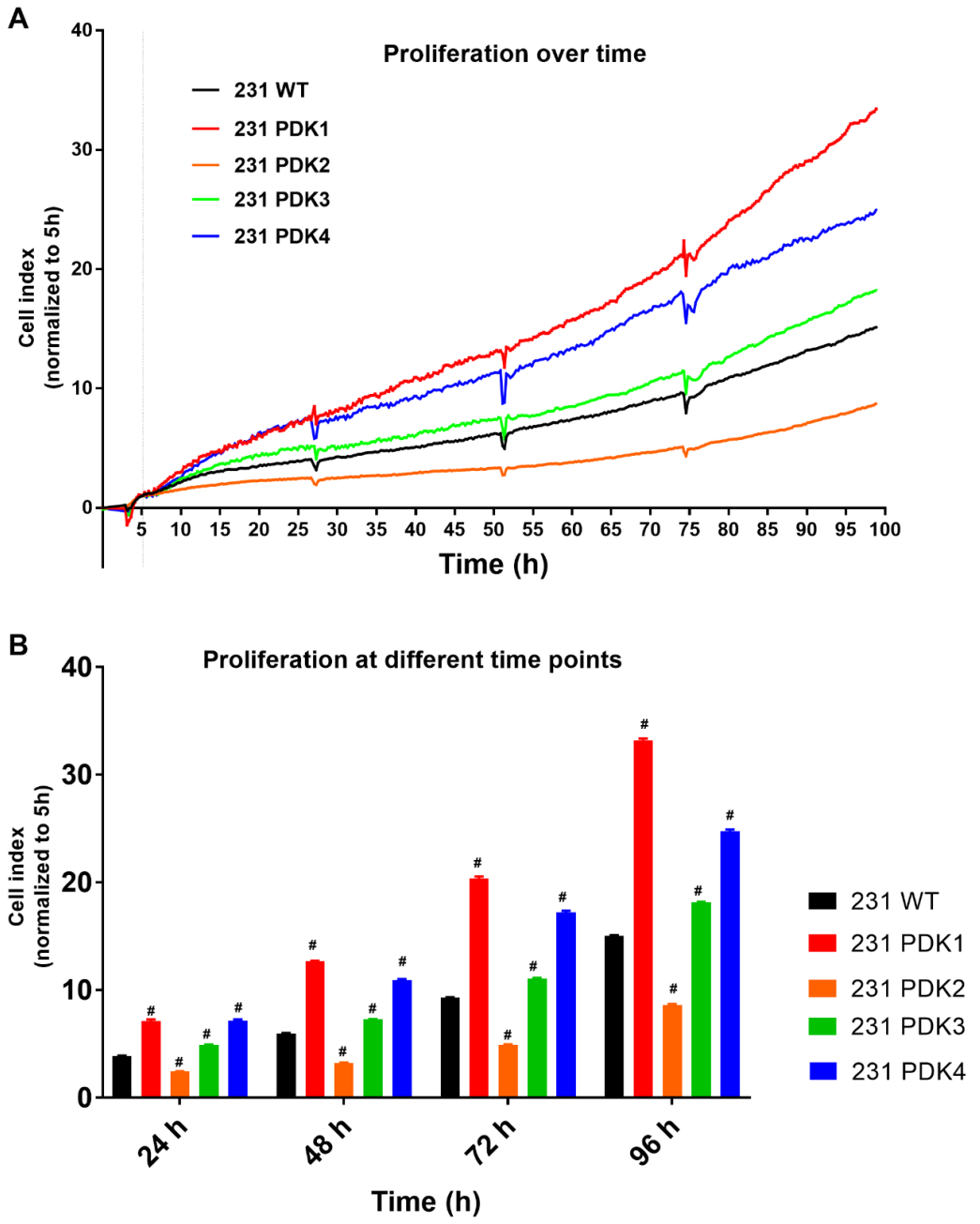

Figure 3.3 Dynamic monitoring of proliferation in the PDK1-4 overexpressed cell lines using the xCELLigence impedance system. (A) Growth curves of 231 WT, PDK1, PDK2, PDK3, and PDK4 cells were recorded over a time period of 96 h in 16-well E-plates with a seeding density 4,000 cells/well. The vertical axis represents the cell index (CI) values that are normalized to first 5 h. The small breaks in the growth curves were due to experimental pause in those time points to collect media from the wells. **(B)** The curves are plotted into standard bar graphs to compare CI values between the cell types at 24 h, 48 h, 72 h, and 96 h. The data are presented as the mean of three replicates ± SD. $^{\#}P < 0.0001$ was obtained by two-way ANOVA for each group relative to the WT control.

3.3.2 Determining glucose and lactate concentrations in culture medium

In the xCELLigence experiment described above, we measured glucose and lactate concentrations in the culture medium at different time points. The process of medium collection caused small breaks in the CI data curve, as seen in Figure 3.3A (experimental pause). Figure 3.4 displays the medium level of glucose and lactate after 24 h, 48 h, 72 h, and 96 h. Initially, the cells had 25 mM glucose in their media and the remaining glucose after 4 days of proliferation (96h) was around 18-20 mmol/L (Figure 3.4A). The level of glucose did not seem to be very different throughout their proliferation time. Further, the 231 WT and 231 PDK1 did not produce lactate until first 24 hours, later they produced up to 4 mmol/L. 231 PDK2 and 231 PDK3 had similar lactate accumulation in the media between 24 h and 48 h, then 231 PDK3 produced more lactate than 231 PDK2 for rest of the period. 231 PDK4 cells produced lactate at the highest rate from 24 h to 96 h, with an amount up to 5mmol/L (Figure 3.4B). The control media did not have any lactate present. The initial medium glucose concentration was measured to be 18-20 mmol/L, some lower than the estimated concentration, and was not found to change significantly in any of the cultures throughout the experiment.

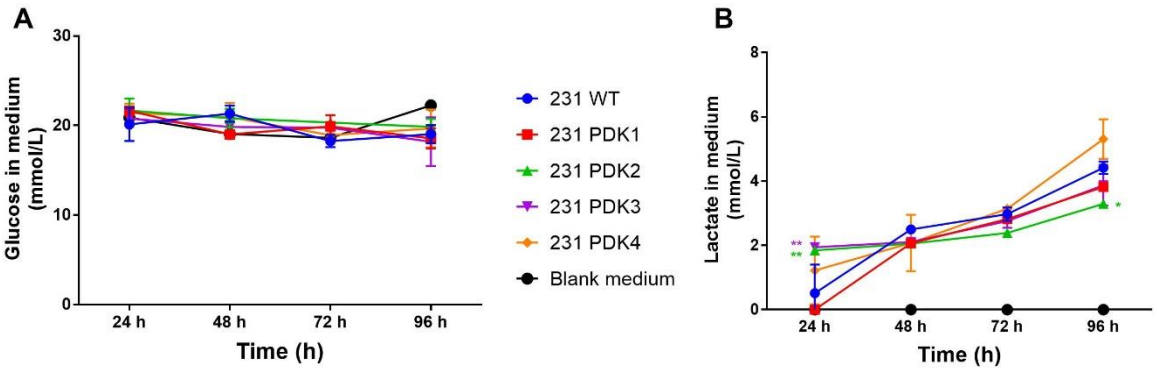

Figure 3.4 Measurement of glucose and lactate present in the cell culture media. The measurements were done during the proliferation study in xCELLigence. **(A)** Estimation of glucose concentration present in the media in the cultures of the 231 WT and PDK1-4 cells after 24 h, 48 h, 72 h, and 96 h **(B)** Estimation of extracellular lactate concentration in the culture media of 231 WT and PDK1-4 cells at the same time points. The amount of glucose and lactate are presented as mmol/L. The graphs represent mean of three replicates ± SD. *P < 0.05; **P < 0.01

3.3.3 Effect of glucose deprivation on the proliferation of PDK1-4 overexpressing cells

The effect of PDK overexpression on cell growth was evaluated by cell culture imaging in IncuCyte® Live Cell Analysis system (IncuCyte) to investigate confluence-dependent proliferation. Unlike from the xCELLigence experiment, high (25 mM), moderate (5 mM), and low (1 mM) concentrations of glucose were used to determine the glucose dependency of the PDK overexpressing cells compared to WT cells.

Figure ***3.5*** presents the morphology as well as proliferation curves of 231 WT and 231 PDK1-4 cells recorded via IncuCyte for 72 h. The growth curves in

Figure ***3.5***B-D are presented as fold change of % confluence values and are normalized to the time point of first image.

In all three glucose conditions, the proliferation rate of PDK1-4 cells was almost same as the WT at least for first 20 h. Then a significant reduction in PDK1-4 cells' proliferation was observed in 1 mM glucose compared to the other two glucose conditions, and it seems like they grew only for around 40h after which they growth curves started to decline. 231 PDK1 and 231 PDK2 were found to be mostly affected by 1 mM glucose condition. Interestingly, the growth of the 231 PDK1-4cells were not affected by 5 mM glucose, whereas a slight increase in the proliferation of 231 PDK2, PDK3, and PDK4 was visible in 25 mM glucose.

Figure 3.5E shows the approximate plateau datapoints that were picked for each cell type in 1 mM glucose and plotted into standard bar graphs which shows subsequent reduction in proliferation in all 231 PDK cells in compared to the 231 WT cell.

For 5 mM and 25 mM conditions, the end-point measurements of growth curves at 71.5h were plotted in standard bar graphs

Figure 3.5F-G). The peak proliferation level for all the PDK overexpressing cell lines were slightly reduced in 1 mM glucose compared to 231 WT cells with statistical significance. This was not observed in higher glucose concentrations, suggesting that overexpression of either of the PDKs causes increased glucose dependency. There was a slight increase in the 231 PDK cells' proliferation in presence of 25 mM glucose, compared to 231 WT cells.

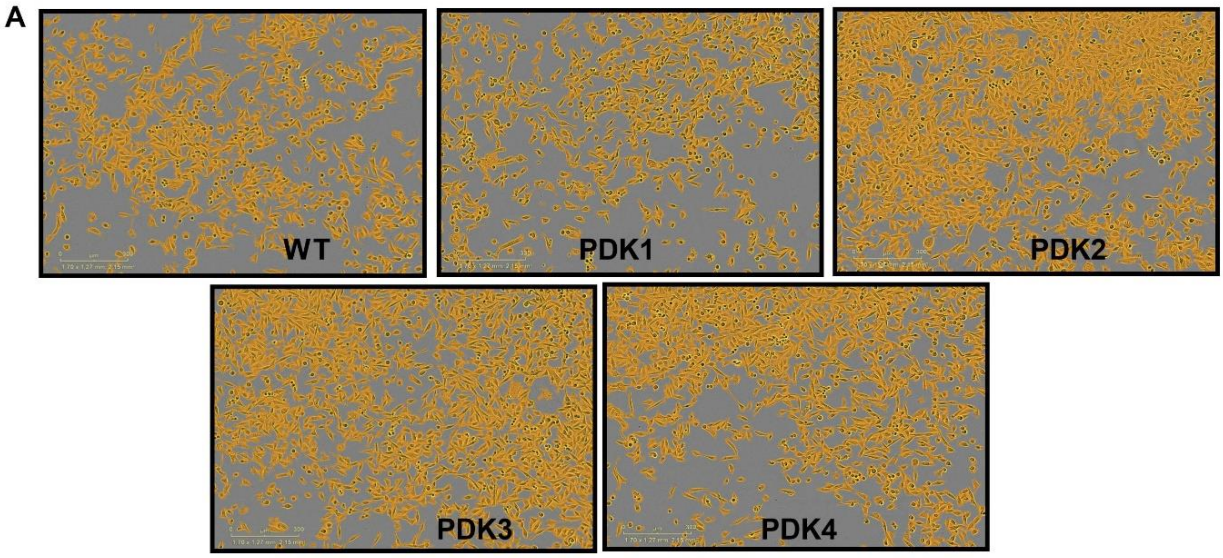
A
WT
PDK1
PDK2
PDK3
PDK4

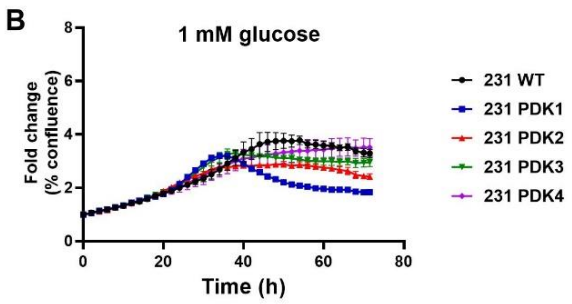
B
1 mM glucose
Fold change (% confluence)
Time (h)
231 WT
231 PDK1
231 PDK2
231 PDK3
231 PDK4

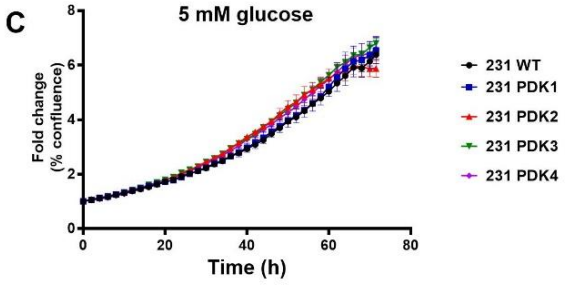
C
5 mM glucose
Fold change (% confluence)
Time (h)
231 WT
231 PDK1
231 PDK2
231 PDK3
231 PDK4

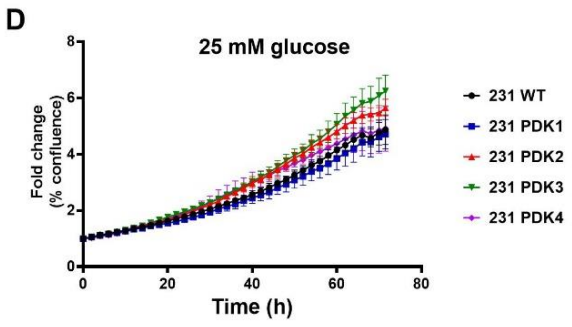
D
25 mM glucose
Fold change (% confluence)
Time (h)
231 WT
231 PDK1
231 PDK2
231 PDK3
231 PDK4

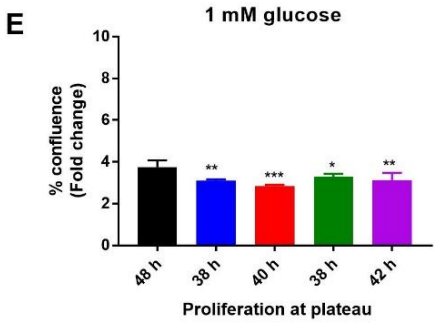
E
1 mM glucose
% confluence (Fold change)
48 h
38 h
40 h
38 h
42 h
Proliferation at plateau

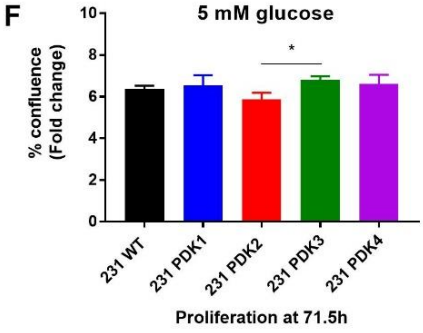
F
5 mM glucose
% confluence (Fold change)
231 WT
231 PDK1
231 PDK2
231 PDK3
231 PDK4
Proliferation at 71.5h

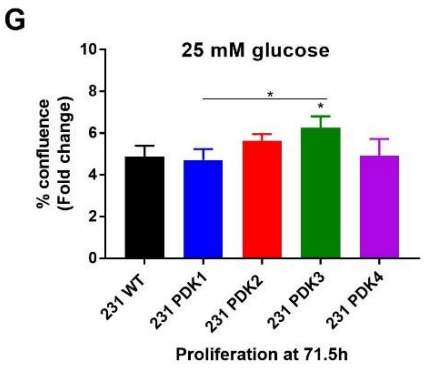
G
25 mM glucose
% confluence (Fold change)
231 WT
231 PDK1
231 PDK2
231 PDK3
231 PDK4
Proliferation at 71.5h

Figure 3.5 IncuCyte® cell proliferation assay of 231 WT & 231 PDK1-4 cells cultured in 1 mM, 5 mM, and 25 mM glucose. The cells were seeded at 3000 cells/100 µl/well and confluence were recorded for 72 h at 10x objective. (A) Live cell morphology captured real-time in 96-well format containing 25 mM glucose at 71.5 h (B-D) Growth curves showing proliferation profile of 231 WT and PDK1-4 cells throughout 72 h. (E) Proliferation of 231 PDK1-4 cells at their plateau datapoints in 1 mM glucose. (F-G) Proliferation at 71.5 h in 5 mM and 25 mM glucose conditions in each glucose condition. The vertical axis represents the fold change of % confluence and are normalized to the time point of first image. The data presented here is representative of two independent experiments. $*P < 0.05$, $**P < 0.01$, $***P < 0.001$.

We also performed a similar experiment where we evaluated viability/proliferation using the metabolic resazurin assay. The cells were first grown for 72 h in presence of 1 mM, 5 mM, or 25 mM glucose, followed by 3 h incubation with resazurin. The fluorescence of resazurin conversion to resorufin by the proliferating cells were measured and the results are presented in Figure 3.6. The resazurin conversion experiment did not suggest that cell viability was reduced under the glucose-limited (1 mM) condition, as could be hypothesized from the previous proliferation data. In contrast, viability was increased in cultures with cells overexpressing PDK2, PDK3 or PDK4, compared to parental cells (Figure 3.6A). Further, the rate of resazurin conversion in the PDK-overexpressing cells were significantly higher than the WT parental cells in the 5 mM and 25 mM glucose condition particularly in the 231 PDK1, PDK2, and PDK3 cells (Figure 3.6B-C). The measurement of resazurin conversion represents a combined indicator of cell viability, proliferation, and metabolic rate.

We also investigated if PDK-overexpression has any effect on proliferation under low-oxygen condition. We incubated the 231 PDK1-4 cells in the same glucose conditions for 72 h, but under physiological oxygen level (5% O_2, 37^0C). However, the 231 PDK1-4 cells did not show any significant differences between normal (atmospheric) and physiological (normoxic) oxygen conditions [113] (data shown in supplementary Figure 8.1).

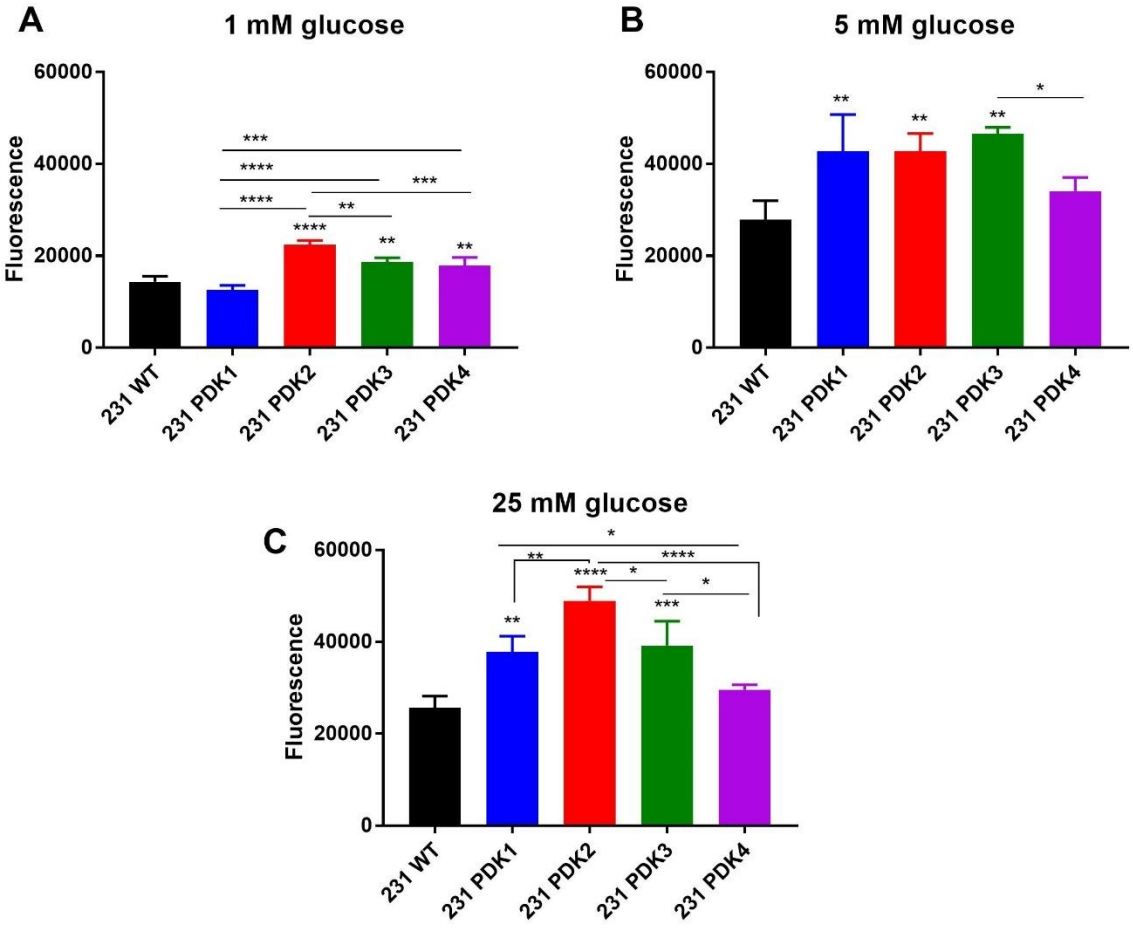

Figure 3.6 Determination of viability in 231 PDK1-4 cells by resazurin-based assay. The 231 PDK1-4 cells were continuously grown for 72 h in 1 mM, 5 mM, and 25 mM glucose media with a seeding a density 3000 cells/100 µl. Following 3 h incubation with resazurin, the fluorescence of resazurin conversion to resorufin was measured at Ex_{560}, Em_{600}. Resazurin conversion rate by the PDK1-4 cells in (A) 1 mM (B) 5 mM, and (C) 25 mM glucose. The vertical axis represents the fluorescence of resorufin and the bars are presented as mean of replicates ± SD; Statistical tests were performed by one-way ANOVA, *P < 0.05, **P < 0.01, ***P < 0.001, ****P < 0.001.

3.3.4 Effect of DCA on proliferation of PDK1-4 cells

Since we observed that PDK overexpression tends to have a positive effect on proliferation, at least when glucose supply is not limiting, we also tested the effects of PDK inhibition on proliferation with the use of DCA. DCA is a well-known inhibitor of all four PDK isoforms [114]. Effects of PDK inhibition on cell proliferation and viability were monitored by incuCyte imaging and resazurin conversion under the same conditions as in section 3.3.3. This was implemented as a part of the previously described experiments, and the effects of DCA were

therefore evaluated to the same untreated cell cultures as in Figure 3.5 and 3.6. 50 mM DCA was added in the selected replicates of 25 mM glucose condition, incubated for 3 days and the effect on PDK-overexpressing cells is showed in Figure 3.7.

A massive reduction in proliferation in each of the PDK-overexpressing cell was observed in terms of resorufin fluorescence as well as percent confluence. Approximately 80-90% reduction in confluence (Figure 3.7A) and 60-65% reduction in resazurin fluorescence (Figure 3.7B) was observed.

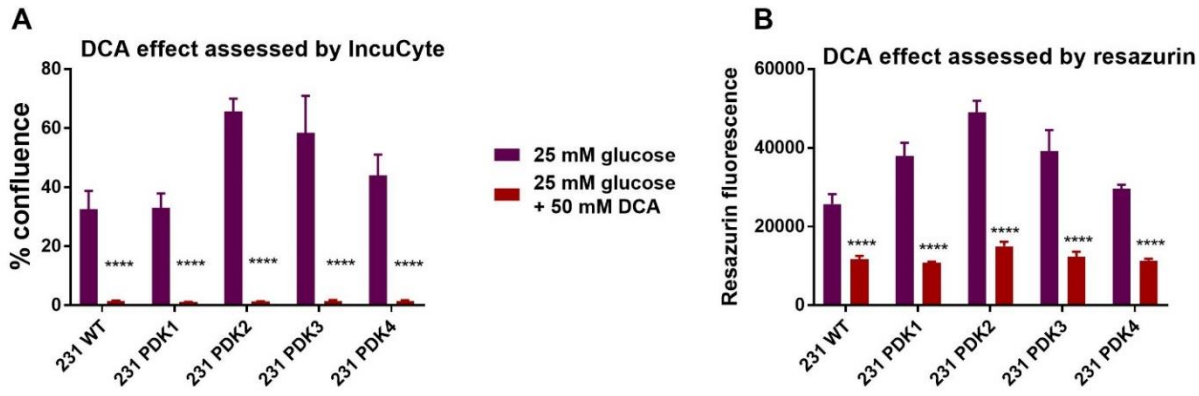

Figure 3.7 Effect of DCA on the growth of 231 PDK1-4 cells assessed using the incuCyte instrument and the resazurin assay. 50 mM DCA in presence of 25 mM glucose was used for treating 3000 cells/100 µl, followed by 3 days incubation. **(A)** Reduction in % confluence due to DCA effect measured by the incuCyte instrument and **(B)** Reduction in resazurin fluorescence due to DCA effect measured by resazurin viability assay in compared to the untreated 25 mM glucose condition. The data are presented as the mean ± SD of 4 duplicated wells. Statistical analysis performed by one-way ANOVA, *P < 0.05, **P < 0.01, ***P < 0.001, ****P < 0.001

3.4 Rates of mitochondrial respiration and glycolysis in PDK1-4 overexpressing cells

In order to investigate how energy metabolism is affected by PDK overexpression, we compared bioenergetic status of the PDK1-4 cells with the WT control based on measuring mitochondrial respiration and glycolysis. We had to first determine the optimal CCCP concentration and 1 µM CCCP was found to stimulate the maximum OCR in 231 WT and 231 PDK4 cell (see supplementary Figure 8.2). Therefore, 1 µM was chosen as optimal CCCP concentration for further experiments.

3.4.1 Effect of PDK1-4 overexpression in mitochondrial respiration

Mitochondrial respiratory analyses were performed by mitochondrial stress test in Agilent seahorse XFe96 analyzer, following overnight incubation with 1 mM, 5 mM, or 25 mM glucose. The overall respiratory rates of 231 PDK1-4 cells in compared to their WT parental cell are presented in Figure 3.8.

Following the measurement of basal respiration, key parameters of mitochondrial function were assessed by sequential addition of pharmacological modulators (Figure 3.8A-C). The inhibitory effect of oligomycin, and the subsequent induction by addition of uncoupler CCCP, confirmed OXPHOS integrity under these conditions. For the 231 WT cells, basal respiration and maximum respiratory capacity tended to be higher in the cultures with 1mM glucose compared to 5 mM glucose (Figure 3.8 D-E). This potential adaptation to the limited glucose appeared to be absent in cells overexpressing PDK1, PDK3 or PDK4, as the respiratory rates were unchanged or higher in cells grown with 5 mM glucose, compared to 1 mM glucose. Due to these differences, the increase in respiratory rates was particularly evident following growth in 5mM glucose. In the PDK2 overexpressing cells, the rates of mitochondrial respiration were similar to the parental cells, apart for an increase in maximum respiration following growth in 1mM glucose. Incubation with 25 mM glucose tended to reduce the respiratory activity, when compared to the 5 mM glucose condition, in the PDK overexpressing cells (Figure 3.8E-F). Hence, the effects of PDK1, PDK3 and PDK4 overexpression were less pronounced under this high glucose condition. There was no significant difference in leak respiration among the groups, apart from a minor increase in PDK1 overexpressing cells.

The maximum OCR in 231 WT cells were almost identical to their basal respiration rate, indicating that the WT cells might operate closer to their maximal capacity at basal levels. All OCR readings are normalized to cells' protein content and presented after background was subtracted. Therefore, non-mitochondrial respiration is not shown in Figure 3.8D-F and the respiration measured after rotenone addition was complex-I independent respiration, which was negligible.

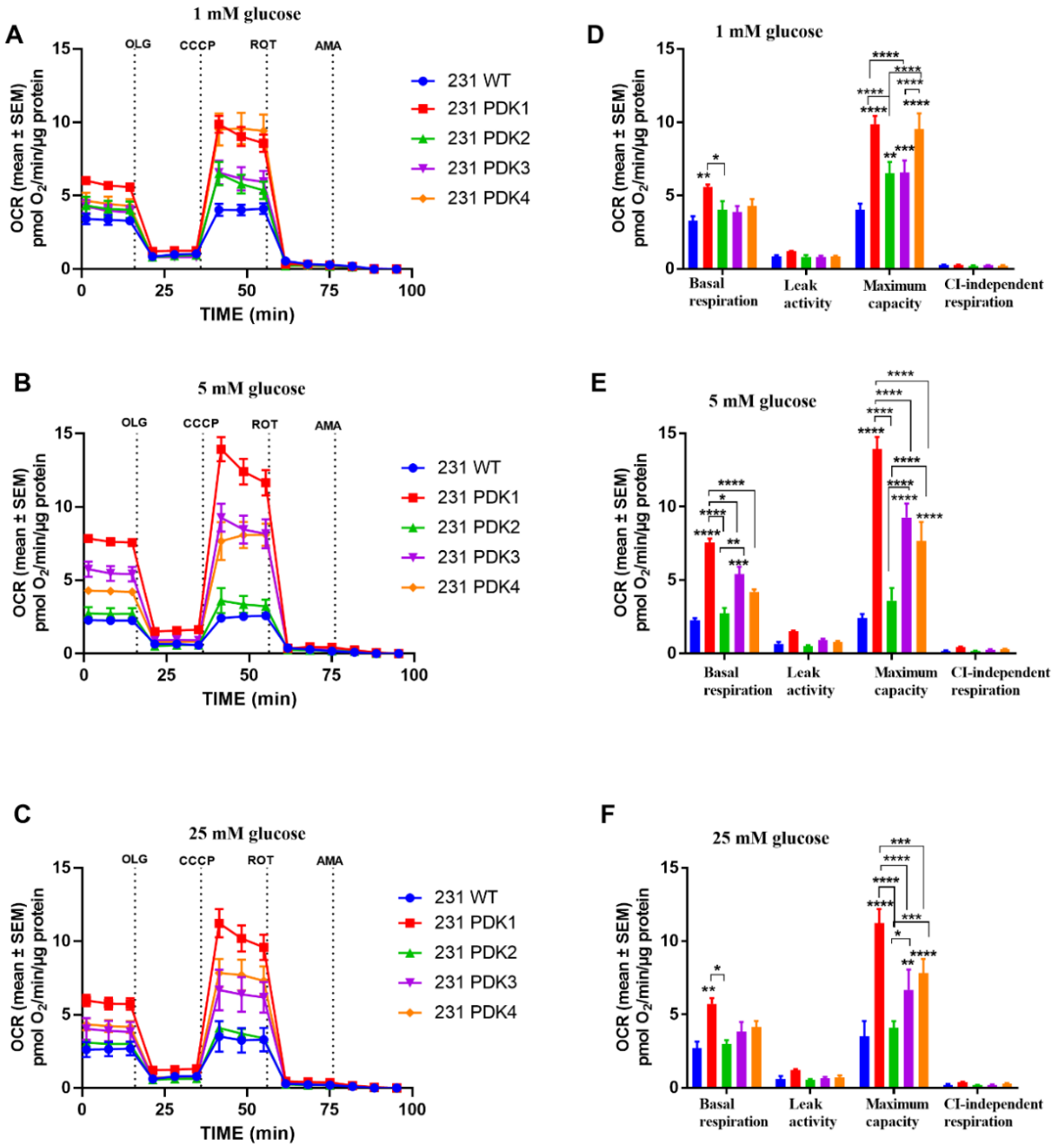

Figure 3.8 Analysis of mitochondrial respiration of 231 WT and 231 PDK1-4 cells. Oxygen consumption rate (OCR) was measured by Seahorse mitochondrial stress test in 1 mM, 5 mM, and 25 mM overnight glucose pretreatment with 30000 cells/well. The analysis was done in basal DMEM assay medium supplemented with 10 mM glucose, 2mM pyruvate, and 2 mM L-glutamine. **(A-C)** Representative traces of OCR (pmol O_2/min/µg protein) obtained after sequential addition of 3 µM oligomycin, 1 µM CCCP, 1 µM rotenone and 1 µM antimycin A. **(D-F)** Data extracted from A-C were analyzed to calculate basal respiration at normal condition; leak respiratory rate due to leakage of protons after oligomycin addition; maximum capacity (uncoupled respiration) after addition of CCCP; and CI-independent respiration after rotenone addition. Non-mitochondrial respiration or residual oxygen consumption is obtained after antimycin A addition. The results presented here are corrected for non-mitochondrial respiration and normalized protein content. The figures display representative data as mean ± SEM. *P < 0.05, **P < 0.01, ***P < 0.001, ****P < 0.0001

3.4.2 Analyzing the glycolytic function

The glycolytic function of the PDK1-4 cells was assessed by measuring the extracellular acidification that is mainly generated by lactate secretion. The glycolysis stress test was performed, and interestingly 231 PDK1-4 cells also showed increased glycolytic rate compared to the 231 WT cells (Figure 3.9A-C). The PDK1-4 and WT cells had apparently same endogenous acidification rate (before adding glucose). After addition of glucose, the glycolysis rate was established and all the 231 PDK1-4 cells displayed higher basal ECAR following pre-incubation in 1 mM glucose (Figure 3.9D). Subsequent addition of oligomycin blocks mitochondrial respiration, which causes a further increase in ECAR, indicative of the glycolytic capacity. The glycolytic capacity was also increased in the 231 PDK1-4 cells pre-incubated in 1 mM glucose (Figure 3.9D). The differences between 231 WT and 231 PDK1-4 cells regarding glycolytic rates were similar when comparing the higher glucose conditions (5 mM and 25 mM glucose) with the glucose restricted condition (1 mM glucose) (Figure 3.9E-F). Hence, these data did not convincingly suggest that differences in glucose supply causes regulatory adaptations of the glycolytic machinery, neither in 231 WT cells nor 231 PDK1-4 cells.

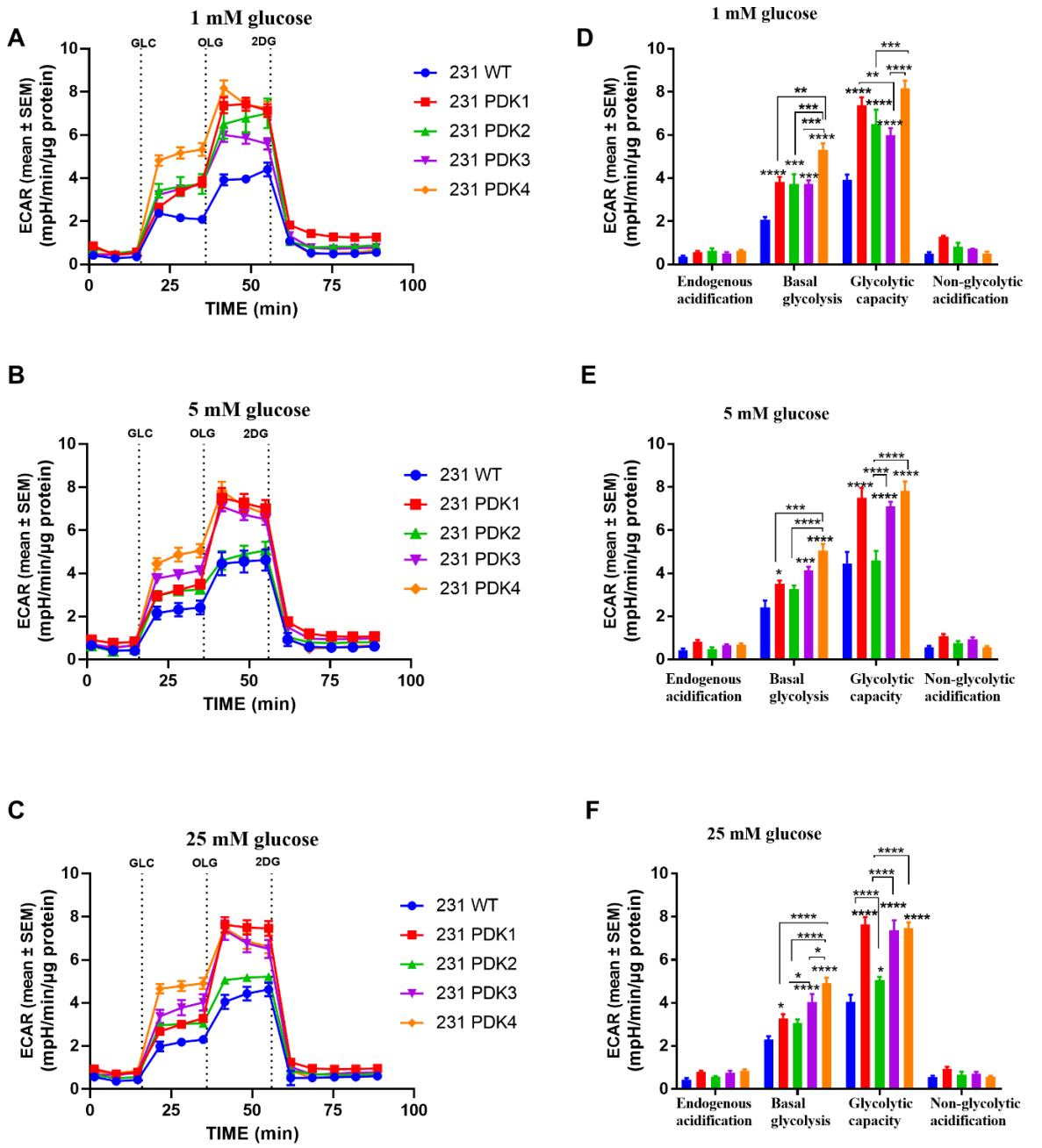

Figure 3.9 Analysis of glycolytic function of 231 WT and 231 PDK1-4 cells. Extracellular acidification rate (ECAR) was measured by Seahorse glycolysis stress test in 1 mM, 5 mM, and 25 mM overnight glucose pretreatment with 30000 cells/well. The analysis was done in basal DMEM assay medium supplemented with 2 mM L-glutamine. **(A-C)** Representative traces of ECAR (mpH/min/µg protein), with sequential addition of 10 mM glucose, 3 µM oligomycin, and 100 mM 2-deoxyglucose (2-DG). **(D-F)** Data extracted from A-C were analyzed to calculate basal glycolysis and glycolytic capacity. Basal glycolysis- ECAR after addition of glucose; Glycolytic capacity- ECAR after addition of both glucose and oligomycin. The results are normalized to cell number and the figures display representative data as mean ± SEM. *P < 0.05, **P < 0.01, ***P < 0.001, ****P < 0.0001

3.5 Characterizing the effect of PDK overexpression on substrate oxidation

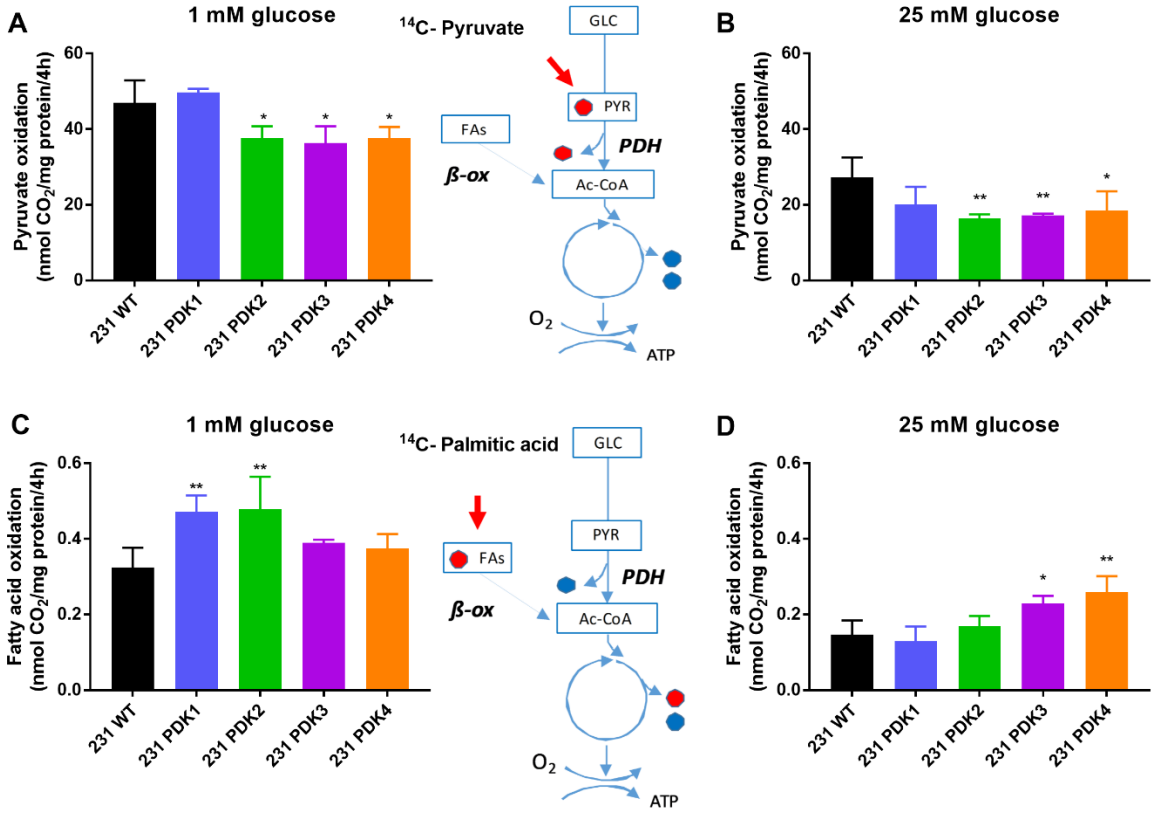

Figure 3.10 Effect of PDK overexpression in pyruvate and fatty acid oxidation was investigated in 231 WT and PDK1-4 overexpressing cells. The cells were pre-incubated (overnight) with **(A)** 1 mM glucose, and **(B)** 25 mM glucose, and pyruvate oxidation was measured by trapping $^{14}CO_2$ during 4h incubation in presence of [1-^{14}C]pyruvic acid (0.25 µCi/ml, 200 µM total pyruvate concentration). The cells were pre-incubated (overnight) with **(C)** 1 mM glucose, and **(D)** 25 mM glucose, and fatty acid oxidation was measured by trapping $^{14}CO_2$-production during 4h incubation with [1-14C]palmitic acid (1 µCi/ml, 100 µM total palmitic acid concentration). The data presented are normalized to cell protein content (mg). The red arrows indicate the entry point of the ^{14}C-labeled substrate into the metabolic pathway. The red and blue circles represent the released CO_2 where the carbon is radiolabeled (red) or non-labeled (blue) respectively. The figures display representative data of three independent experiments with mean of replicates ± SD. *P < 0.05, **P < 0.01, ***P < 0.001.

3.5.1 Determining pyruvate and fatty acid oxidation rate and preferred substrate

We wanted to investigate if increased PDK1-4 expression confers any changes in substrate oxidation rates of the cells, or causes a metabolic switch towards preferred substrate. To address such question, we used radiolabeled [1-^{14}C]pyruvic acid and [1-^{14}C]palmitic acid in assay medium together with respective non-radiolabeled substrates to determine pyruvate and

fatty acid oxidation rate by measuring $^{14}CO_2$-production. Further, to evaluate effects related to glucose supply, the 231 WT cells and 231 PDK1-4 cells were pre-incubated overnight in 1 mM or 25 mM glucose. Generally, and especially regarding fatty acid oxidation, the oxidation rates were significantly higher in cultures pre-incubated with 1 mM glucose, compared to 25 mM glucose (Figure 3.10C-D).

PDK-overexpression was expected to cause reduced PDH activity. Accordingly, we observed reduced pyruvate oxidation in 231 PDK1-4 cells compared to the WT parental cells, except for 231 PDK1 cells pre-incubated with 1 mM glucose (Figure 3.10A-B). The relative effect of PDK1-4 expression in reduced pyruvate oxidation was some more significant following pre-incubation in 25 mM compared to 1 mM glucose.

On the other hand, 231 PDK1 and 231 PDK2 cells exhibited increased fatty acid oxidation following pre-incubation in 1 mM glucose, whereas 231 PDK3 and 231 PDK4 cells demonstrated increased fatty acid oxidation following pre-incubation in 25 mM glucose (Figure 3.10C-D). Apparently, the cells overexpressing PDK 1 or PDK2, similarly to the 231 WT cells, were able to activate fatty acid oxidation to a higher extent than the 231 PDK3 and 231 PDK4 cells, when they were placed in the low glucose condition compared to the high.

In similar conditions, we also investigated glucose oxidation when [^{14}C(U)]glucose was used as major substrate and no significant differences were observed in glucose oxidation between 231 WT and 231 PDK1-4 cells (Supplementary Figure 8.3). We also collected media from the wells before adding radiolabeled substrates to determine the amount of glucose and lactate present in the media. Due to overnight incubation, there was no glucose left in the media in 1 mM glucose treated cells. Supplementary Figure 8.4 shows glucose consumption and lactate production rate of 25 mM glucose treated cells.

3.5.2 Characterizing pyruvate and fatty acid oxidation rates after specific pathway modulations

We also wanted to investigate if uncoupling of mitochondrial inner membrane has any effect on pyruvate and fatty acid oxidation of the PDK-overexpressing cells. Besides, we treated the cells with inhibitors of pyruvate and fatty acid oxidation to test at what extent oxidation of these two substrates is inhibited. We used the same radiolabeled substrates in $^{14}CO_2$-trapping method as described in section 3.5.1. This experiment was performed in association with the experiment presented in Figure 3.10 and the pyruvate and fatty acid oxidation data in Figure 3.10 have been used as control data in Figure 3.11. The use of 1 µM CCCP did not seem to

have very much effect on pyruvate oxidation (Figure 3.11A-B). Conversely, CCCP caused a drastic increase in palmitic acid oxidation in both glucose conditions (1 mM and 25 mM), again indicating fatty acids as preferred substrate for the 231 PDK1-4 cells (Figure 3.11C-D)

Upon treatment with MPC inhibitor UK-5099 and CPT-1 inhibitor etomoxir, pyruvate and fatty acid oxidation was almost blocked. The residual portions of the pyruvate and fatty acid oxidation after UK-5099 and etomoxir treatment indicates non-mitochondrial substrate oxidation.

Furthermore, the cell associated radioactivity was calculated after the trapping procedure upon lysing of the cells with 0.1 M NaOH. No significant differences were observed associated with [1-^{14}C]pyruvic acid activity but a slight increase in [1-^{14}C]palmitic acid activity was visible in compared to WT. Supplementary Figure 8.5 shows the concentration-dependent changes in the cell-associated [1-^{14}C]pyruvic acid and [1-^{14}C]palmitic acid activity.

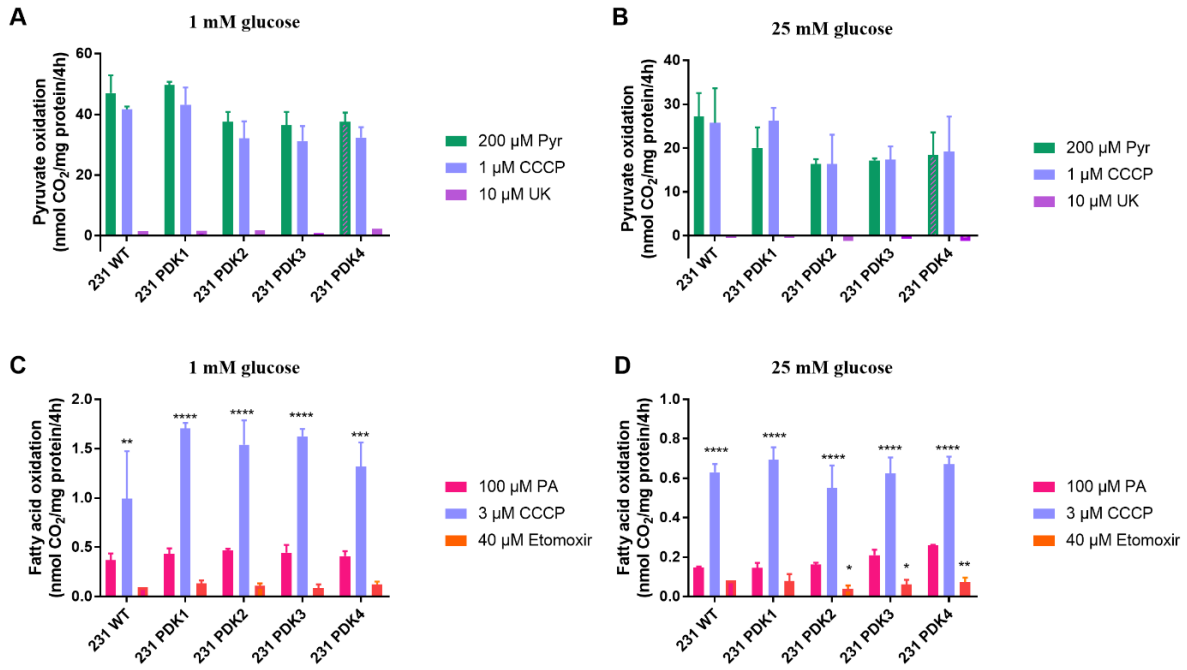

Figure 3.11 Effect of mitochondrial uncoupler and pyruvate and fatty acid oxidation inhibitors on 231 PDK1-4 cells. Pyruvate oxidation was measured from [1-^{14}C]pyruvic acid (0.25 µCi/ml, 200 µM) after being treated with an uncoupling agent CCCP (1 µM) , and MPC blocker, UK-5099 (10 µM) in **(A)** 1 mM and **(B)** 25 mM pre-treated glucose condition . Fatty acid oxidation was measured with [1-^{14}C]palmitic acid (1 µCi/ml, 100 µM) after treated with CCCP (3µM) and mitochondrial β-oxidation inhibitor, etomoxir (40 µM). Data presented as mean of replicates ± SD. *P < 0.05, **P < 0.01, ***P < 0.001, ****P < 0.0001. MPC-mitochondrial pyruvate carrier.

3.5.3 Effect of DCA-mediated PDK inhibition on pyruvate and fatty acid oxidation

Further we wanted to investigate if DCA-mediated inhibition of PDKs can reactivate PDH function, thereby increasing pyruvate oxidation. We also wanted to look at associated effects of DCA on palmitic acid oxidation. To study this, we performed $^{14}CO_2$-trapping analysis with [1-^{14}C]pyruvic acid (0.25 µCi/ml, 200 µM) and [1-^{14}C]palmitic acid (1 µCi/ml, 100 µM) as described above sections, following incubation under normal culturing conditions (25 mM glucose). The experiment was performed with 20 µM, 30 µM, 40 µM, and 50 µM DCA in order to find out the dose-dependent effects of DCA on PDH activity.

Figure 3.12 represents the rate of substrate oxidation in presence of different DCA concentrations. Following 4 h of trapping, no significant differences were observed in pyruvate oxidation between the untreated and DCA-treated groups (Figure 3.12A-E). Though 231 PDK3 cells tended to have slightly increased pyruvate oxidation in presence of 30, 40 and 50 µM DCA, this was not statistically significant. Hence, these data did not support that DCA causes increase pyruvate oxidation upon regaining of PDH activity. Interestingly, significant differences were observed in fatty acid oxidation. Higher DCA concentrations (40, 50 µM) almost blocked palmitic acid oxidation (Figure 3.12 F-J) in each of the cell types. The lowest DCA concentration (20 µM) inhibited fatty acid oxidation in 231 WT and 231 PDK1 cells, but not the others. The results from this experiment need further validation since it was not possible to reproduce the experiment due to time shortage.

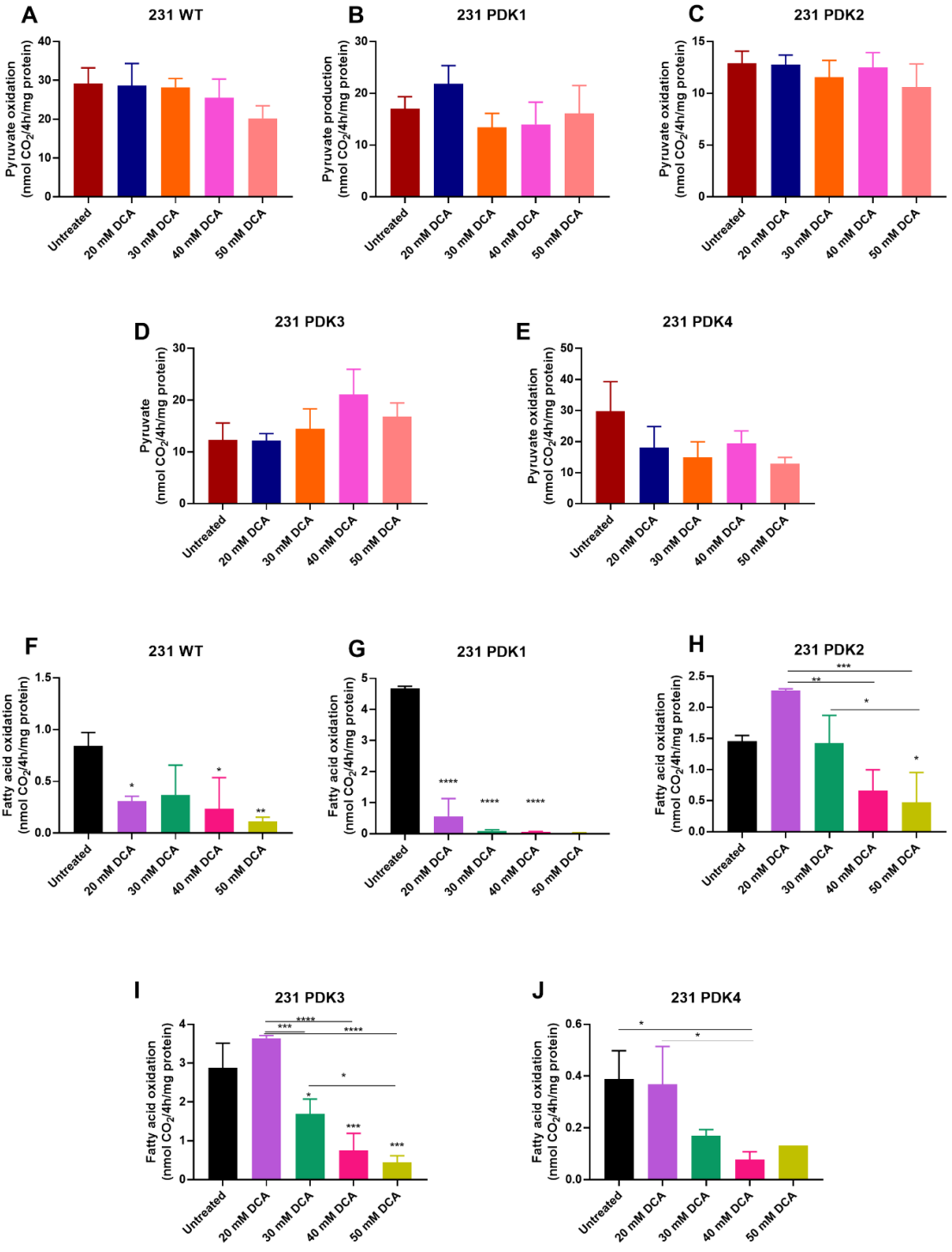

Figure 3.12 Effect of DCA treatment on pyruvate and fatty acid oxidation. 231 WT and PDK1-4 cells were seeded as 45000 cells/well in 96-well CellBind® microplates and incubated overnight in 25 mM glucose condition. DCA titration with 20 µM, 30 µM, 40 µM, and 50 µM concentrations was done prior to 4 h trapping in presence of radiolabeled pyruvic acid (0.25 µCi/ml, 200 µM) and palmitic acid (1 µCi/ml, 100 µM). (A-E) Pyruvate oxidation rate in cell affected by varying DCA concentrations compared to untreated (F-J) Fatty acid oxidation rate in each cell affected by varying DCA concentrations compared to untreated. Data presented as mean of replicates ± SD. *P < 0.05, **P < 0.01, ***P < 0.001, ****P < 0.0001.

4 Discussion

In this study, we investigated the effect of PDK overexpression in cultured cells under different conditions of energy stress. We explored changes in cellular features and metabolic functions due to PDK overexpression, and found that the given metabolic defects triggered potential rescue mechanisms involving metabolic adaptations to the conditional changes.

Since energy is vital for survival, cells are provided with precise mechanisms to maintain proper energy balance and to elicit stress protection responses when needed [51]. Cells have metabolic flexibility that enables them to switch between different pathways or substrates depending on the cellular energy demand or the availability of nutrients and oxygen. Metabolic defects may compromise such ability when the limit exceeded resulting in cellular energy failure with possible consequences of mild cellular stress to cell death [12]. To counteract energy depleted cellular state, cells must activate adaptive mechanisms which theoretically can be referred as metabolic rewiring. Some of the effects of metabolic stress or defects can be mimicked *in vitro* in cultured cell models, and thus can help to characterize mechanisms of metabolic adaptation triggered by those metabolic defects and energy stress.

In this thesis, we interfered with the PDH activity by inducing upregulation of its negative regulator, PDK and then investigated how the cell metabolism and mitochondrial functions are affected in the manipulated cells due to PDK overexpression. The cell model used for this manipulation was the immortalized cell line MDA-MB-231 that represents a highly malignant and poorly differentiated human breast adenocarcinoma line [115]. The use of immortalized cell lines offers enormous possibilities of easy handling and limitless replicative potential. Since they are immortalized and can be grown continuously in culture, they produce comparably a more homogeneous population of cells. They provide advantage experimental replications, and often can tolerate robust treatment conditions which make them ideal to be used as stable cell model. The use of immortal cell lines is not always optimal. Since they are not normal human cells anymore and many of them have been passaged for decades, they do not resemble original cell state since they are prone to genotypic and phenotypic changes [116-118] .

Besides genetic manipulation via PDK overexpression, we created environmental stress by variable glucose conditions, low oxygen, treatment with different metabolic inhibitors and modulators and mitochondrial uncouplers. We then employed different strategies to investigate changes in cell morphology, growth, substrate use and metabolic functions which are discussed below in line with the results obtained.

4.1 Stable transduction leads to significant upregulation of PDK

All four isoforms of PDK were introduced in MDA-MB-231 cell by retroviral transduction and this study demonstrates characterization of these four PDK1-4 overexpressing cells. This overexpression strategy facilitated comparison of the metabolic status and mitochondrial function of 231 PDK1-4 cells with their WT parental cell. At first, induced expression of all four PDKs was confirmed by qPCR and western blot analysis. The PDK1, PDK2, PDK3 and PDK3 probes used were sensitive enough to detect high mRNA expression of respective PDK isoforms in the transduced cells whereas the non-overexpressed PDKs had significantly lower level, comparable to the WT parental mRNA sample (Figure 3.1). The presence of other endogenous PDKs in each of the PDK overexpressing cells were also found to be low. This might not due to the sensitivity of the probes, rather might be the cell and tissue -specific expression manner of the PDK isoforms [54]. This has been reported by many that PDK2 and PDK4 are predominantly expressed in metabolically active tissues like liver, skeletal muscle, heart, and kidney during starvation whereas PDK1 exclusively expressed in heart and PDK3 in brain and testes [72, 119]. Since we used MDA-MB-231 cell line for our study, these cells predominantly express PDK2 and low levels of the other PDK isoforms naturally [120]. However, qPCR analysis confirmed significant upregulation of PDK1-4 upon overexpression, based on their high fold change, though the level of expression was very different among the PDKs, ranging between 60-2000-fold. This might due to the variation in copy number of the PDK mRNAs since a high copy number positively correlates with high expression, which in turn can affect the overall expression of the proteins [121].

A second qPCR quantification also confirmed the presence of inserted constructs (Figure 3.1B) again after a selection process, but the fold changes were reduced to 30- to 350-fold, particularly for the PDK1 and PDK4. One possible reason behind this may be that the part of the vector genes might be lost from the pool because of continuous passaging or the cycles of freezing and thawing somehow affected the gene expression. Another anticipation is that we did not make the cell population from a single clone, rather with all surviving clones after the selection process. Some of them might express the gene required to survive selection, but not the gene we want to over-express. They might grow together with overexpressing cells and eventually result in loss of expression of the target gene within the population (selection processes) [122]. Even though having lower expression than the first measurement, PDK4 was the highest expressed isoform among the other three. The high expression of PDK4 suggests that it may contribute to the regulation of long-term adaptive response of PDH activity [119].

We quantified qPCR data by normalizing to the endogenous reference control, 18S rRNA. Kuchipudi et al. reported that 18S rRNA is the best reference gene upon testing and comparing a set of housekeeping genes [123]. It has a low turnover rate, less prone to changes due to physiological perturbation, and has invariant expression in different organisms, tissues, treatments and developmental stages. One technical limitation of using 18S rRNA is that it lacks poly-A tail, therefore random primers must be used rather than oligo-(DT). Another problem is that 18S rRNA is more abundant than any other typical mRNA transcripts and thus requires dilution to reach the threshold value within the dynamic range of qPCR reaction [123, 124].

Western blot data in Figure 3.2 that shows the protein level expression of PDK1-4 isoforms are also in agreement with the qPCR data. The anti-PDK (1-4) antibodies detected the expression of target PDKs (1-4) in the respective overexpressed cell with high intensity bands. We had all five protein samples (including the 231WT) in a single blot and the expression of other PDK proteins in each overexpressed cell was detected as low. The same was observed in the WT protein sample, indicating downregulation of all four PDK proteins due to poor intensity signals. We used separate blots for each anti-PDK antibody because the four PDK1-4 proteins have very close molecular weight (MW, 46-49 KDa) and the bands are detected at approximately 46 KDa, otherwise the bands might be produced in overlapped with each other making them difficult to differentiate. The same problem happened with the use of α-tubulin as a loading control, α-tubulin has a MW of approximately 50 KDa which is close to the PDKs' MW. Thus, the bands detected via anti- α-tubulin were in overlapping position with the PDK bands that made the quantification procedure difficult. As a result, we continued with the anti-GAPDH antibody which has a MW of 35.8 KDa, and the bands produced were clear enough to perform a proper quantification. Though some researchers recommend not to use GAPDH since it is a metabolic enzyme and can bind to other proteins and the expression is sometimes not stable [125], it was found to be quite good but for our purpose. The molecular weight for the bands of interest was evaluated by comparison to the size of the standard protein bands and was found as reproducible.

4.2 PDK overexpression is associated with increased proliferation in 231 PDK1-4 cells and is affected by glucose limitation

Proliferation study found that the PDK1,3 and 4 overexpressing cells tended to grow faster than the parental WT cells, whereas the 231 PDK2 had slightly reduced proliferation. This was

confirmed by measurement of impedance analysis in the xCELLigence instrument. Unlike from the conventional end-point based proliferation assays, the xCELLigence system provides the advantage of non-invasive monitoring of cell growth including cell adhesion, spreading and proliferation [126]. Since the system detects impedance based on cell attachment, the data we have shown in Figure 3.3 was normalized to first 5 hours after the experiment started (i.e 2h after cell seeding) so that the cells were properly attached to the bottom of the wells. The cell number we used (4000 cells/well) was previously been optimized for similar types of cells in our lab, but the growth curves of 231 PDK1-4 did not seem to reach to their maximum cell index, indicating that the cell number was not optimal for these cells. Since cell number correlates very well with impedance-based monitoring of proliferation, we tried measuring proliferation with higher cell densities but the results were not satisfactory. One possible reason behind this was explained by Man I et al, who found that the quality of the assay is limited by overgrowth of the cells in the wells at very high cell densities, as well as lack of nutrients in the culture media [126]. Therefore, we continued with the 4000 cells/well density. We calculated proliferation rate of the 231 PDK1-4 cells every 24 hours and obtained the similar trend in each time points (Figure 3.3B); 231 PDK1, PDK3, and PDK4 had increased proliferation while PDK2 had reduced proliferation compared to the WT. Our findings suggest that the overexpression caused metabolic adaptation and a subsequent change in their proliferation rate compared to their parental line.

Media was collected form the wells at 24h, 48h, 72h, and 96h, and the concentrations of glucose and lactate present in media was measured (Figure 3.4). This was done mainly to investigate how much glucose was utilized by the cells and how much lactate was produced as a consequence. Interestingly, the glucose level was not that much reduced throughout the 96 hours of growth, and remained around 18-20 mmol/L. This was surprising, since the cells produced up to 5 mmol/L lactate, which is anticipated to originate via glycolytic breakdown of glucose. One possible explanation is that the cells might use another energy source present in the media, for instance glutamine, thus maintaining the glucose concentration at a high level. Another possibility is, we used FBS in media which might contribute to dilution of the glucose concentration in the media. This is the probable reason that we observed 18-20 mM glucose in blank medium instead of 25 mM.

We also characterized effect of glucose deprivation on 231 PDK1-4 proliferation by incuCyte image sequence analysis and resazurin conversion. Several studies have shown that the level of glucose has important effect on cellular responses, and the range of its effect varies from

cell type to cell type [62, 127, 128]. Moreover, the required concentration of glucose in commercial cell culture media often exceeds the glucose level of normal physiological condition (during fasting ~4 mM, after meal ~7.8 mM) [129, 130]. We hypothesized that regulation of the PDH complex through altered expression of PDKs may lead to metabolic adaptations that changes the response to glucose variations, with regards to cell growth. Therefore, we treated the 231 PDK1-4 cells with three different concentrations of glucose, limited supply (1 mM), average supply (5 mM), and high glucose state (25 mM). The growth of the cells was then monitored using the incuCyte imaging instrument, under the same incubation condition as the cells were usually maintained (21% O_2, 5% CO_2, 37^0C). The growth of the 231 PDK1-4 cells were significantly affected by the glucose limited condition (1 mM) compared to the two conditions with higher glucose concentrations, as presented by the growth curves in

Figure ***3.5***. The cultures provided 1 mM glucose grew for approximately 40 h before the cell density reached a plateau and later started to decline, probably due to glucose deprivation. Interestingly, the 231 PDK1 and 231 PDK2 cells appeared to reach glucose deprivation before the three other cell types, however, the growth curves of all the 231 PDK1-4 cultures tended to be below the 231 WT cells in the critical phase when glucose became limiting. This may indicate that the PDK overexpressing cells are more dependent on glucose, but this will have to be confirmed in repeated studies. Overexpression of PDK1-4 did not change the growth in 5 mM glucose, compared to the control, but 231 PDK3 cells displayed slightly increased growth in 25 mM glucose.

To investigate effects on cell viability, the cells were cultured for 72 h under the same glucose conditions as the incuCyte experiment, before we carried out the resazurin conversion assay (Figure 3.6). The data did not suggest the PDK1-4 overexpressing cells have reduced tolerance for low glucose availability (1 mM glucose), compared to the parental cells. However, this represents an endpoint measurement, and comparing with the incuCyte analysis, it may seem that this timepoint (72 h) was too late to cover the most critical phase. In 5 mM and 25 mM glucose, we generally observed increased viability in PDK overexpressing cultures compared to WT cultures. This is relatively consistent with the effects we observed with the other methods of cell proliferation. It is important to be aware that the methods of cell viability and growth employed in this project (xCELLigence, incuCyte, resazurin) assess different cellular features, and therefore may show some variability. For example, 231 PDK1 was found to have the highest proliferation rate, and the 231 PDK2 had the lowest, in xCELLigence analysis,

whereas the same was not observed in incuCyte and resazurin assay. Such differences may be explained by variations between the detected features (e.g. metabolism *versus* cell number), as well as inter-experimental variations that is always an issue in cell culture experiments. Further, cellular resazurin conversion depends on metabolic activity, and may be affected by changes in mitochondrial metabolism which we found changed in the 231 PDK1-4 cells. Besides, the concentration and incubation time of resazurin is also important due to its ability to induce stress mechanisms that lead to reduced proliferation and mitochondrial dysfunction in cultured cells. According to Erikstein et al resazurin exposure was used as a model in investigating cellular stress mechanisms in two leukemia cell lines, HL-60 and Jurkat in one of their studies. They showed that resazurin reduced cell proliferation which ultimately led to autophagy and cell death through the generation of ROS, and concluded resazurin as a toxic mediator of cultured cells [131]. So, care should be taken while using this reagent since it affects vital mechanisms of cellular homeostasis. Therefore, we used 1x diluted concentration of 20x 2.5mg/ml resazurin stock and exposed the cells only for 3h to resazurin.

4.3 PDK overexpression is associated with increased mitochondrial respiration and glycolysis

In order to investigate if metabolic adaptation occurred in 231 PDK1-4 cells, we measured mitochondrial respiration and glycolysis by the seahorse analyzer. The OCR measurement by the mitochondrial stress test indicates how the mitochondria operate when exposed to their weaknesses and also an indicator of overall cellular health [87, 132]. Similarly, measurement of ECAR is the determinant of glycolytic capacity [110].

Analysis of OCR revealed that 231 PDK1-4 cells had higher rates of mitochondrial respiration compared to the WT parental cells; however, this difference was some less pronounced after culturing in 1 mM glucose, compared to 5 mM glucose. In particular, the 231 PDK1, PDK3, and PDK4 cells demonstrated markedly increased basal mitochondrial respiration, ATP-linked respiration as well as maximum capacity in 5 mM glucose condition (Figure 3.8 C-D). Interestingly, the rate of increased mitochondrial respiration in 231 PDK1, PDK3, and PDK4 was somewhat less evident in 25 mM glucose in compared to 5 mM glucose. These glucose-dependent effects on mitochondrial respiration was found to be different in PDK2 overexpressing cell, almost similar to the rate of mitochondrial respiration in 231 WT cell, particularly in 5 mM and 25 mM glucose. Apparently, very low proton leak was observed in each condition (See Figure 3.8D-F) indicating that the mitochondrial integrity is intact, and the

mitochondrial membrane potential remained unchanged in these cells. So, based on the data observed in this study, we interpret that PDK overexpression causes an increased electron flow throughout the respiratory chain in 231 PDK1, PDK3, and PDK4 cells and is coupled to elevated oxidative phosphorylation. However, the optimal CCCP concentration we chose for this study was 1 µM, even though 1.5 µM and 2 µM did also produce quite good respiration profile. CCCP is a strong uncoupler and too high concentration of uncouplers can inhibit mitochondrial function or cause mitochondrial dysfunction [133].

Similarly, we observed increased rates of glycolysis in the 231 PDK1-4 cells, compared to 231 WT cells. The basal glycolysis as well as the glycolytic capacity of the 231 PDK1-4 were significantly higher than WT cells in all glucose conditions (Figure 3.9). When cells experience loss of ATP production in mitochondria due to inhibition of oxidative phosphorylation, either blockage by oligomycin or by low-oxygen tension, they divert cellular metabolism towards glycolysis to make more ATP to maintain cellular energy homeostasis [134]. Similarly, for 231 PDK1-4 cells, we assessed their maximum capacity upon inhibition of mitochondrial respiration by oligomycin. Nevertheless, the ECAR profile of 231 PDK1-4 cells demonstrates very high glycolysis rate in these cells than the parental cells but that does not necessarily mean that the cells are highly glycolytic, since the effects on mitochondrial respiration and glycolysis seemed relatively balanced. Furthermore, the ECAR data suggests that difference in glucose supply does not cause any metabolic adaptation in the glycolytic machinery of the PDK-overexpressing cells. However, if the conditions changed, for example nutrient restriction, use of other substrates except glucose (e.g galactose), and treatment with different modulators might produce different OCR and ECAR profile in these cells. Again, the measurement of complex-I independent OCR by rotenone, non-mitochondrial OCR by antimycin-A and non-glycolytic ECAR by glucose analog 2-DG provided true baseline measurement of OCR and ECAR respectively, at the same time indicated the high sensitivity of the seahorse technique [109].

4.4 PDK overexpression in 231 PDK1-4 cells leads to increased fatty acid oxidation

Cells tend to rewire their metabolic pathways in order to meet their metabolic energy demands and homeostasis. We hypothesize that in contexts of limited glucose supply, there might be a metabolic switch towards increased fatty acid oxidation in the 231 PDK1-4 cells. In this project, we investigated pyruvate and fatty acid oxidation capacity of 231 PDK1-4 cells and particularly focused, and searched for any shift in substrate preference under high and limited

glucose supplied conditions. During *in vitro* studies with cultured cells, mitochondrial pyruvate and fatty acid oxidation can be assessed by using radiolabeled pyruvate and fatty acid substrates as described by Wensaas et al [112]. Therefore, we used [1-^{14}C]pyruvic acid (0.25 µCi/ml) and [1-^{14}C]palmitic acid (1 µCi/ml) followed by trapping and quantifying the $^{14}CO_2$ produced from the 231 PDK1-4 cells. The advantage of this method is that it uses 96-well tissue culture plates with an inverted filter plate on top to capture the $^{14}CO_2$ produced by the cells instead of using conventional tissue culture flasks to trap the $^{14}CO_2$ from isolated organelles, enzymes or intact cells.

We observed that upregulated PDK3 and PDK4 expression tended to cause increased basal mitochondrial fatty acid oxidation rate particularly in 25 mM glucose whereas PDK1 and PDK2 tended to cause increased fatty acid oxidation in 1 mM glucose, compared to their WT parental cells. Conversely, PDK-overexpression was associated with reduced pyruvate oxidation rate in these cells (Figure 3.10). Since PDK1-4 are the four regulatory kinases of PDH that phosphorylate and inhibit PDH [72], the PDH enzyme might be inactive or less active due to PDK overexpression in the 231 PDK1-4 cells. Therefore, the cells were found to mediate a metabolic switch from pyruvate to fatty acid oxidation. Interestingly, the PDK-overexpressing cells were able to activate fatty acid oxidation to a higher extent in glucose limited condition (1 mM) than in the 25 mM glucose, supporting the fact that the adaptation to fatty acid metabolism is stimulated by glucose deprived or glucose limiting conditions.

This kind of metabolic shift towards increased oxidation of fatty acid instead of glucose substrate indicates a causative relationship between PDK overexpression and fatty acid oxidation [135]. Several studies have shown rewiring of metabolic pathways in contexts of substrate utilization in relation to PDK4. Pettersen et al (unpublished work) showed that PDK4 was simultaneously upregulated with fatty acid oxidation related genes in rat liver and heart. They also reported increased fatty acid oxidation in cultured MDA-MB-231 and Hela cells with overexpression of PDK4, concluding that PDK4 can be used as a surrogate marker for stimulated fatty acid oxidation [135]. Chambers et al showed that cardiac specific overexpression of PDK4 in transgenic (myosin heavy chain (MHC)-PDK4) mice exhibits insulin-resistant substrate oxidation profile, characterized by low glucose but high fatty acid oxidation flux [136].

4.5 Characterizing the effects associated with metabolic inhibitors and modulators in 231 PDK1-4 cells

We evaluated the effects of different modulators and inhibitors on 231 PDK1-4 cells in relation to cell proliferation, substrate utilization, and cellular and mitochondrial functions. The effects of respiratory chain and glycolysis modulators have been discussed in the seahorse section. However, we examined some other conditions to further investigate the effect of PDK overexpression in substrate oxidation in presence of inhibitors of glucose and fatty acid metabolism. Since, CPT1 controls the mitochondrial import of fatty acids for β-oxidation as well as MPC controls the pyruvate import [137], we incubated the 231 PDK1-4 cells with the inhibitors of CPT1, etomoxir and MPC inhibitor, UK-5099. Both of them markedly inhibited pyruvate and fatty acid oxidation (Figure 3.11), indicating that both pyruvate and fatty acids need specific transporters for their import to mitochondria. This is also an indicator that mitochondria have vital role in substrate oxidation as well as maintain a balanced metabolic state in the cell. In contrast with these inhibitory effects, incubation with the uncoupling agent CCCP resulted in a small increase in the rate of fatty acid conversion into $^{14}CO_2$, but the effect was not visible in pyruvate oxidation.

We also looked at how DCA-mediated inhibition of PDK influence 231 PDK1-4 cells' proliferation and substrate oxidation rate. Since the cells were found to be dependent on glucose, we used 25 mM glucose condition to execute the effect of DCA. Initially we tried with lower concentration of DCA (10 mM, 20 mM for instance), but no effect was observed, and finally we were able to see a significant effect on cell proliferation at 50 mM DCA concentration. This concentration was found to be effective in some other cells as well in our laboratory. As suggested by Bell et al and Woo et al, PDK2 is most susceptible to DCA due to its ubiquitous expression pattern whereas PDK3 is least sensitive [66, 76], we found such effect in very small extent in our cells. Rather, DCA inhibited proliferation in each of the cells (Figure 3.7). This finding can provide insights on the usefulness of DCA in targeting cancer cells with increased PDK expression. Michelakis's group in 2007 reported that DCA is uniquely toxic to human cancer cells and particularly inhibited the proliferation of human non-small cell lung cancer (A549) tumor xenografts in rats [138]. Other researchers also support that DCA therapy could slow down the formation of cancer, decrease the tumor volume, reduce the rate of proliferation, and could trigger cancerous cell apoptosis. DCA was also found to downregulate

expression of few genes required for cancer survival, for example, suppression of HIF-α expression in cancer cells with high PDK4 expression [139].

We also aimed that inhibition of PDK by DCA might increase mitochondrial pyruvate oxidation by activating the PDH complex. It is also an established therapeutic strategy for reversing the Warburg effect in cancer cells that eventually increase the OXPHOS [139]. For our 231 PDK1-4 cells, instead of increasing, DCA showed a negative effect on the conversion of [1-^{14}C]pyruvate into $^{14}CO_2$, though a minimal effect was visible in 231 PDK3 cells. One possible reason is, since PDK1-4 are highly expressed in the 231 PDK1-3 cells, higher concentration of DCA even more than 50 mM might be needed to fully inhibit the PDKs. Fatty acid oxidation was also drastically reduced upon treatment with DCA, indicating that PDK1-4 were actually inhibited (Figure 3.12). Both these findings gave rise to contradictory interpretations. Therefore, a measurement of end-point lactate level can be an indicator of PDK inhibition. A decreased level of lactate in the media is the immediate result of PDK inhibition in cells [140]. However, we do not rely very much on this finding since we need to optimize the DCA concentration further and also need to repeat this experiment few times.

5 Concluding remarks

In this study, our main aim was to investigate mechanisms of metabolic adaptation upon genetic manipulation in cultured cells, and how these are influenced by energy stress and mitochondrial modulation. We introduced PDK1-4 overexpression in MDA-MB-231 cells and gene expression study confirmed that the PDK1-4 are highly expressed in the respective cells. Subsequently, metabolism in cells overexpressing PDK1, PDK3, and PDK4 was found to be characterized by increased rates fatty acid oxidation, glycolysis and mitochondrial respiration, and generally accompanied by increased proliferation. Interestingly, high PDK1-4 expression appeared to reduce the capacity of metabolic adaptation in response to reduced glucose supply, possibly since the rates mitochondrial oxidation and respiration were already high under well-supplied glucose conditions. Taken together, and supported by the proliferation studies, the findings further support that the PDK overexpressing cells are more dependent on glucose for optimal growth.

The increased metabolic rates are consistent with increased growth. Modulation of mitochondrial ETC and glycolysis confirmed that the integrity of glycolysis and mitochondrial respiration was intact. One remarkable finding of our study was that PDK overexpression

tended to cause a metabolic shift from pyruvate to fatty acid oxidation, indicating a metabolic adaptation towards increased rates of mitochondrial fatty acid oxidation. Inhibitors of pyruvate and fatty acid transporters were used to confirm the specificity of the measurements. The PDK inhibitor DCA was found to be a highly capable inhibitor of proliferation and fatty acid oxidation in this model.

The data generated from this study put insights on how cells rewire their metabolism upon genetic modulation and conditional energy demands and also some implications related to PDH impairment in cell.

6 Future perspectives

In our study, we have investigated the effect of PDK overexpression and characterized the associated mechanisms of metabolic adaptation in terms of proliferation, viability, glucose dependency, mitochondrial respiration, glycolytic capacity, and substrate oxidation rate in cultured cells. Though most of the other studies that have been done so far related to PDK overexpression are based on PDK4 expression, we have been able to characterize increased expression of all four PDK4 isoforms in our cell model. Some of the works need to be repeated for more reliable data. For example, we tried to regain PDH activity and subsequent pyruvate oxidation by inhibiting PDK with DCA. This could be a good approach to confirm the effects of PDK overexpression. However, some further optimization of experimental methods and DCA concentration will be necessary. Treatment with other inhibitors, such as PDK subtype specific inhibitors, may also be included to further pursue the experimental findings in this thesis. We found potential effect on glucose dependency of the PDK overexpressing cells. To further investigate this effect, it could be a good idea to study cellular proliferation in presence of other carbohydrate sources, such as galactose which is known to require mitochondrial metabolism to obtain a net yield of ATP. Due to time limitation, we were not able to investigate the effect of hypoxia in cell growth, which we intend to do in future; however, we managed to see the effect under normoxic condition to some extent.

Our next plan is to carry out gene expression study on OXPHOS proteins and fatty acid oxidation related genes in these cells as well as to look at nutrient- and energy-sensitive factors such as expression of AMPK, the family of peroxisome proliferator-activated receptor transcription factors (PPARs), and the activation of Akt/mTOR. Besides, we will be looking at mitochondrial respiration and substrate oxidation rate after treatment with different modulators

such as pharmacological activator of AMPK (5-aminoimidazole-4-carboxamide ribonucleotide, AICAR), PPARα-agonists, such as WY-14,643, modified fatty acids (e.g tetradecylthioacetic acid, TTA) and other uncouplers such as 2,4-Dinitrophenol (DNP). Another future direction might include investigating the effect of metabolic modulation on ROS production for instance, by flow cytometry.

We also look forward to investigate the involvement of PDK overexpression in any particular disease and if it contributes to therapy resistance. Furthermore, data generated from *in vitro* studies often require validation via *in vivo* studies. Since PDKs are extremely tissue specific, in vivo studies will provide tissue specific expression profile of PDK 1-4 isoforms as well as substrate oxidation rate in different tissues after being treated with modified high-fat or glucose-rich diet. We also have other cell lines with PDK overexpression in our lab (e.g Hela, C2C12, Huh7), so comparing the effects of PDK overexpression in cellular and metabolic changes between cell lines will be another possible approach for rewiring of metabolism. In a manuscript currently under evaluation for publication in a scientific journal, we characterized PDK4 mRNA expression as a sensitive surrogate marker of fatty acid oxidation. Therefore, we aim to investigate PDK4 expression in clinical samples from patients with relevant diseases.

7 References

1. Ernster, L. and G. Schatz, Mitochondria: a historical review. The Journal of cell biology, 1981. **91**(3 Pt 2): p. 227s-255s.
2. Lunt, S.Y. and M.G.V. Heiden, Aerobic Glycolysis: Meeting the Metabolic Requirements of Cell Proliferation. 2011. **27**(1): p. 441-464.
3. Salway, J.G., Metabolism at a glance. 4th ed. 2017, Chichester: Willey-Blackwell.
4. Goodpaster, B.H. and L.M. Sparks, Metabolic Flexibility in Health and Disease. Cell Metab, 2017. **25**(5): p. 1027-1036.
5. Galgani, J.E., C. Moro, and E. Ravussin, Metabolic flexibility and insulin resistance. Am J Physiol Endocrinol Metab, 2008. **295**(5): p. E1009-17.
6. Friedman, J.R. and J. Nunnari, Mitochondrial form and function. Nature, 2014. **505**(7483): p. 335-343.
7. Hodneland Nilsson, L.I., et al., A new live-cell reporter strategy to simultaneously monitor mitochondrial biogenesis and morphology. Scientific reports, 2015. **5**: p. 17217-17217.
8. van Wijk, R. and W.W. van Solinge, The energy-less red blood cell is lost: erythrocyte enzyme abnormalities of glycolysis. Blood, 2005. **106**(13): p. 4034-42.
9. Bruce Alberts, A.J., Julian Lewis, Martin Raff, Keith Roberts, and Peter Walter, The Mitochondrion, in Molecular Biology of the Cell. 2002, Garland Science: New York.
10. Khalifat, N., et al., Membrane deformation under local pH gradient: mimicking mitochondrial cristae dynamics. Biophysical journal, 2008. **95**(10): p. 4924-4933.
11. Tronstad, K.J., et al., Regulation and quantification of cellular mitochondrial morphology and content. Curr Pharm Des, 2014. **20**(35): p. 5634-52.
12. Nikolaisen, J., et al., Automated Quantification and Integrative Analysis of 2D and 3D Mitochondrial Shape and Network Properties. PLOS ONE, 2014. **9**(7): p. e101365.
13. Ryan, M.T. and N.J. Hoogenraad, Mitochondrial-nuclear communications. Annu Rev Biochem, 2007. **76**: p. 701-22.
14. Nass, M.M. and S. Nass, INTRAMITOCHONDRIAL FIBERS WITH DNA CHARACTERISTICS. I. FIXATION AND ELECTRON STAINING REACTIONS. J Cell Biol, 1963. **19**: p. 593-611.
15. Aziz, A., Understanding Mitochondrial DNA in Brain Tumorigenesis. 2015. p. 3-27.
16. Birky, C.W., Jr., The inheritance of genes in mitochondria and chloroplasts: laws, mechanisms, and models. Annu Rev Genet, 2001. **35**: p. 125-48.
17. Smith, E. and H.J. Morowitz, Universality in intermediary metabolism. 2004. **101**(36): p. 13168-13173.
18. DeBerardinis, R.J. and C.B. Thompson, Cellular metabolism and disease: what do metabolic outliers teach us? Cell, 2012. **148**(6): p. 1132-44.
19. Alberts B, J.A., Lewis J, How Cells Obtain Energy from Food, in Molecular Biology of the Cell. 2002, Garland Science: New York.
20. Cura, A.J. and A. Carruthers, Role of monosaccharide transport proteins in carbohydrate assimilation, distribution, metabolism, and homeostasis. Comprehensive Physiology, 2012. **2**(2): p. 863-914.
21. Berg, J.M., Metabolism, in Biochemistry. 2015, Macmillan learning.
22. Reinmuth, O.M., et al., Total cerebral blood flow and metabolism in human brain stem disease. Neurology, 1968. **18**(3): p. 280-1.
23. Bing, R.J., et al., Metabolism of the human heart. II. Studies on fat, ketone and amino acid metabolism. Am J Med, 1954. **16**(4): p. 504-15.
24. Owen, O.E., et al., Brain metabolism during fasting. J Clin Invest, 1967. **46**(10): p. 1589-95.
25. Van de Vyver, C., et al., An Exceptional Case of Diabetic Ketoacidosis. Case reports in emergency medicine, 2017. **2017**: p. 4351620-4351620.
26. Coyle, E.F., Substrate utilization during exercise in active people. Am J Clin Nutr, 1995. **61**(4 Suppl): p. 968s-979s.
27. Trayhurn, P. and J.H. Beattie, Physiological role of adipose tissue: white adipose tissue as an endocrine and secretory organ. Proc Nutr Soc, 2001. **60**(3): p. 329-39.

28. Ebeling, P., H.A. Koistinen, and V.A. Koivisto, Insulin-independent glucose transport regulates insulin sensitivity. FEBS Lett, 1998. **436**(3): p. 301-3.
29. TeSlaa, T. and M.A. Teitell, Techniques to monitor glycolysis. Methods Enzymol, 2014. **542**: p. 91-114.
30. Berg JM, T.J., Stryer L, The Glycolytic Pathway Is Tightly Controlled in Biochemistry. 2002, W H Freeman: New York.
31. Abuelgassim, A.O., A.M. Salem, and S.M. Khoja, Allosteric control of 6-phosphofructo-1-kinase from rat lung. Comp Biochem Physiol B, 1992. **101**(1-2): p. 135-8.
32. Anderson, N.M., et al., The emerging role and targetability of the TCA cycle in cancer metabolism. Protein Cell, 2018. **9**(2): p. 216-237.
33. Berg JM, T.J., Stryer L, The Citric Acid Cycle, in Biochemistry. 2002, W H freeman: New York.
34. Herzig, S., et al., Identification and functional expression of the mitochondrial pyruvate carrier. Science, 2012. **337**(6090): p. 93-6.
35. Akram, M., Citric acid cycle and role of its intermediates in metabolism. Cell Biochem Biophys, 2014. **68**(3): p. 475-8.
36. Raimundo, N., B.E. Baysal, and G.S. Shadel, Revisiting the TCA cycle: signaling to tumor formation. Trends in molecular medicine, 2011. **17**(11): p. 641-649.
37. Ryan, D.G., et al., Coupling Krebs cycle metabolites to signalling in immunity and cancer. Nature Metabolism, 2019. **1**(1): p. 16-33.
38. Salway, J.G., Medical biochemistry at a glance. 3rd ed. ed. At a glance series. 2012, Chichester: Wiley-Blackwell.
39. Smeitink, J., L. van den Heuvel, and S. DiMauro, The genetics and pathology of oxidative phosphorylation. Nat Rev Genet, 2001. **2**(5): p. 342-52.
40. Boyer, P.D., THE ATP SYNTHASE—A SPLENDID MOLECULAR MACHINE. 1997. **66**(1): p. 717-749.
41. Cooper, G.M., The Mechanism of Oxidative Phosphorylation, in The Cell: A Molecular Approach. 2000, Sinauer Associates: Sunderland, MA.
42. C Rodick, T., et al., Potential role of coenzyme Q10 in health and disease conditions. Vol. Volume 10. 2018. 1-11.
43. Jump, D.B. and S.D. Clarke, Regulation of gene expression by dietary fat. Annu Rev Nutr, 1999. **19**: p. 63-90.
44. Eaton, S., Control of mitochondrial beta-oxidation flux. Prog Lipid Res, 2002. **41**(3): p. 197-239.
45. Su, X. and N.A. Abumrad, Cellular fatty acid uptake: a pathway under construction. Trends Endocrinol Metab, 2009. **20**(2): p. 72-7.
46. Bonnefont, J.P., et al., Carnitine palmitoyltransferases 1 and 2: biochemical, molecular and medical aspects. Mol Aspects Med, 2004. **25**(5-6): p. 495-520.
47. Kerner, J. and C. Hoppel, Fatty acid import into mitochondria. Biochim Biophys Acta, 2000. **1486**(1): p. 1-17.
48. Houten, S.M. and R.J. Wanders, A general introduction to the biochemistry of mitochondrial fatty acid beta-oxidation. J Inherit Metab Dis, 2010. **33**(5): p. 469-77.
49. Wanders, R.J.A., et al., The enzymology of mitochondrial fatty acid beta-oxidation and its application to follow-up analysis of positive neonatal screening results. Journal of inherited metabolic disease, 2010. **33**(5): p. 479-494.
50. Hiltunen, J.K. and Y. Qin, beta-oxidation - strategies for the metabolism of a wide variety of acyl-CoA esters. Biochim Biophys Acta, 2000. **1484**(2-3): p. 117-28.
51. Fulda, S., et al., Cellular Stress Responses: Cell Survival and Cell Death %J International Journal of Cell Biology. 2010. **2010**: p. 23.
52. Poljšak, B. and I. Milisav, Clinical implications of cellular stress responses. Bosn J Basic Med Sci, 2012. **12**(2): p. 122-6.
53. Smith, R.L., et al., Metabolic Flexibility as an Adaptation to Energy Resources and Requirements in Health and Disease. Endocrine Reviews, 2018. **39**(4): p. 489-517.
54. Zhang, S., et al., The pivotal role of pyruvate dehydrogenase kinases in metabolic flexibility. Nutr Metab (Lond), 2014. **11**(1): p. 10.

55. Kelley, D.E. and L.J. Mandarino, Fuel selection in human skeletal muscle in insulin resistance: a reexamination. 2000. **49**(5): p. 677-683.
56. Wang, S., P. Song, and M.H. Zou, AMP-activated protein kinase, stress responses and cardiovascular diseases. Clin Sci (Lond), 2012. **122**(12): p. 555-73.
57. Hardie, D.G., F.A. Ross, and S.A. Hawley, AMPK: a nutrient and energy sensor that maintains energy homeostasis. Nat Rev Mol Cell Biol, 2012. **13**(4): p. 251-62.
58. Hardie, D.G., AMPK and autophagy get connected. The EMBO journal, 2011. **30**(4): p. 634-635.
59. Uttara, B., et al., Oxidative stress and neurodegenerative diseases: a review of upstream and downstream antioxidant therapeutic options. Current neuropharmacology, 2009. **7**(1): p. 65-74.
60. Perlman, J.M., Summary proceedings from the neurology group on hypoxic-ischemic encephalopathy. Pediatrics, 2006. **117**(3 Pt 2): p. S28-33.
61. Naifeh J, V.M., Aerobic glycolysis, in Biochemistry. 2019, StatPearls Publishing.
62. Elstrom, R.L., et al., Akt stimulates aerobic glycolysis in cancer cells. Cancer Res, 2004. **64**(11): p. 3892-9.
63. Burgering, B.M. and P.J. Coffer, Protein kinase B (c-Akt) in phosphatidylinositol-3-OH kinase signal transduction. Nature, 1995. **376**(6541): p. 599-602.
64. Yamada, K.M. and M. Araki, Tumor suppressor PTEN: modulator of cell signaling, growth, migration and apoptosis. J Cell Sci, 2001. **114**(Pt 13): p. 2375-82.
65. Lopaschuk, G.D., I.M. Rebeyka, and M.F. Allard, Metabolic modulation: a means to mend a broken heart. Circulation, 2002. **105**(2): p. 140-2.
66. Bell, H. and E. Thomas Parkin, Pyruvate dehydrogenase kinase inhibition: Reversing the Warburg effect in cancer therapy. Vol. 4. 2016. 4215.
67. Patel, M.S., L.G. Korotchkina, and S. Sidhu, Interaction of E1 and E3 components with the core proteins of the human pyruvate dehydrogenase complex. Journal of molecular catalysis. B, Enzymatic, 2009. **61**(1-2): p. 2-6.
68. Jeoung, N.H., Pyruvate Dehydrogenase Kinases: Therapeutic Targets for Diabetes and Cancers. Diabetes & metabolism journal, 2015. **39**(3): p. 188-197.
69. Sradhanjali, S. and M.M. Reddy, Inhibition of Pyruvate Dehydrogenase Kinase as a Therapeutic Strategy against Cancer. Curr Top Med Chem, 2018. **18**(6): p. 444-453.
70. Klyuyeva, A., et al., Tissue-specific kinase expression and activity regulate flux through the pyruvate dehydrogenase complex. J Biol Chem, 2019. **294**(3): p. 838-851.
71. Stacpoole, P.W., Therapeutic Targeting of the Pyruvate Dehydrogenase Complex/Pyruvate Dehydrogenase Kinase (PDC/PDK) Axis in Cancer. JNCI: Journal of the National Cancer Institute, 2017. **109**(11).
72. Jeong, J.Y., et al., Transcriptional regulation of pyruvate dehydrogenase kinase. Diabetes & metabolism journal, 2012. **36**(5): p. 328-335.
73. Fluge, Ø., et al., Metabolic profiling indicates impaired pyruvate dehydrogenase function in myalgic encephalopathy/chronic fatigue syndrome. JCI insight, 2016. **1**(21): p. e89376-e89376.
74. Sousa, B., J. Pereira, and J. Paredes, The Crosstalk Between Cell Adhesion and Cancer Metabolism. 2019. **20**(8): p. 1933.
75. Epstein, T., R.A. Gatenby, and J.S. Brown, The Warburg effect as an adaptation of cancer cells to rapid fluctuations in energy demand. PloS one, 2017. **12**(9): p. e0185085-e0185085.
76. Woo, S.H., et al., Dichloroacetate potentiates tamoxifen-induced cell death in breast cancer cells via downregulation of the epidermal growth factor receptor. Oncotarget, 2016. **7**(37): p. 59809-59819.
77. Robbins, D. and Y. Zhao, New aspects of mitochondrial Uncoupling Proteins (UCPs) and their roles in tumorigenesis. International journal of molecular sciences, 2011. **12**(8): p. 5285-5293.
78. Ledesma, A., M.G. de Lacoba, and E. Rial, The mitochondrial uncoupling proteins. Genome Biol, 2002. **3**(12): p. Reviews3015.
79. Busiello, R.A., S. Savarese, and A. Lombardi, Mitochondrial uncoupling proteins and energy metabolism. Front Physiol, 2015. **6**: p. 36.
80. Ricquier, D. and F. Bouillaud, Mitochondrial uncoupling proteins: from mitochondria to the regulation of energy balance. J Physiol, 2000. **529 Pt 1**(Pt 1): p. 3-10.

81. Marchi, S., et al., Mitochondria-ros crosstalk in the control of cell death and aging. Journal of signal transduction, 2012. **2012**: p. 329635-329635.
82. Trotta, A.P., et al., Disruption of mitochondrial electron transport chain function potentiates the pro-apoptotic effects of MAPK inhibition. The Journal of biological chemistry, 2017. **292**(28): p. 11727-11739.
83. Terada, H., Uncouplers of oxidative phosphorylation. Environmental health perspectives, 1990. **87**: p. 213-218.
84. Wyatt, C.N. and K.J. Buckler, The effect of mitochondrial inhibitors on membrane currents in isolated neonatal rat carotid body type I cells. The Journal of physiology, 2004. **556**(Pt 1): p. 175-191.
85. Ruas, J.S., et al., Underestimation of the Maximal Capacity of the Mitochondrial Electron Transport System in Oligomycin-Treated Cells. PLOS ONE, 2016. **11**(3): p. e0150967.
86. Won, J.H., et al., Rotenone-induced Impairment of Mitochondrial Electron Transport Chain Confers a Selective Priming Signal for NLRP3 Inflammasome Activation. J Biol Chem, 2015. **290**(45): p. 27425-37.
87. Agilent Seahorse XF Cell Mito Stress Test Kit User Guide. 2017, Agilent Technologies, Inc: Wilmington, DE 19808-1610 USA.
88. Stewart, J.B. and P.F. Chinnery, The dynamics of mitochondrial DNA heteroplasmy: implications for human health and disease. Nat Rev Genet, 2015. **16**(9): p. 530-42.
89. Taylor, R.W. and D.M. Turnbull, Mitochondrial DNA mutations in human disease. Nature reviews. Genetics, 2005. **6**(5): p. 389-402.
90. Johannsen, D.L. and E. Ravussin, The role of mitochondria in health and disease. Current opinion in pharmacology, 2009. **9**(6): p. 780-786.
91. Taylor, M.R., et al., A zebrafish model for pyruvate dehydrogenase deficiency: Rescue of neurological dysfunction and embryonic lethality using a ketogenic diet. 2004. **101**(13): p. 4584-4589.
92. Atherton, H.J., et al., Role of pyruvate dehydrogenase inhibition in the development of hypertrophy in the hyperthyroid rat heart: a combined magnetic resonance imaging and hyperpolarized magnetic resonance spectroscopy study. Circulation, 2011. **123**(22): p. 2552-2561.
93. Simsek, T., et al., The distinct metabolic profile of hematopoietic stem cells reflects their location in a hypoxic niche. Cell Stem Cell, 2010. **7**(3): p. 380-90.
94. Liberti, M.V. and J.W. Locasale, The Warburg Effect: How Does it Benefit Cancer Cells? Trends in biochemical sciences, 2016. **41**(3): p. 211-218.
95. Vander Heiden, M.G., L.C. Cantley, and C.B. Thompson, Understanding the Warburg effect: the metabolic requirements of cell proliferation. Science (New York, N.Y.), 2009. **324**(5930): p. 1029-1033.
96. Adekola, K., S.T. Rosen, and M. Shanmugam, Glucose transporters in cancer metabolism. Current opinion in oncology, 2012. **24**(6): p. 650-654.
97. Domblides, C., L. Lartigue, and B. Faustin, Metabolic Stress in the Immune Function of T Cells, Macrophages and Dendritic Cells. Cells, 2018. **7**(7): p. 68.
98. Mathupala, S.P., A. Rempel, and P.L. Pedersen, Glucose catabolism in cancer cells: identification and characterization of a marked activation response of the type II hexokinase gene to hypoxic conditions. J Biol Chem, 2001. **276**(46): p. 43407-12.
99. Mathupala, S.P., Y.H. Ko, and P.L. Pedersen, Hexokinase II: cancer's double-edged sword acting as both facilitator and gatekeeper of malignancy when bound to mitochondria. Oncogene, 2006. **25**(34): p. 4777-4786.
100. King, A., M.A. Selak, and E. Gottlieb, Succinate dehydrogenase and fumarate hydratase: linking mitochondrial dysfunction and cancer. Oncogene, 2006. **25**(34): p. 4675-82.
101. Maziveyi, M. and S.K. Alahari, Cell matrix adhesions in cancer: The proteins that form the glue. Oncotarget, 2017. **8**(29): p. 48471-48487.
102. Strober, W., Trypan blue exclusion test of cell viability. Curr Protoc Immunol, 2001. **Appendix 3**: p. Appendix 3B.
103. Joyce, C., Quantitative RT-PCR. A review of current methodologies. Methods Mol Biol, 2002. **193**: p. 83-92.

104. Karlen, Y., et al., Statistical significance of quantitative PCR. BMC Bioinformatics, 2007. **8**: p. 131.
105. Rao, X., et al., An improvement of the 2ˆ(-delta delta CT) method for quantitative real-time polymerase chain reaction data analysis. Biostatistics, bioinformatics and biomathematics, 2013. **3**(3): p. 71-85.
106. Ke, N., et al., The xCELLigence system for real-time and label-free monitoring of cell viability. Methods Mol Biol, 2011. **740**: p. 33-43.
107. Borra, R.C., et al., A simple method to measure cell viability in proliferation and cytotoxicity assays. 2009. **23**(3): p. 255-262.
108. Riss, T., M. O'Brien, and R.J.C.n. Moravec, Choosing the right cell-based assay for your research. 2003. **6**(1): p. 6.
109. Yang, M., et al., Bioenergetic profile of human coronary artery smooth muscle cells and effect of metabolic intervention. PLOS ONE, 2017. **12**(5): p. e0177951.
110. Agilent Seahorse XF Glycolysis Stress Test Kit User Guide. 2017, Agilent Technologies, Inc.: Wilmington, DE 19808-1610 USA.
111. Collins, C.L., et al., Multiwell 14CO2-capture assay for evaluation of substrate oxidation rates of cells in culture. Biotechniques, 1998. **24**(5): p. 803-8.
112. Wensaas, A.J., et al., Cell-based multiwell assays for the detection of substrate accumulation and oxidation. J Lipid Res, 2007. **48**(4): p. 961-7.
113. McKeown, S.R., Defining normoxia, physoxia and hypoxia in tumours-implications for treatment response. Br J Radiol, 2014. **87**(1035): p. 20130676.
114. Nayak, M.K., et al., Dichloroacetate, an inhibitor of pyruvate dehydrogenase kinases, inhibits platelet aggregation and arterial thrombosis. Blood advances, 2018. **2**(15): p. 2029-2038.
115. Burdall, S.E., et al., Breast cancer cell lines: friend or foe? Breast cancer research : BCR, 2003. **5**(2): p. 89-95.
116. Freshney, R.I., Culture of Animal Cells: A Manual of Basic Technique and Specialized Applications. 2016, Wiley-Blackwell: New Jersey.
117. Nagaraja, G.M., et al., Gene expression signatures and biomarkers of noninvasive and invasive breast cancer cells: comprehensive profiles by representational difference analysis, microarrays and proteomics. Oncogene, 2006. **25**(16): p. 2328-2338.
118. Stacey, G., Primary Cell Cultures and Immortal Cell Lines, in eLS. 2006, John Wiley & Sons, Ltd.
119. Bowker-Kinley, M.M., et al., Evidence for existence of tissue-specific regulation of the mammalian pyruvate dehydrogenase complex. Biochem J, 1998. **329 (Pt 1)**: p. 191-6.
120. Gang, B.P., et al., Targeting of two aspects of metabolism in breast cancer treatment. Cancer biology & therapy, 2014. **15**(11): p. 1533-1541.
121. Myhre, S., et al., Influence of DNA copy number and mRNA levels on the expression of breast cancer related proteins. Molecular oncology, 2013. **7**(3): p. 704-718.
122. Zitzmann, J., et al., Single-cell cloning enables the selection of more productive Drosophila melanogaster S2 cells for recombinant protein expression. Biotechnology reports (Amsterdam, Netherlands), 2018. **19**: p. e00272-e00272.
123. Kuchipudi, S.V., et al., 18S rRNA is a reliable normalisation gene for real time PCR based on influenza virus infected cells. Virology journal, 2012. **9**: p. 230-230.
124. Nestorov, J., et al., Gene Expression Studies: How to Obtain Accurate and Reliable Data by Quantitative Real-Time RT PCR / IZUČAVANJE EKSPRESIJE GENA: KAKO DOBITI TAČNE I POUZDANE PODATKE KVANTITATIVNIM RT PCR-OM U REALNOM VREMENU. 2013. **32**(4): p. 325.
125. Goasdoue, K., et al., Standard loading controls are not reliable for Western blot quantification across brain development or in pathological conditions. Electrophoresis, 2016. **37**(4): p. 630-4.
126. Man, I., et al., Novel real-time cell analysis platform for the dynamic monitoring of ionizing radiation effects on human tumor cell lines and primary fibroblasts. Mol Med Rep, 2015. **12**(3): p. 4610-1619.
127. Berger, E., et al., Gene Network Analysis of Glucose Linked Signaling Pathways and Their Role in Human Hepatocellular Carcinoma Cell Growth and Survival in HuH7 and HepG2 Cell Lines. BioMed research international, 2015. **2015**: p. 821761-821761.

128. Han, J., M.A. Hughes, and G.W. Cherry, Effect of glucose concentration on the growth of normal human dermal fibroblasts in vitro. J Wound Care, 2004. **13**(4): p. 150-3.
129. Buzzai, M., et al., The glucose dependence of Akt-transformed cells can be reversed by pharmacologic activation of fatty acid beta-oxidation. Oncogene, 2005. **24**(26): p. 4165-73.
130. Kleman, A.M., et al., Physiological glucose is critical for optimized neuronal viability and AMPK responsiveness in vitro. J Neurosci Methods, 2008. **167**(2): p. 292-301.
131. Erikstein, B.S., et al., Cellular stress induced by resazurin leads to autophagy and cell death via production of reactive oxygen species and mitochondrial impairment. Journal of cellular biochemistry, 2010. **111**(3): p. 574-584.
132. Haylett, W., et al., Altered Mitochondrial Respiration and Other Features of Mitochondrial Function in Parkin-Mutant Fibroblasts from Parkinson's Disease Patients. Parkinsons Dis, 2016. **2016**: p. 1819209.
133. Lou, P.-H., et al., Mitochondrial uncouplers with an extraordinary dynamic range. The Biochemical journal, 2007. **407**(1): p. 129-140.
134. Pike Winer, L.S. and M. Wu, Rapid Analysis of Glycolytic and Oxidative Substrate Flux of Cancer Cells in a Microplate. PLOS ONE, 2014. **9**(10): p. e109916.
135. Ina Katrine Nitschke Pettersen, D.T., Lena Hansen, Sissel Elisabeth Dyrstad, Hanan Ashrafi, Xiao-Zheng Liu, Linn IH Nilsson, Nils Gunnar Løvsletten, Kjetil Berg, Hege Wergedahl, Bodil Bjørndal, Olav Mella, Øystein Fluge, Ove Bruland, Arild Rustan, Nils Halberg, Gro Vatne Røsland, Rolf Kristian Bergem, Karl Johan Tronstad, Increased PDK4 mRNA expression is a sensitive marker of upregulated fatty acid oxidation. 2019.
136. Chambers, K.T., et al., Chronic inhibition of pyruvate dehydrogenase in heart triggers an adaptive metabolic response. The Journal of biological chemistry, 2011. **286**(13): p. 11155-11162.
137. Fillmore, N. and G.D. Lopaschuk, Targeting mitochondrial oxidative metabolism as an approach to treat heart failure. Biochimica et Biophysica Acta (BBA) - Molecular Cell Research, 2013. **1833**(4): p. 857-865.
138. Bonnet, S., et al., A mitochondria-K+ channel axis is suppressed in cancer and its normalization promotes apoptosis and inhibits cancer growth. Cancer Cell, 2007. **11**(1): p. 37-51.
139. Zhang, W., et al., Targeting Tumor Metabolism for Cancer Treatment: Is Pyruvate Dehydrogenase Kinases (PDKs) a Viable Anticancer Target? International journal of biological sciences, 2015. **11**(12): p. 1390-1400.
140. Michelakis, E.D., L. Webster, and J.R. Mackey, Dichloroacetate (DCA) as a potential metabolic-targeting therapy for cancer. British journal of cancer, 2008. **99**(7): p. 989-994.

8 Appendix

8.1 Effect of low oxygen condition in the viability of PDK-overexpressing cells

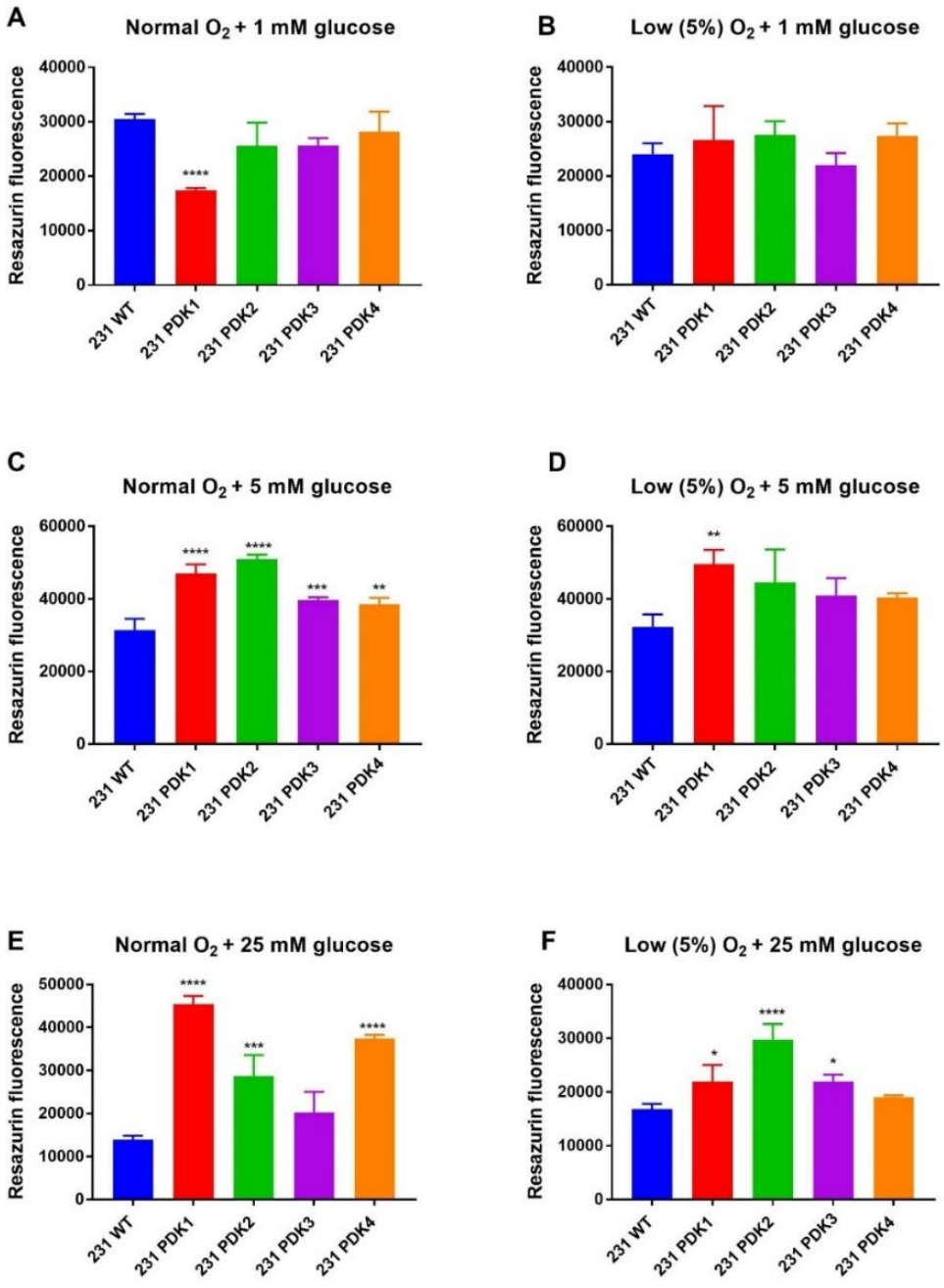

Figure 8.1 Comparison of cell viability in PDK-overexpressing cells under normal and physiological oxygen condition. The measurements were done with 3000 cells/well after 72 h incubation, followed by 3h resazurin conversion assay. Resazurin fluorescence indicating differences in viability between normal (21%) and low oxygen (5%) condition in (A-B) 1 mM glucose, (C-D) 5 mM glucose, and (E-F) 25 mM glucose. The graphs represent mean of three technical replicates ± SD. *P < 0.05, **P < 0.01, ***P < 0.001, ****P < 0.0001.

8.2 Determination of optimal CCCP concentration for assessing maximum mitochondrial respiration

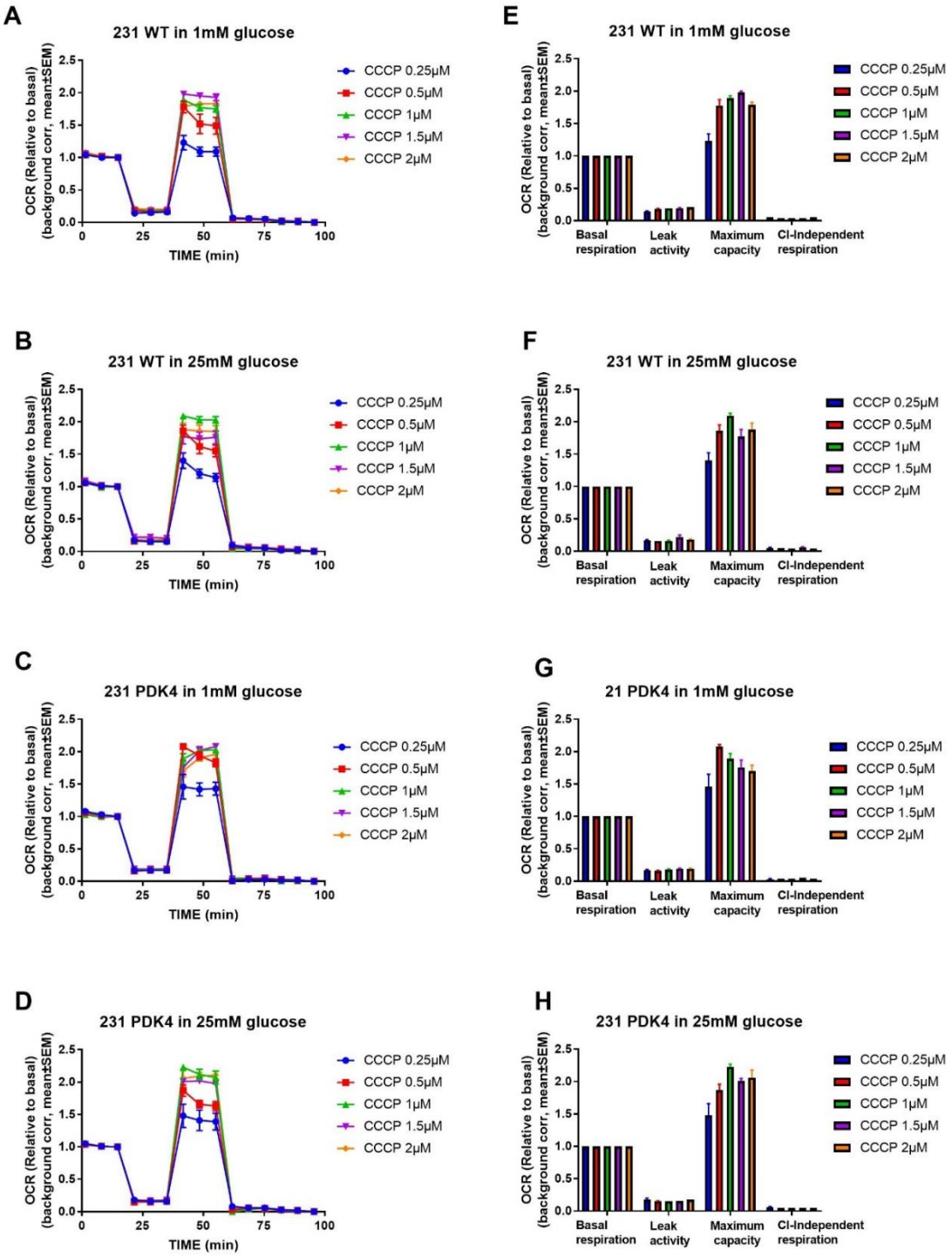

Figure 8.2 Mitochondrial stress test to determine optimal CCCP concentration. Oxygen consumption rate (OCR) was measured in basal DMEM assay medium supplemented with 10 mM glucose, 2mM pyruvate, and 2 mM L-glutamine with 30000 cells/well. Representative traces of OCR (pmol O_2/min/μg protein) obtained after sequential addition of 3 μM oligomycin, CCCP (0.25 μM, 0.5 μM, 1 μM, 1.5 μM, and 2 μM), 1 μM rotenone and 1 μM antimycin A in **(A-B)** 231 WT cells and **(C-D)** 231 PDK4 cells after overnight pretreatments with 1 mM and 25 mM glucose respectively. **(E-H)** Data extracted from **A-B** and **C-D** were

analyzed to calculate basal respiration, leak respiratory rate due to leakage of protons after oligomycin addition; maximum capacity (uncoupled respiration) after addition of CCCP, and CI-independent respiration after rotenone addition. The results presented here are corrected for non-mitochondrial respiration and normalized protein content. The figures display representative data as mean ± SEM.

8.3 Effect of PDK overexpression in the oxidation of glucose by 231 PDK1-4 cells

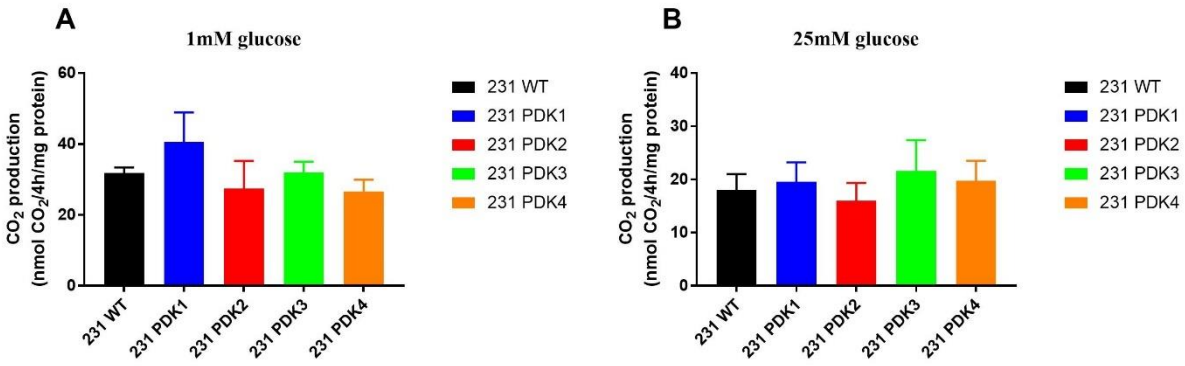

Figure 8.3 Effect of PDK overexpression in the glucose oxidation of 231 WT and 231 Glucose oxidation was measured by trapping $^{14}CO_2$-production during 4h incubation with [U-^{14}C]Glucose (4 µCi/ml, 5 mM total glucose concentration) after overnight pre-treatment with (A)1 mM glucose, and **(B)** 25 mM glucose **(C)** After overnight pre-treatment with 1 mM glucose, and **(D)** 25 mM glucose. The data presented here are normalized to cell protein content (mg). The figures display representative data of three independent experiments with mean of replicates ± SD. [U-^{14}C] Glucose - U indicates all carbons of glucose substrate is ^{14}C labeled.

8.4 Measurement of media glucose and lactate

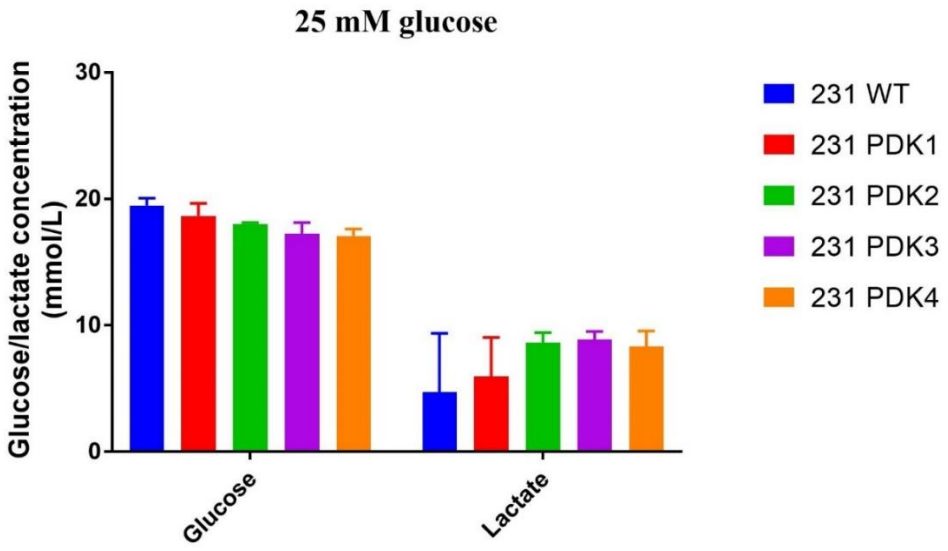

Figure 8.4 Measurement of glucose and lactate present in the cell culture media after overnight pretreatment in 25 mM glucose. The measurements were done before substrate oxidation experiment by $^{14}CO_2$-trapping. Estimated glucose concentration present in the media was ranging between 18-20 mmol/L in 231 WT and 231PDK1-4 cells. Estimation of extracellular lactate concentration was higher in 231 PDK1-4 than 231 WT culture media, ranging up to 5-9 mmol/L. The graphs represent mean of three replicates ± SD.

8.5 Determination of cell-associated radioactivity in 231 PDK1-4 cells

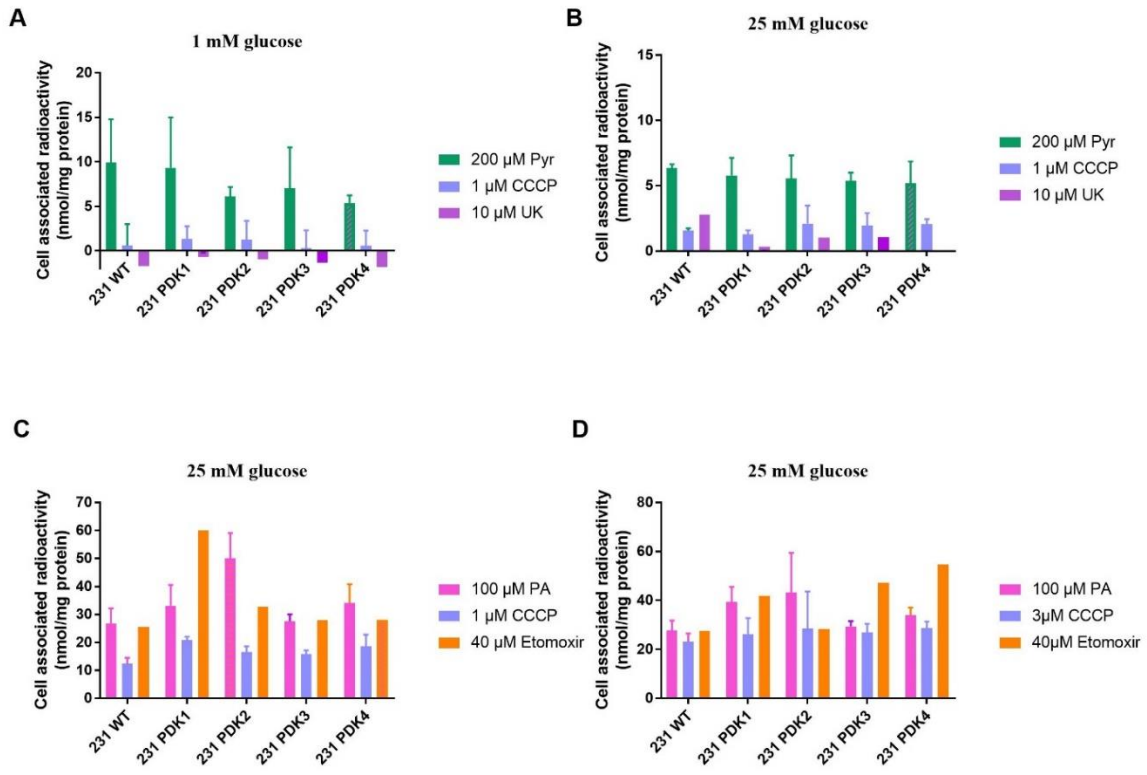

Figure 8.5 Cell associated radioactivity measured from the cell lysates of 231 WT and 231 PDK1-4 cells. (A-B) Accumulation of [1-^{14}C]pyruvic acid in presence of 1 µM CCCP and 10 µM UK-5099 in 1 mM and 25 mM pre-treated glucose condition respectively. (C-D) Accumulation of [1-^{14}C]palmitic acid after treated with 3µM CCCP and 40 µM etomoxir in 1 mM and 25 mM pre-treated glucose condition respectively. Measurements were after 2 hincubation with UltimaGold XR scintillation liquid. Data presented as mean of replicates ± SD.

Table 8.1 The qPCR ddCT values of the all PDK expression in each of the PDK-overexpressing cell

Cell types	PDK1+18S	PDK2+18S	PDK3 +18S	PDK4+18S
231 WT	1.00	1.00	1.00	1.00
231 PDK1	**35.80**	0.89	0.78	1.28
231 PDK2	0.72	**82.74**	0.33	0.80
231 PDK3	0.68	1.16	**145.74**	0.98
231 PDK4	0.25	0.67	0.36	**344.21**